Permeability studies of lipid vesicles by Fluorescence Correlation Spectroscopy and Monte Carlo simulations

A Master's Thesis

at the University of Copenhagen

Andreas Blicher

Submitted 2 August 2007

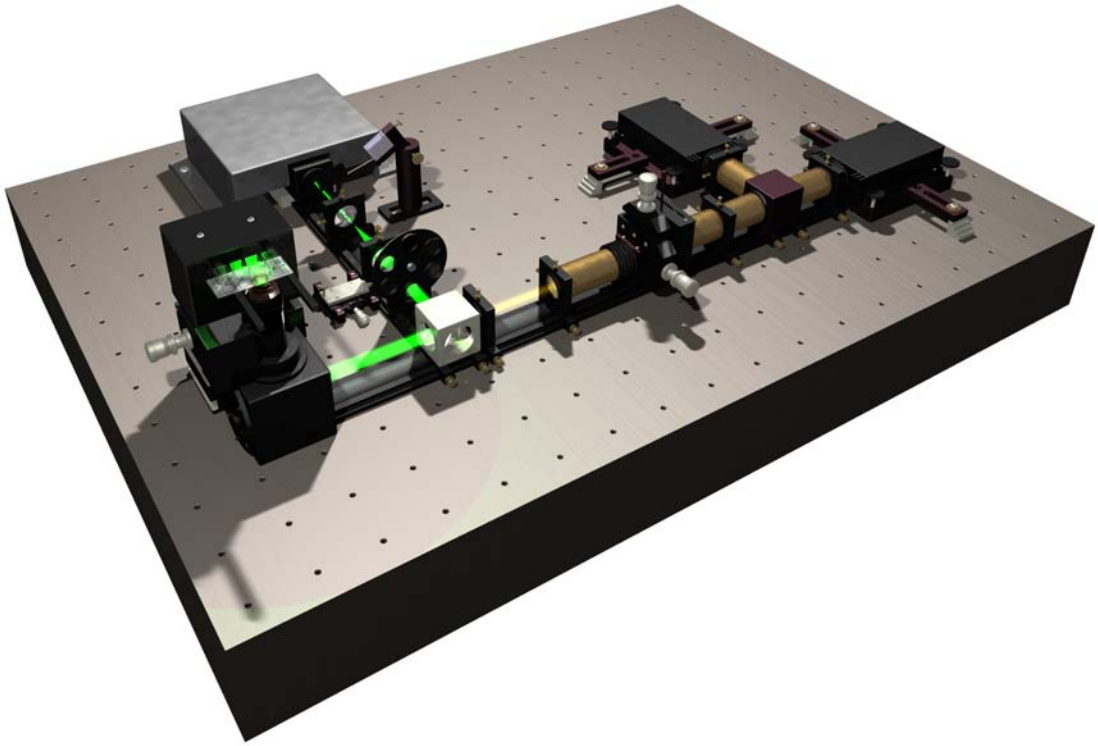

Imagination is more important than knowledge. For knowledge is limited to all we now know and understand, while imagination embraces the entire world, and all there ever will be to know and understand.

– Albert Einstein

Abstract

Unmodified phospholipid membranes show a pronounced increase in the transmembrane permeability in the gel-fluid phase transition regime. Fluorescence correlation spectroscopy was used to determine the characteristic time it takes for the fluorescence dye rhodamine 6G chloride to escape from large unilamellar vesicles composed of dipalmitoylphosphatidylcholine. The observed self-diffusion rates of the fluorophores could be changed by more than six orders of magnitude by inducing a phase transition in the membranes by adjusting the temperature or adding a general anaesthetic to the phospholipid membranes. The results are compared to numerical simulations based on the Monte Carlo method. In the numerical model the pore formation processes are similarly found to be closely coupled to the area fluctuations of the membrane, which are also strongest at the transition point.

Acknowledgements

First of all, I wish to thank my supervisor Thomas Heimburg. He has been a great source of inspiration, and without his help this project would not have been possible.

I also wish to thank the members of the NBI Membrane Biophysics Group for their patience and willingness to help, and in particular Konrad Kaufmann for an excellent discussion about the history of the field.

I would also like to show my gratitude to the people on the Kb-floor at the Niels Bohr Institute for keeping me entertained and sane during the writing of this thesis.

Lastly, I wish to thank Lars Holm Øgendal for providing the Dynamic Light Scattering data as well as thoughtful discussion and good genes.

A note on figures

All of the figures in this thesis were made using

- IGOR Pro (www.wavemetrics.com)
- CorelDRAW X3 (www.corel.com)
- PyMOL (pymol.sourceforge.net)
- POVray (www.povray.org)

Unless explicitly noted otherwise, all figures were made by Andreas Blicher. Some figures have been adapted from other sources, meaning that the data was extracted from the original figure and then replotted.

Contents

Part I
Introduction

More than three decades ago Papahadjopoulos et al. (1973) showed that the permeation rate of Na^+ ions through unmodified phospholipid bilayers could be increased by several orders of magnitude when the temperature was close to the melting temperature of the membrane.

Similar findings were made by other groups that same year. It was found that the electrical conductivity of DPPC membranes exhibited a pronounced maximum in the vicinity of the transition temperature (Wu and McConnell (1973)), and that the rate of transport through bacterial membranes is enhanced at the onset of the lateral phase separation in the membranes (Linden et al. (1973)).

The following year it was found by Yafuso et al. (1974) that under certain conditions, spontaneous conductance changes (ion channels) could be induced in oxidised cholesterol lipid films.

Half a dozen years later Antonov et al. (1980) and Boheim et al. (1980) demonstrated that the appearance of ion channels could be induced in pure lipid membranes by lowering the temperature to the melting temperature of the membrane. Even more interestingly, this could be done in a reversible manner.

A few years later Kaufmann and Silman (1983a,b) similarly demonstrated that they could also reversibly induce ion channels by changing the pH of the bulk solution on one side of the bilayer. Additionally, by increasing the proton concentration even further, they could return the system to a state of low conductance.

These findings led them to suggest that *any* mechanism that would lead to large fluctuations in the membranes should similarly induce ion channels – a fact that has since then been shown in a number of studies (Strom-Jensen et al. (1984), Maynard et al. (1985), Antonov et al. (1985), Yoshikawa et al. (1988), Kaufmann et al. (1989), Woodbury (1989), Antonov et al. (2005)).

Up till then – and to a large degree still – most studies on ion channels have implicitly been assuming that the lipid bilayer serves as an essentially inert matrix of high resistance and that the channels observed occur within the pore-forming proteins that are present in the bilayer.

However, the spontaneously formed pores give rise to discrete conductance jumps, which have an uncanny resemblance to the conductance of protein-channels. This spontaneous and stochastic gating process across the membrane may be due to the repeated opening and recovery of defects induced by lateral density fluctuations, as this would account for the increased permeability of the membrane when the fluctuations are strong, as is the case when near a phase transition.

The melting transition of biological membranes tends to lie just below body temperature, thus making it easy to get into the melting transition by changing the local pH, pressure or voltage across the membrane. It has been shown that anaesthetics shift the melting transition to lower temperatures. This means that the membranes are further from the transition conditions and thus less likely to enter the phase transitions, which are necessary for the biological function. Therefore, it is not unreasonable to speculate that the lipid bilayer could play an active part in the functional control of biological membranes.

The purpose of this project is to study – both theoretically and experimentally – how the permeability of lipid membranes varies with temperature and how this dependence changes if another membrane variable is varied.

For this purpose we have chosen to study synthetic, unilamellar lipid vesicles, as these offers a simple, well-defined system that makes it possible to measure permeation rates, and how these change with temperature and other membrane variables.

This is done in two ways: by measuring the rates directly with the use of Fluorescence Correlation Spectroscopy (FCS), and by means of Monte Carlo simulations.

With FCS it should be possible to measure how fast fluorescent molecules leak out of the vesicles at a given temperature by looking at the time evolution of the correlation curves of the system.

The Monte Carlo simulation will be based on a two-state Ising model with the various parameters being determined – where possible – by calorimetric measurements. These simulations of the lipid membrane provide information about both the thermodynamic properties of the system and domain formation and fluctuations, and consequently the permeability of the system. The results of the numerical work can then be compared with the FCS measurements to allow for a detailed description of the system and the possible implications for the physiology of biological cells.

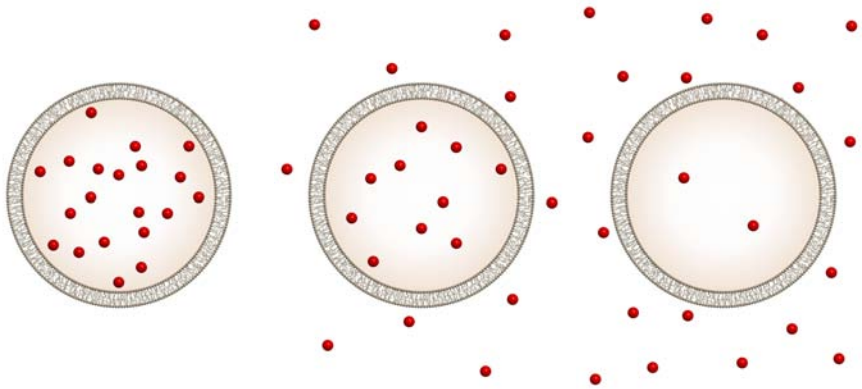

FIG. 1: The basic idea behind the FCS experiments. *Left:* The initial state of the system, where all of the dye is trapped inside the vesicles. *Middle:* After a while some of the dye will have leaked out due to spontaneous pore formation. *Right:* In the end there will be no concentration gradient, and the vesicles will be mostly empty.

1 Composition of Membranes

Lipid bilayers are found everywhere in the living world, with plasma membranes forming a 5nm thick skin around every eukaryotic and prokaryotic cell. Organelles and other intracellular structures such as the endoplasmic reticulum, the nucleus of eukaryotic cells, mitochondria, and the chloroplasts of green plant cells are all surrounded by lipid membranes, as are several animal and plant viruses.

Cell membranes are primarily constructed from lipids and proteins, and are generally arranged in topologically closed surfaces which physically separate the intracellular components from the extracellular environment. At the most fundamental level they function as selective barriers, which allow living cells to maintain an intracellular composition that is different from that of the extracellular solution. The barrier function is provided by the lipid bilayer, as the hydrophobic core of the bilayer has a very low dielectric constant compared to water (a factor of ~ 40). This results in a prohibitively large transfer energy for moving ions from the aqueous solution into the bilayer core (Paula et al. (1998)).

Ever since Overton (1899) concluded that cells must be surrounded by a "fatty oil", there have been speculations on the structure and properties of the cell membranes. The first evidence of a bilayer structure was obtained by Gorter and Grendel (1925), who predicted and demonstrated that the lipid membrane was indeed a bilayer by comparing the surface area of different animal (and human) erythrocytes to the "surface occupied by all of the lipoids of the chromocytes."

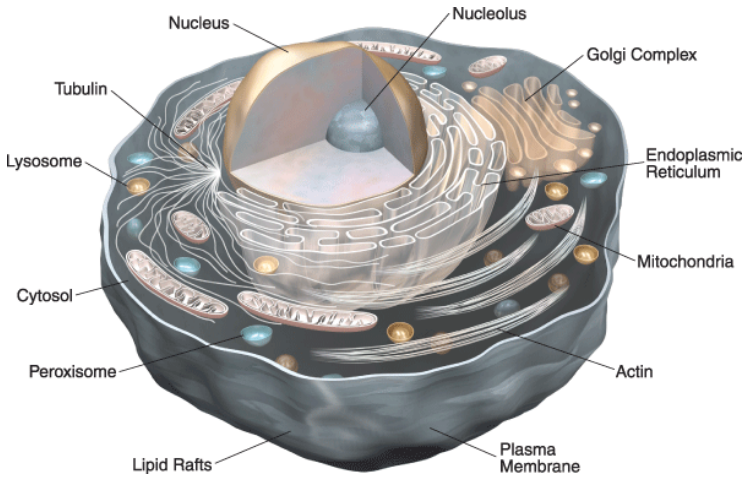

FIG. 2: Illustration of an idealised animal cell. The plasma membrane is a thin phospholipid bilayer that acts a selective barrier between the inner and outer part of the cell. Inside the cell itself, membranes also appear in different organelles like the endoplasmic reticulum, the Golgi complex and the mitochondria. The endoplasmic reticulum is involved in the synthesis of e.g. lipids, steroids and proteins. The Golgi complex is a network of flat membranous sacs that produce, change and store proteins, while the mitochondria are involved cellular respiration and the production of ATP from nutrients. The picture was taken from `http://probes.invitrogen.com`.

FIG. 3: Models for cell membranes. *Left:* The fluid mosaic model of Singer and Nicolson (1972). The phospholipids are arranged in a discontinuous bilayer with the polar head regions being exposed to the aqueous phases while the hydrocarbon tails are sequestered away. The proteins are partially or fully embedded in the fluid membrane and are largely randomly distributed, though they may locally form aggregates. *Right:* The mattress model of Mouritsen and Bloom (1984). Transmembrane proteins or polypeptides are located in an environment that is primarily determined by the mismatch in the hydrophobic regions of the lipids and the amphiphilic molecules.

The first commonly accepted membrane model came ten years later. It was proposed by Danielli and Davson (1935), who suggested that cells must be surrounded by "lipoidal material" that was sandwiched in between two layers of proteins. The membrane itself was considered to be homogeneous and it could be either solid or liquid.

This model persisted for several decades, undergoing only some minor revisions with the introduction of the electron microscope studies, where Robertson (1957) observed a characteristic trilaminar appearance consisting of two darker outer lines and a lighter inner region. The interpretation was that all cell membranes must have a common structure (the "unit membrane"), where the darker lines must be protein layers and the light region the lipid bilayer.

This model was eventually refined by Singer and Nicolson (1972), where they proposed a fluid mosaic model for the gross organisation and structure of the proteins and lipids of biological membranes. In their model the lipids are arranged in the form of a bilayer, in which the proteins are embedded and can diffuse freely (see Fig. (3)).

Since its proposal this model has been subjected to further refinement to take into account that lipids and proteins may distribute inhomogeneously (Mouritsen and Bloom (1984), Jacobsen et al. (1995)), and that domains rich in sphingolipids and cholesterol (so-called "rafts") may form in the membrane. This lateral heterogeneity has a strong influence on diffusion and directed transport in the membrane as well as signalling pathways (Simons and Ikonen (1997)).

The lipid and protein composition of the various membranes shows a large variation. For instance, in nerve membranes (myelin) one finds a high percentage of sphingomyelin lipids. One also finds a large range for the percentage of unsaturated fatty acids as well the amount of charged lipids between different membranes (Heimburg (2007)). The reason behind this diversity in membrane composition still remains unresolved (Tien and Ottova-Leitmannova (2003)).

When bacteria are grown under different environmental conditions (different

temperature, pressure, salinity, pH), they display a different lipid composition (Hazel and Williams (1990), Heimburg (2007)). They can regulate the composition of their membranes by either changing the number of double bonds in the hydrocarbon chains, or by changing the chain lengths. Desaturases – that is enzymes that can introduce carbon-carbon double bonds – are normally synthesised by expression of the relevant genes when the temperature is lowered. At higher temperatures, a protein binds to the enzymes and thereby inactivates them (Jensen and Prentø (1994)). This ability to regulate the composition of the membranes to cope with the effects of different environmental conditions is known as homeoviscous adaptation (Marr and Ingraham (1962), Sinensky (1974)), and numerous examples of this phenomenon have been found (see MacDonald (1988) and the references therein).

The cells of eukaryotic organisms also make use of both the regulation of the number of double bonds in the hydrocarbon chains as well as adjusting the concentration of cholesterol to control the state of the membranes. Therefore, the number of double bonds and amount of cholesterol will increase with decreasing temperature for poikilothermic animals[1]. Similarly, it has been found that the cell membranes of deep sea fish also show homeoviscous adaptation to pressure[2] (MacDonald (1988), Hazel and Williams (1990)).

Another example can be found in trouts that have been raised at different temperatures. Here it has been found that the lipid composition of their livers changes with temperature. Likewise, it has been found that the brain synaptic membranes of teleost fish display different lipid compositions depending on whether their habitat is arctic, temperate, or tropical (Logue et al. (2000)). Arctic animals, such as seagulls and reindeer, also have high amounts of unsaturated lipids in the membranes near the feet/hooves, whereas membranes near the thigh have relatively few double bonds (Fox (1972), MacDonald (1988)).

It is also known that hibernating animals will start off by adjusting their membranes to function at lower temperatures (Aloia and Raison (1989), Jensen and Prentø (1994)).

This adaptation can even be found in humans, where it is a well-established fact that chronic alcoholics have higher amounts of saturated lipids and cholesterol in their red blood cells (Benedetti et al. (1987), Parmahamsa et al. (2004)), to compensate for the changes induced by the alcohol.

A different – and still not quite understood – change in the membranes happens during anaesthesia. Anaesthesia occurs when the membranes of the nerve cells absorb certain hydrophobic compounds, which changes their state as a result. This change inhibits the cells' ability to receive and process signals. A couple of thermodynamically based explanations have been proposed.

One theory is that the anaesthetic alter the transverse pressure profile of the membrane, thereby influencing the conformations and function of the embedded proteins (Cantor (1997a,b)).

Another possibility has been proposed by Heimburg and Jackson (2005), who argue that the nerve pulse is in fact a propagating density pulse (soliton). The effect of the anaesthetic would then solely be due to the induced melting

[1] I.e. vertebrate animals, such as fish and reptiles, where the body temperature varies with the temperature of its surroundings.

[2] For lipid bilayers the transition temperature increases with pressure by 0.1–0.4K/MPa, depending on the exact composition. For most phospholipids, this value lies in the vicinity of $\approx$ 0.23K/MPa (Hazel and Williams (1990)).

point depression which alters the amount of free energy needed to generate a pulse. It thus predicts that anaesthesia can be reversed by adjusting e.g. the hydrostatic pressure, pH or pCa, so that the free energy of the membrane returns to its original value (Heimburg and Jackson (2007a,b), Seeger et al. (2007)).

In conclusion, the composition and state of the lipid membranes must play an important role for biological function, as it would be rather easy to lower the melting temperature significantly by introducing unsaturated lipids or cholesterol, if only soft and fluid membranes were required.

1.1 Fatty acids and phospholipids

Fatty acids are carboxylic acids of the form RCOOH, where the R represents a long hydrocarbon chain. They are usually not found in their free state in cells, but are instead components of covalently bonded molecules, such as phospholipids or triglycerides where two or three fatty acids are linked to a glycerol backbone. In the case of the phospholipids, the remaining -OH group in the glycerol is replaced by a phosphate group -PO_4 which, in turn, is linked to yet another group that is normally referred to as the polar head group.

Like all lipids in biological membranes, phospholipids are amphiphilic in nature (i.e. they have both a polar and a non-polar region). The length of the non-polar hydrocarbon chains lies in the range from 12 to 24 carbons with the typical value being 16 or 18 (Eisenberg and McLaughlin (1976), Heimburg (2007)).

The polar head groups of phospholipids may be chosen from a variety of organic compounds, such as choline, ethanolamine, serine and glycerol.

Both serine and glycerol phospholipids have negative charge due to the phosphate group, while choline and ethanolamine are zwitterionic but have no net charge. The naming convention for a phospholipid reflects, in part, its fatty

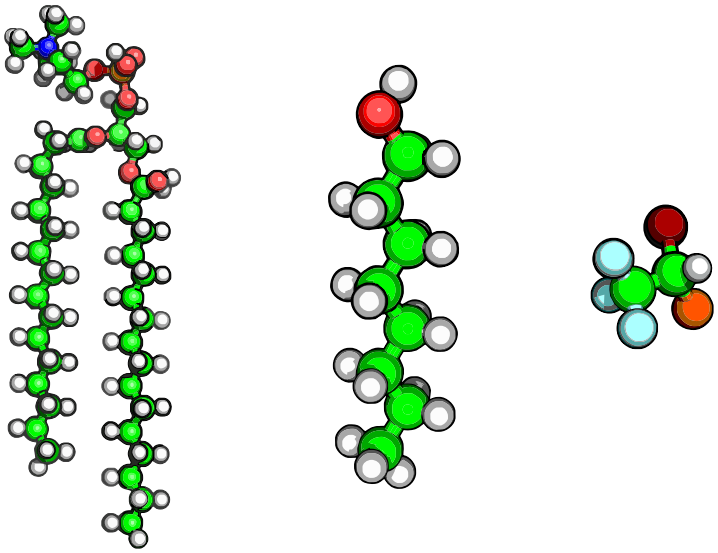

FIG. 4: *Left:* Dipalmitoyl phosphatidylcholine (DPPC). *Middle:* 1-Octanol. *Right:* 2-Bromo-2-chloro-1,1,1-trifluoroethane (halothane).

acid composition. For example, a phospholipid containing two palmitic acids (16 carbons each) and a choline group is called dipalmitoyl phosphatidylcholine or DPPC for short. Common abbreviations include:

- phosphatidylcholine: PC
- phosphatidylethanolamine: PE
- phosphatidylserine: PS
- phosphatidylglycerol: PG

In many membranes the fraction of charged lipids is around $10-20\%$, though it can be as high as 40%, as is the case for mitochondria (Heimburg (2007)). This will of course have an influence on the electrostatic potential of the membranes.

While the phospholipids are major component of cellular membranes, there are other kinds of lipids present, such as glycolipids and cholesterol.

Glycolipids are similar to phospholipids in that they have a pair of hydrocarbon chains, but the phosphate group is replaced by a sugar residue (based on a ring of five carbons and one oxygen).

Cholesterol, on the other hand, is a member of the steroid family and is commonly found in the membranes of eukaryotic cells. For instance, in erythrocytes the cholesterol content may be 20% or even higher (Parmahamsa et al. (2004), Heimburg (2007)).

2 An Incomprehensive Summary of Previous Permeability Studies

Present theories of ion channel formation (whether in artificial bilayers or in cell membranes) favour the notion of ion channels being formed by specific proteins that are embedded in the membrane and provide pathways for fast and controlled flow of selected ions along their electrochemical gradients.

This activity is used to explain action potentials in nerves, muscles and other excitable cells, and is thought to form the basis of all movement, sensation and thought processes in living beings.

While it is well-known that certain proteins and peptides can create selective ion channels and thereby regulate the permeability of the membrane, it seems less well-known that pores can transiently form in protein-free membranes due to thermal fluctuations. This phenomenon can make permeation rates much higher than expected from the Arrhenius law, especially in states where there are strong lateral density fluctuations (Papahadjopoulos et al. (1973), Wu and McConnell (1973), Nagle and Scott (1978), Antonov et al. (1980), Cruzeiro-Hansson and Mouritsen (1988) Kaufmann and Silman (1989), Corvera et al. (1992), Seeger et al. (2007), Heimburg (2007)).

An interesting feature of these spontaneously formed pores is that they exhibit features normally considered to be indicative of protein channels including stepwise conductance changes, flickering, ion selectivity, and inactivation (Woodbury (1989)).

While physiological studies provide detailed information about the functional properties of ion channels, there has been a notorious lack of structural

knowledge about them. Even the famous potassium channel from the Hodgkin-Huxley theory was only crystallised in 1998 by Roderick MacKinnon (who was awarded the Nobel Prize already in 2003 for this feat), even though the Hodgkin-Huxley theory was proposed more than 50 years ago (Hodgkin and Huxley (1952)).

Prior to the publication of the first studies of quantised currents through proteins by patch clamp, Yafuso et al. (1974) reported spontaneous conductance changes and multilevel conductance states in pure black lipid membranes made from oxidised cholesterol.

Two years later Neher and Sakmann (1976) performed the first patch clamp experiments (which also won them the Nobel Prize in 1991). This was the first time single-channel currents were recorded in biological membranes. Since then an enormous number of patch clamp studies have been performed, so for a thorough discussion of this field see Hille (2001).

Despite the omnipresence and vital nature of lipid membranes, most studies have for a long time tended to ignore them and simply consider them as being homogeneous and impermeable barriers without any noteworthy properties (Tien and Ottova-Leitmannova (2003)).

The fact that the membrane permeability increases strongly under certain conditions is rarely considered in measurements on protein-channels. For instance, the simple act of applying suction or a transmembrane voltage in patch clamp experiments can induce a phase transition in the membrane (Kaufmann and Silman (1989)).

Furthermore, even when some protein-channels are found to be influenced by the lipid membrane (Schmidt et al. (2006), Lee (2006)), it is usually only specific binding/interaction with proteins that is considered, and rarely the thermodynamics of the system as a whole.

Consequently, the studies of pure lipid membrane systems are few and far between, though their importance is starting to dawn on the scientific community (Hilgemann (2003)).

In Antonov et al. (1980) the electrical conductance of protein-free membranes made from synthetic DSPC was examined. It was discovered that at the phase transition temperature long-lived current fluctuations appeared. In this article they tentatively proposed that such channels could in fact conduct the known transmembrane ionic currents, without the direct involvement of protein-channels.

In Antonov et al. (1985) (and also more recently, such as in Antonov et al. (2005)) they followed up on their findings. The capacitive and ionic currents through bilayer lipid membranes formed from dipalmitoylphosphatidic acid were studied, and it was found that by causing a phase transition by introducing Ca^{2+} ions, they could observe single ion channel events in the bilayer lipid membranes.

Two years before that, Kaufmann and Silman (1983b) published a systematic study on how ion channels through lipid bilayer membranes could be induced by changes in the pH of the system. Specifically, they found that there was a certain threshold for the proton concentration at which otherwise stable lipid bilayers of very low conductivity would show resolved ion channels. Further acidification would reduce the permeability of the membrane to a much lower value, indicating that this was related to a transition in the membrane.

In Kaufmann et al. (1989) they published their extensive studies on how ion channel fluctuations in pure lipid bilayer membranes could be controlled in a

deterministic fashion by changing any of the intensive thermodynamic variables, such as voltage, surface pressure, pH, and temperature. This led them to conclude that the reversible fluctuations in the membrane are responsible for the opening and closing of aqueous defects in the lipid bilayer.

Other groups have observed similar properties of protein-free phospholipid membranes. Boheim et al. (1980) and Yoshikawa et al. (1988) both verified that fluctuations and stepwise changes in the electrical current across a synthetic membrane could be induced by having the system near its phase transition temperature.

Likewise, Woodbury (1989) found that channel-like current fluctuations in planar lipid bilayers could be observed when pure lipid vesicles fused with the membranes.

Finally, it has been found that the membrane phospholipid composition and state affects the function (conductivity, opening and closing statistics, midpoints of activation, etc.) of certain protein-channels. (Turnheim et al. (1999), Schmidt et al. (2006)). Furthermore, the various channel activity parameters also show a pronounced peak in the transition regime (Cannon et al. (2003)).

In summary, it has been found that

- The permeability of lipid membranes depends strongly on the temperature, with a pronounced peak at the phase transition temperature (Papahadjopoulos et al. (1973), Georgallas et al. (1987), Corvera et al. (1992), Heimburg (2007)).
- Ion channels appear in any lipid bilayer even in the absence of any further membrane component, and they reversibly open and close. These fluctuating channels are thought to be due to structural changes (transient pores) in the lipid bilayer during the melting-transition of the phospholipids (Yafuso et al. (1974), Antonov et al. (1980), Boheim et al. (1980), Antonov et al. (1985), Yoshikawa et al. (1988), Woodbury (1989), Kaufmann and Silman (1989), Antonov et al. (2005)).
- The spontaneously formed pores exhibit stepwise conductance changes, flickering, ion selectivity, and inactivation (Woodbury (1989)).
- The probability of an event can be controlled by all of lipid variables, such as voltage, surface pressure, pH, pCa, and temperature (Antonov et al. (1980), Boheim et al. (1980), Kaufmann and Silman (1983a), Kaufmann and Silman (1983b), Antonov et al. (1985), Kaufmann and Silman (1989), Antonov et al. (2005)).
- The typical time scales of ion channel opening and closing in both transient pores as well as in protein-channels are similar to the characteristic relaxation time of the membrane (Seeger (2006), Seeger et al. (2007)).
- The function of certain protein-channels depends strongly on the composition and state of the lipid environment (Turnheim et al. (1999), Cannon et al. (2003), Schmidt et al. (2006), Lee (2006)).

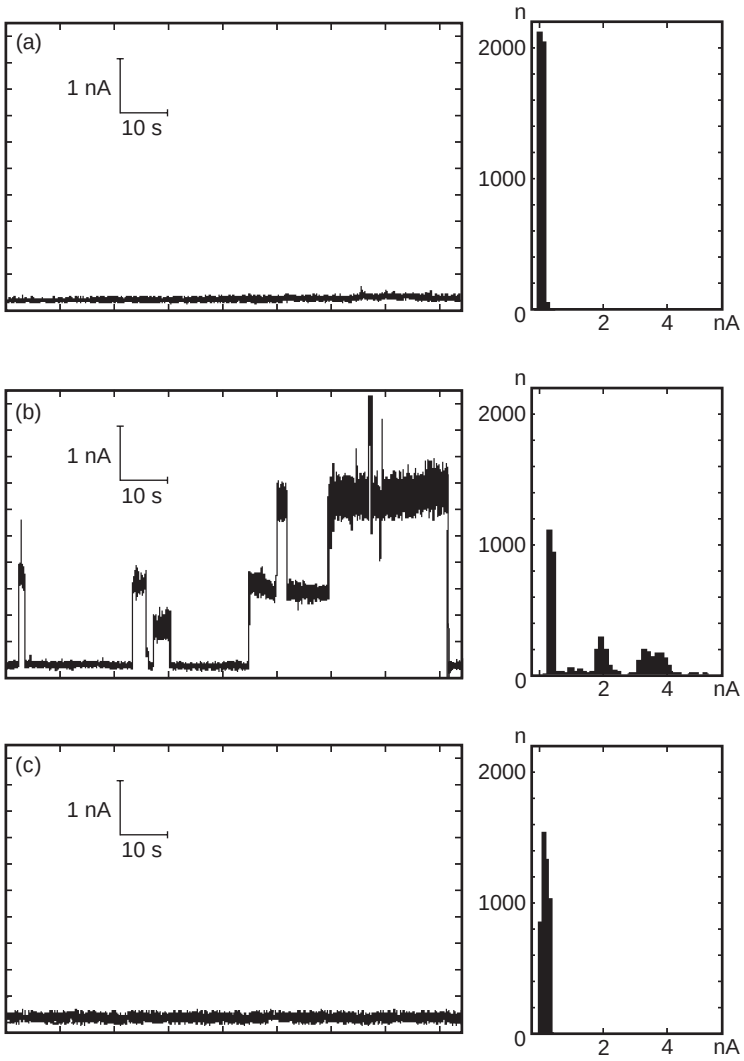

FIG. 5: Electric current fluctuations *(left)* and corresponding histograms *(right)* recorded in planar BLM from DPPC in 1M LiCl with the transmembrane potential clamped at 50mV. At temperatures above (*a:* $T = 50°\mathrm{C}$) and below (*c:* $T = 35°\mathrm{C}$) the current fluctuations are practically absent and only noise is observed. At the temperature of the main phase transition of the system (*b:* $T = 43°\mathrm{C}$) one can see a series of single and double current fluctuations with a well-defined amplitude. Adapted from Antonov et al. (2005).

Part II
Theory

This part introduces all of the theory needed for this project. As the phenomenon investigated in the thesis is a thermodynamic one, the first section will describe some of the basic thermodynamics of lipid membranes.

As the two primary methods of investigation used in this thesis are Fluorescence Correlation Spectroscopy and Monte Carlo simulations, the basics of both of these methods will also be discussed in some detail.

3 The Thermodynamics of Membranes

3.1 Phase transitions

Phase transitions occur when there is a singularity in a system's free energy or one of its derivatives. This can normally be observed as a sharp change in one or more of the properties of the system. There are many examples of this, such as the transition from solid to liquid, from paramagnet to ferromagnet, or from normal conductivity to superconductivity.

Another example is, of course, amphiphilic molecules in solution, which can exhibit fairly exotic behaviour. These molecules have a hydrophilic polar head group and two hydrophobic hydrocarbon tails, which means that in an aqueous system, the polar heads of the lipids will be orientated towards the polar, aqueous environment, while the hydrophobic tails seek to minimise their contact with the water as shown in Fig. (6).

If there is a surface they will migrate there and as a result lower the surface tension – hence their use as soaps.

The phase diagrams of solutions of lipids – and surfactant molecules in general – are mainly determined by the concentration of the solute, though pH, salinity, pressure and temperature can also have a strong influence, as in the case of DMPG, which displays quite complex (and still not fully understood)

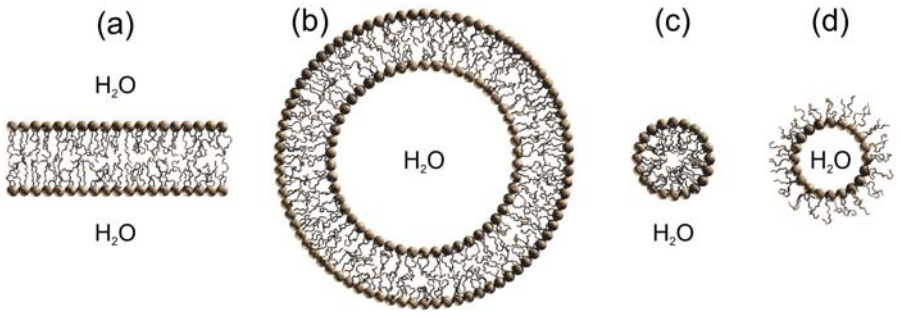

Fig. 6: Self-assembly of lipids in water gives different structure, depending on the lipid concentration, the molecular structure, etc. *(a)* Bilayer. *(b)* Unilamellar vesicle. *(c)* Micelle. *(d)* Inverse micelle.

phase behaviour (Heimburg and Biltonen (1994)). In fact, lipids display a great diversity of structure over a very narrow range of chemical and physical parameters that are close to physiological conditions – more so than any other class of biological molecules (Hazel and Williams (1990)).

When the concentration is increased micelles form. These are groups of lipids arranged in a spherical or cylindrical configuration, so that the polar heads shield the hydrocarbon tails from the aqueous environment. If the concentration is increased even further, the system can undergo a transition to other geometries, such as a state where micelles are ordered in a cubic or hexagonal array or a sponge phase where the intervening spaces are filled with water. Other transitions are also possible, such as when the lipids are arranged into bilayers but move freely within it like a two-dimensional fluid, and a further transition to a so-called ripple phase, where lines of lipids are in in the fluid state (Heimburg (2000)), and finally a fully fledged crystalline state, where the lipids are ordered on a triangular lattice.

One will find different states of lipid membranes depending on the temperature. When the temperature is decreased, four different states occur:

- $\mathbf{L}_\alpha$: In this state all the lipid chains are disordered (fluid) and the lateral order of lipids is random (liquid). Therefore, this phase is also called the liquid-disordered phase, or simply the fluid phase.
- $\mathbf{P}'_\beta$: This is the so-called 'ripple'-phase, where the system is partially solid and partially fluid, and has a periodic super structure (Heimburg (2000)).
- $\mathbf{L}_\beta$: Crystalline molecular order (solid) in the membrane phase, chains are 'all-trans' (ordered) and tilted. This phase is sometimes called the solid-ordered phase, or alternatively the gel phase.
- $\mathbf{L_c}$: Crystalline in three dimensions.

The transition between these four phases occurs at well-defined temperatures. The transition temperature depends on a number of factors, such as the chain length, chain saturation (number of carbon-carbon double bonds), head group size and charge, etc. The transition temperatures can also be altered by co-addition of cholesterol, peptides, general anaesthetics (e.g. halothane or chloroform), binding of molecules to the surface, etc.

3.2 Transitions in phospholipids

The physical properties of the lipid membranes can be studied in detail by using model systems prepared from pure (synthetic) lipids, and has been done so extensively in the last couple of decades (Hinz and Sturtevant (1972), Heimburg (2007)).

As described in Sec. (1.1) a phospholipid has two hydrocarbon chains. Each of the C–C bonds of the hydrocarbon chains allows for rotations to take place, with three distinct energy minima at $\pm 120°$ angles as shown in Fig. (7).

Of the three minima, the trans configuration displays the lowest energy, with a difference of approximately 2.5kJ/mol with respect to the gauche$^-$ and gauche$^+$ configurations.

In the ground state of the system both chains adopt an all-trans configuration, and as this can only be done in one way, the state has an entropy of

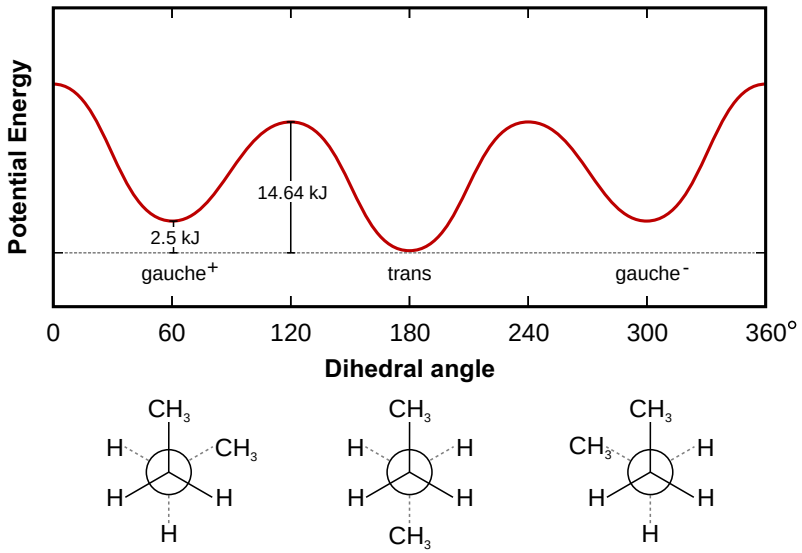

FIG. 7: Lipid chains may have various conformations. Different conformations can be generated by rotation around the C–C bonds in the chains ('trans-gauche' isomerizations). The configuration with the lowest energy is the 'all-trans' configuration, which has a characteristic zig-zag pattern as shown in Fig. (4). The conformations with 'gauche'-isomers display higher internal energy, but also have a much higher degeneracy. Thus the conformation of the chains will depend strongly on the temperature. Furthermore, the different lipid conformations will occupy different volumes and areas, so the lipid conformations will also depend on bulk and lateral pressure. Figure adapted from Gennis (1989).

$S_0 = S_0^0 + R\ln(1) = S_0^0$. If we let γ denote the mean probability to find a gauche-isomerization in a CH_2–CH_2 bond (an exited state), the entropy of the chains will be given by

$$\Delta S_{CH_2} = -k_B \sum_i P_i \ln P_i = -k_B \cdot 2 \cdot \left(\frac{\gamma}{2}\ln\frac{\gamma}{2}\right) - k_B(1-\gamma)\ln(1-\gamma), \qquad (1)$$

where $P_{gauche^-} = P_{gauche^+} = \gamma/2$ and $P_{trans} = (1-\gamma)$.

At high temperatures all the trans and the gauche states will be equally probable, so for $T \to \infty$ we have that $\gamma \to 2/3$ and

$$\Delta S_{CH_2} = -k_B \cdot 3 \cdot \left(\frac{1}{3}\ln\frac{1}{3}\right) = k_B \ln 3. \qquad (2)$$

A hydrocarbon chain with n carbon atoms has $(n-2)$ bonds which lead to distinguishable configurations after rotation, and the entropy of the disordered chain is therefore

$$\Delta S = \Delta S^0 + 2(n-2)\Delta S_{CH_2}, \qquad (3)$$

that is, it is proportional to the length of the chain. The factor 2 stems from the fact that there are two chains in each lipid.

For the enthalpy of the excited state we similarly find

$$\Delta H = \Delta H^0 + 2(n-2)\Delta H_{CH_2} \tag{4}$$

with $\Delta H_{CH_2} = \gamma \cdot 2.5\text{kJ/mol}$.

If we assume that a the lipid will only be found in one of two states – all-trans and disordered – the (chain) melting point can be defined as the temperature at which the ground state and the excited states are equally likely:

$$\frac{P_{disordered}(T_m)}{P_{all-trans}(T_m)} = K(T_m) = 1 \tag{5}$$

$$\Rightarrow \quad \Delta\mu = \Delta H - T_m \Delta S = 0 \Rightarrow T_m = \frac{\Delta H}{\Delta S} \tag{6}$$

As is evident from Eqs. (3)–(6) this temperature depends on the length of the hydrocarbon tails. However, in general there are a number of other factors which can strongly influence its value. As mentioned in Sec. (1) the presence of double bonds will generally reduce the melting point of the system, thus allowing organisms to easily adjust the melting point of their lipid membranes by adjusting the ratio of unsaturated/saturated lipids. Electrostatic interactions between the lipids' head groups also plays a major role, as the strength of this effect depends strongly on pH and salt concentrations, making it possible to quickly induce changes. Pressure as well as the electric potential across the membrane will also influence its state.

For most natural lipids the melting temperatures are in the biologically relevant temperature regime (−20°C to +60°C) (Tien and Ottova-Leitmannova (2003), Ivanova et al. (2003)), and in general biological membranes have a transition temperature approximately 15K below the organism's temperature (Heimburg and Jackson (2005)), though the transition is rather broad (≈ 10–15°C).

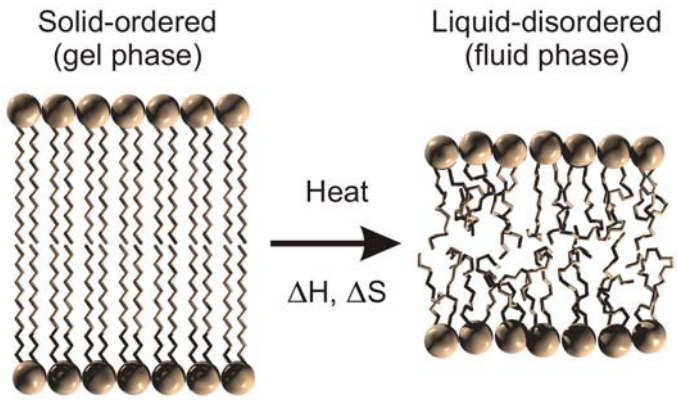

FIG. 8: Chain-melting transition of a phospholipid bilayer. When going from low to high temperature there is an increase in the enthalpy, ΔH, and the entropy, ΔS. The change in the chain configurations also means that the membrane changes area by approximately 33% and thickness by approximately −13% (Heimburg (1998)).

3.3 Fluctuations

The lipid bilayer fluctuates reversibly in any state, and from these fluctuations a large number of properties of the system can be derived.

The excess heat capacity at constant pressure of a system, c_p, can easily be derived from the fluctuation-dissipation theorem (Hill (1962)) as follows.

$$c_p \equiv \left(\frac{d\langle H\rangle}{dT}\right)_p \tag{7}$$

$$= \left(\frac{d}{dT}\right)_p \sum_i \frac{H_i \cdot e^{-H_i/RT}}{Z}, \quad \text{where} \quad Z \equiv \sum_i e^{-H_i/RT} \tag{8}$$

$$= \sum_i \frac{H_i^2 \cdot e^{-H_i/RT}}{RT^2 \cdot Z} - \sum_i \frac{H_i \cdot e^{-H_i/RT}}{Z} \sum_j \frac{H_j \cdot e^{-H_j/RT}}{RT^2 \cdot Z} \tag{9}$$

$$= \frac{\langle H^2\rangle - \langle H\rangle^2}{RT^2}, \tag{10}$$

where R is the gas constant and T the temperature. Here the sums are over all the possible states of the system.

Another example is the isothermal area compressibility, κ_T^A, which can be derived in a similar fashion:

$$\kappa_T^A \equiv -\left(\frac{1}{\langle A\rangle}\frac{d\langle A\rangle}{d\Pi}\right)_T \tag{11}$$

$$= -\frac{1}{\langle A\rangle}\left(\frac{d}{d\Pi}\right)_T \sum_i \frac{A_i \cdot e^{-H_i/RT}}{Z} \tag{12}$$

$$= \frac{\langle A^2\rangle - \langle A\rangle^2}{\langle A\rangle RT}, \tag{13}$$

where Π is the lateral pressure (where $H = E + pV + \Pi A + \ldots$).

Thus the excess heat capacity is proportional to the fluctuations in the enthalpy, while the area compressibility is proportional to the fluctuations in the area of the system. This turns out to be extremely useful relations when performing Monte Carlo simulations.

Since the membrane volume only changes by $\approx 4\%$ during the transition (Heimburg (1998)), the relative thickness fluctuations must be approximately equal to the relative area fluctuations. This means that the membrane thickness fluctuations are large when the isothermal area compressibility is large.

Furthermore, it is known that membranes become more pliable during the chain-melting transition (Heimburg (1998)). In fact, it has been found that the lateral compressibility and the excess heat capacity are proportional functions near the chain-melting transition (Heimburg (1998), Ebel et al. (2001)), meaning that both the area and the enthalpy fluctuates strongly during the transition.

Moreover, it has been shown that the relaxation time after a perturbation of the system is similarly related to the fluctuations of the system (Grabitz et al. (2002), Seeger (2006), Seeger et al. (2007)).

The presence of these fluctuations means that the hydrophobic barrier of the flexible hydrocarbon chains will inevitably disappear locally given sufficient time.

As a pore (hydrophilic or not) is an allowed state of the membrane, it seems reasonable to assume that the probability of occurrence would be much higher when the lateral density and thickness fluctuations of the membrane are strongest, such as during the chain-melting transition.

3.4 Models for permeability

As mentioned in Part (I) the permeation rate of ions and small molecules through unmodified lipid membranes increases by several orders of magnitude in the transition regime. The reason for this anomaly is still not fully understood, though a possible explanation is offered by at least two models, which – for ease of reference – will be called the 'line defect model' and the 'pore model'. Both of them are based on thermodynamic grounds and they should not be considered to be mutually exclusive.

The line defect model was first proposed by Träuble and Haynes (1971) and later Papahadjopoulos et al. (1973) and subsequently followed up on by Cruzeiro-Hansson and Mouritsen (1988). They proposed that the increase in permeability is caused by line defects that occur at the interfaces between domains and the bulk, which can facilitate the solubility and diffusion of water and other small solutes through the membrane. These defects appear because of the mismatch in the area of fluid state and gel state lipids, which makes it impossible to have optimal (hexagonal) packing of the lipids. This theory would thus predict that the permeability should increase in the phase transition when domain formation and local fluctuations are strong. Furthermore, the permeability should increase with increasing interfacial area, which happens when the cooperativity (line tension) of the system is decreased.

Another possible mechanism (the pore model) was proposed by a number of people (Linden et al. (1973), Wu and McConnell (1973), Nagle and Scott (1978), Doniach (1978), Kaufmann and Silman (1983a,b), Kaufmann et al. (1989), Ivanova et al. (2003)). This mechanism assumes that the particles permeate through transient hydrophilic pores that are the result of thermal fluctuations. Thus no dehydration or hydrophobic barrier has to be involved. They suggested that the probability of forming a pore should solely depend on the fluctuations in the area (and consequently the lateral compressibility) of the system. As this quantity is directly proportional to the heat capacity (Ebel et al. (2001)), this theory predicts that the permeability would decrease at the transition midpoint if the cooperativity of the system is reduced, as this lowers and broadens the heat capacity profile. Thus the permeability would decrease near the phase transition temperature, but increase in the wings of the heat capacity profile.

These thermodynamic models are, in a sense, very minimalistic models in that they incorporate the fewest possible assumptions about the diffusion mechanism, and neither implies a detailed structural model of the defects.

As mentioned, these two models are not mutually exclusive, but one of the mechanisms will be the dominant one, while the other will simply provide an alternative pathway for permeation.

It was shown in Paula et al. (1998) that the permeation of halide ions through phospholipid bilayers seems to favour the solubility-diffusion mechanism. However, it seems difficult to explain the discrete nature of the ion channel currents based on this mechanism. However, under certain conditions the pore mechan-

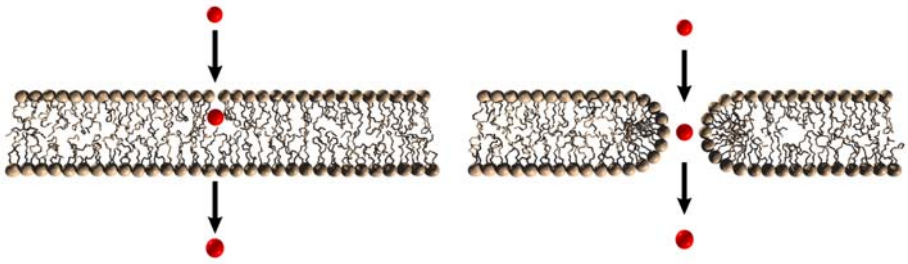

FIG. 9: Models for permeation. *Left:* The solubility-diffusion mechanism. Particles enter the hydrophobic core through some small defect and then diffuse across the bilayer. *Right:* The pore mechanism. Particles traverse the bilayer through transient hydrophilic pores caused by thermal fluctuations.

ism may be more favourable and could give rise to the transient and stepwise conductance changes.

Whatever the specific case may be, these thermodynamic interpretations of ion channel opening and closing due to lipid bilayer fluctuations are free of adjustable parameters, and make several testable predictions.

3.4.1 Model of passive ion transport

The following is loosely based on the derivation found in Cruzeiro-Hansson and Mouritsen (1988).

Let us consider a vesicle of volume $V(T)$ with an internal ion concentration, $c(t) = N(t)/V(T)$. For such as system the number of ions leaving the vesicle, $dN(t)$, at time t will be given by

$$dN(t) \propto c(t)v(T)A(T)P(T)dt, \tag{14}$$

where $v(T)$ is the velocity of the colliding ion, $A(T)$ is the internal area of the vesicle, and $P(T)$ is the probability of the ion crossing the membrane once it hits it.

From the kinetic theory of gases we know that the velocity of the ions follows a Maxwell-Boltzmann distribution, with $\langle v(T)\rangle \propto \sqrt{RT/\mathcal{M}}$, where $\mathcal{M}$ is the molar mass of the ion. Inserting this expression into Eq. (14), we have that

$$dN(t) \propto \mathcal{M}^{-1/2}A(T)^{-1/2}T^{1/2}P(T)N(t)dt. \tag{15}$$

In the line defect model (Papahadjopoulos et al. (1973), Cruzeiro-Hansson and Mouritsen (1988)) it is assumed that the probability, $P(T)$, of an ion crossing should be closely related to the boundaries between the fluid and gel domains. In this model $P(T)$ can be written as a sum of three terms, namely

$$P(T) = a_i(T)p_i + a_g(T)p_g + a_f(T)p_f, \tag{16}$$

where a_i, a_g and a_f are the fractions of the membrane area occupied by the interfaces, and by the gel and fluid lipids not associated with an interface. The corresponding regional probabilities of permeation are p_i, p_g and p_f respectively.

As previously mentioned, the line defect model assumes that the interfacial area is associated with a very high relative regional permeability, $p_i \gg p_g, p_f$.

The idea behind this is that there should be a high defect density in the interfacial region which could cause leakiness due to imperfect molecular packing.

In the pore model the probability is phenomenologically related to the isothermal area compressibility by (Nagle and Scott(1978))

$$P(T) = P_0 + P_2\kappa_T^A = P_0 + P_2'\Delta c_p, \tag{17}$$

where P_0 is the crossing probability for the homogeneous states, and is assumed to be a monotonously increasing function of the fluid fraction (due to the increase in the average lipid spacing). The second equality sign stems from the observation that the lateral compressibility is a linear function of the excess heat capacity (Ebel et al. (2001), Heimburg (2007)). Both P_0, P_2 and P_2' may be temperature dependent, though it is assumed to be relatively weak.

By integrating Eq. (15) one arrives at a simple expression for the fraction, $f(t,T)$, of ions still inside the vesicle

$$f(t,T) = \frac{N(t)}{N(t=0)} = e^{-k_p t} \quad \text{with} \quad k_p \propto \mathcal{M}^{-1/2} A(T)^{-1/2} T^{1/2} P(T), \tag{18}$$

where k_p is the characteristic permeation rate of the system. For a constant $P(T)$ the temperature dependence of k_p would be rather weak, as it would only change by a factor of ≈ 0.9 when going from 25°C to 45°C for a DPPC membrane.

4 Fluorescence Correlation Spectroscopy

Fluorescence Correlation Spectroscopy (FCS) was first introduced by Magde et al. (1972) to measure the chemical rate constants and diffusion coefficients of a chemically reactive system at equilibrium. This was done by measuring the temporal correlations of the fluctuations in the fluorescence intensity, arising from the thermodynamic concentration fluctuations.

Since then the experimental method has been improved upon and has successfully been used to make concentration and aggregation measurements and study confined, anomalous, and rotational diffusion, active transport processes, bacterial motility, and even conformational changes in proteins (Schwille and Haustein (2002)).

This section will introduce the basic theory behind FCS which will be needed for the data analysis.

4.1 Basic correlation function

The correlation function is a measure of the self similarity of a signal, $F(t)$. It is normally defined as

$$G(\tau) \equiv \frac{\langle F(t+\tau) \cdot F(t) \rangle}{\langle F(t) \rangle^2} \tag{19}$$

or alternatively, as the correlation of the fluctuations in the signal,

$$G(\tau) \equiv \frac{\langle \delta F(t+\tau) \cdot \delta F(t) \rangle}{\langle F(t) \rangle^2}, \tag{20}$$

which will only differ from Eq. (19) by an additive constant (namely -1).

In FCS one measures the fluorescence of the sample (hence the name), which for a dilute system can be expressed as

$$F(t) = \kappa \varepsilon Q \int_{all\ space} \Omega(\mathbf{r}) \cdot c(\mathbf{r}, t) d\mathbf{r}, \tag{21}$$

where κ is the efficiency of the fluorescence detector (including the detector quantum efficiency, its sensitivity to the particular wavelength range, and losses in the optical system), ε is the molar extinction coefficient of the fluorophore at the wavelength of the exciting laser radiation, Q is the fluorescence quantum yield of the fluorophore, $\Omega(\mathbf{r})$ is the fluorescence detection efficiency profile, and $c(\mathbf{r})$ is the concentration of fluorescent particles.

By writing the concentration as a mean plus a deviation, $c(\mathbf{r}) = \langle c \rangle + \delta c(\mathbf{r}, t)$, Eq. (21) becomes

$$F(t) = \langle F \rangle + \kappa \varepsilon Q \int_{all\ space} \Omega(\mathbf{r}) \cdot \delta c(\mathbf{r}, t) d\mathbf{r} \quad \Rightarrow \tag{22}$$

$$G(\tau) = \frac{\iint \Omega(\mathbf{r}) \Omega(\mathbf{r}') \cdot \langle \delta c(\mathbf{r}, t+\tau) \cdot \delta c(\mathbf{r}', t) \rangle d\mathbf{r} d\mathbf{r}'}{\langle c \rangle^2 (\int \Omega(\mathbf{r}) d\mathbf{r})^2}. \tag{23}$$

Assuming free diffusion in three dimensions and a Gaussian detection efficiency profile, one can with a bit of effort show that (see e.g. Widengren (1996) or

Petrov (2005)) for a system with only one fluorescent species, the correlation function is given by

$$G(\tau) = \frac{1}{\langle N \rangle} \left[1 + \frac{\tau}{\tau_D}\right]^{-1} \left[1 + \frac{\tau}{\omega^2 \tau_D}\right]^{-1/2}, \tag{24}$$

where $\langle N \rangle$ is the mean number of fluorophores in the observation volume, τ_D is the characteristic diffusion time, and $\omega \equiv \frac{z_0}{r_0}$ is the ratio of the longitudinal and radial dimensions of the fluorescence detection efficiency profile.

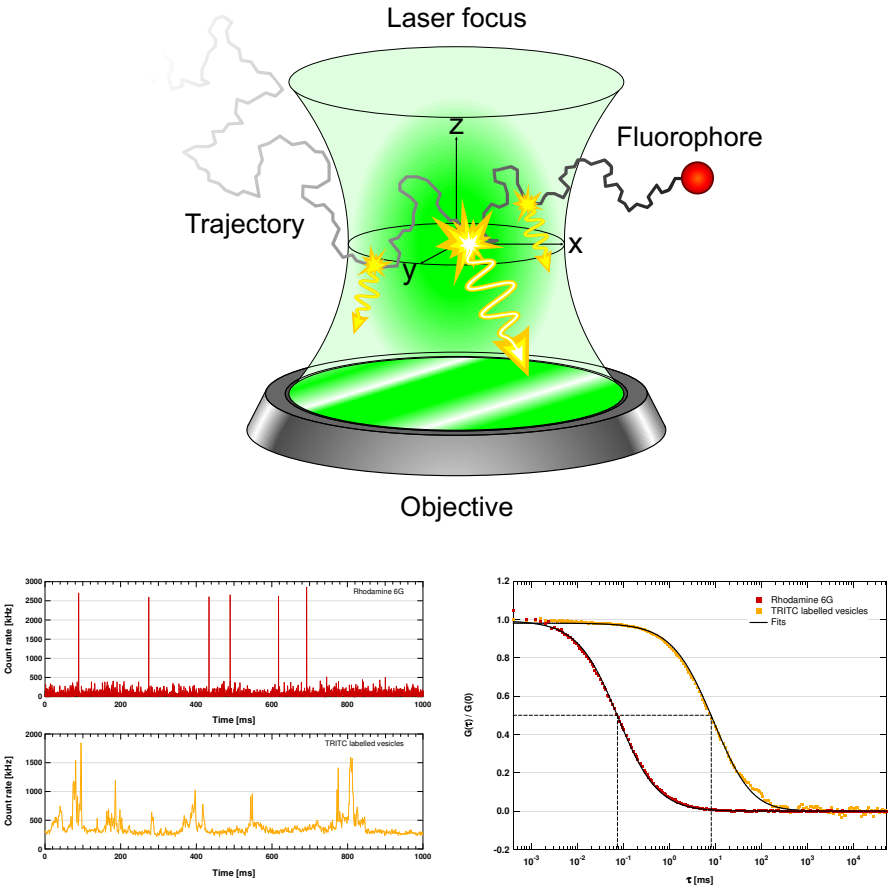

FIG. 10: *Top:* Schematic illustration of a fluorophore diffusing through the confocal volume. As the particle gets closer to centre of the focus the fluorescence intensity increases, resulting in a peak in the intensity trace. *Bottom left:* Fluorescence intensity traces for two different samples recorded with a multichannel counter and then integrated with different bin widths. *Bottom right:* The resulting auto correlation curves. As can be seen from the figure, τ_D is the time value at half height. The black, solid lines are fits by Eq. (24).

4.2 Multiple species

The system to be studied will be composed of several fluorescent species with various and changing brightnesses, so Eq. (24) will need to be expanded. As this kind of FCS study has not been published at the time of this writing, a substantial part of the theoretical work was to derive the relations necessary for the description of such a system.

For a system containing several types of fluorophores, each with their own characteristic diffusion times and brightnesses, the fluorescence signal will then be given by

$$F(t) = \sum_i F_i(t) \tag{25}$$

$$= \sum_i \kappa_i \varepsilon_i Q_i \int_{all\ space} \Omega(\mathbf{r}) \cdot c_i(\mathbf{r},t) d\mathbf{r}. \tag{26}$$

Again, we can define $c_i(\mathbf{r}) = \langle c_i \rangle + \delta c_i(\mathbf{r},t)$, together with a "brightness", $B_i \equiv \kappa_i \varepsilon_i Q_i$, and we thus have that

$$\delta F(t) = \sum_i B_i \int \Omega(\mathbf{r}) \cdot \delta c_i(\mathbf{r},t) d\mathbf{r} \tag{27}$$

$$\Rightarrow G(\tau) = \frac{\sum_{i,j} \langle \delta F_i(t+\tau) \cdot \delta F_j(t) \rangle}{\langle \sum_k F_k(t) \rangle^2} \tag{28}$$

$$= \frac{\sum_{i,j} \iint \Omega(\mathbf{r}) \Omega(\mathbf{r}') B_i B_j \cdot \langle \delta c_i(\mathbf{r},t+\tau) \cdot \delta c_j(\mathbf{r}',t) \rangle d\mathbf{r} d\mathbf{r}'}{(\sum_k B_k \langle c_k \rangle)^2 (\int \Omega(\mathbf{r}) d\mathbf{r})^2}. \tag{29}$$

If we assume that there is no correlation between different species, we will have that

$$\langle \delta c_i(\mathbf{r},t+\tau) \cdot \delta c_j(\mathbf{r}',t) \rangle = \delta_{ij} \langle \delta c_i(\mathbf{r},t+\tau) \cdot \delta c_i(\mathbf{r}',t) \rangle, \tag{30}$$

which means that our correlation function simplifies to

$$G(\tau) = \frac{\sum_i B_i^2 \iint \Omega(\mathbf{r}) \Omega(\mathbf{r}') \cdot \langle \delta c_i(\mathbf{r},t+\tau) \cdot \delta c_i(\mathbf{r}',t) \rangle d\mathbf{r} d\mathbf{r}'}{(\sum_j B_j \langle c_j \rangle)^2 (\int \Omega(\mathbf{r}) d\mathbf{r})^2}. \tag{31}$$

Recalling the solution for a single species, Eq. (24), we can define a function

$$G_i(\tau) \equiv \frac{\iint \Omega(\mathbf{r}) \Omega(\mathbf{r}') \cdot \langle \delta c_i(\mathbf{r},t+\tau) \cdot \delta c_i(\mathbf{r}',t) \rangle d\mathbf{r} d\mathbf{r}'}{\langle c_i \rangle^2 (\int \Omega(\mathbf{r}) d\mathbf{r})^2} \tag{32}$$

$$= \frac{1}{\langle N_i \rangle} \left[1 + \frac{\tau}{\tau_{Di}} \right]^{-1} \left[1 + \frac{\tau}{\omega^2 \tau_{Di}} \right]^{-1/2}. \tag{33}$$

Using this definition, our final equation becomes

$$G(\tau) = \frac{\sum_i B_i^2 \langle c_i \rangle^2 G_i(\tau)}{(\sum_j B_j \langle c_j \rangle)^2} \tag{34}$$

$$= \frac{\sum_i B_i^2 \langle N_i \rangle}{(\sum_j B_j \langle N_j \rangle)^2} \left[1 + \frac{\tau}{\tau_{Di}} \right]^{-1} \left[1 + \frac{\tau}{\omega^2 \tau_{Di}} \right]^{-1/2}. \tag{35}$$

Note how the relative amplitude of a given species is proportional to its brightness squared, B_i^2. This means that bright fluorophores will tend to dominate the measured correlation curve, which can make it difficult to observe dim fluorophores, even if their relative concentration is high.

4.3 Extruded vesicles

When extruding vesicles in a solution containing free dye, the number of fluorophores trapped inside a given vesicle will follow a Poisson distribution.

So let us consider a system consisting of equal-sized vesicles (thus $\tau_{Di} = \tau_{Dj} \equiv \tau_D$), but with different brightnesses, as they contain different amounts of fluorophore.

If we first consider the denominator of Eq. (35), we have that

$$\sum_{i=0}^{\infty} B_i \langle N_i \rangle = \sum_{i=0}^{\infty} B_i p(B_i) \langle N_v \rangle, \tag{36}$$

where $\langle N_v \rangle$ is the mean number of vesicles (of any brightness) in the observation volume, and $p(B_i)$ is the probability of finding a vesicle with brightness B_i.

If we let i be the number of fluorophores contained in a single vesicle, and assume that this will follow a Poisson distribution[3], we have that

$$p(B_i) = \frac{e^{-\widetilde{B}} \widetilde{B}^i}{i!} \qquad \text{and} \qquad B_i = iB_1 \tag{37}$$

where we have introduced the brightness of a single fluorophore, B_1, and the average number of fluorophores per vesicle, $\widetilde{B} \equiv \frac{\langle B \rangle}{B_1}$. Also, it has been assumed that there is no self-quenching.

Now the sum trivially yields

$$\begin{aligned} \sum_{i=0}^{\infty} B_i \langle N_i \rangle &= \langle N_v \rangle \sum_{i=0}^{\infty} B_i p(B_i) & (38) \\ &= \langle N_v \rangle \langle B \rangle, & (39) \end{aligned}$$

which is the same as for a system with a well-defined vesicle brightness.

The nominator can easily be evaluated as follows

$$\begin{aligned} \sum_{i=0}^{\infty} B_i^2 \langle N_i \rangle &= \langle N_v \rangle B_1^2 \sum_{i=0}^{\infty} i^2 \frac{e^{-\widetilde{B}} \widetilde{B}^i}{i!} & (40) \\ &= \langle N_v \rangle B_1^2 \widetilde{B} \sum_{i=1}^{\infty} i \frac{e^{-\widetilde{B}} \widetilde{B}^{i-1}}{(i-1)!} & (41) \\ &= \langle N_v \rangle B_1^2 \widetilde{B} \sum_{i=0}^{\infty} (i+1) \frac{e^{-\widetilde{B}} \widetilde{B}^i}{i!} & (42) \\ &= \langle N_v \rangle B_1^2 \widetilde{B} (\widetilde{B} + 1) & (43) \\ &= \langle N_v \rangle \langle B \rangle^2 \left[1 + \frac{B_1}{\langle B \rangle} \right] & (44) \end{aligned}$$

Thus the correlation function for a system consisting of equal-sized vesicles with a Poisson distribution of brightnesses is

$$G(\tau) = \frac{1 + B_1/\langle B \rangle}{\langle N_v \rangle} \left[1 + \frac{\tau}{\tau_{D,v}} \right]^{-1} \left[1 + \frac{\tau}{\omega^2 \tau_{D,v}} \right]^{-1/2}. \tag{45}$$

Note the factor $1 + B_1/\langle B \rangle$ compared to Eq. (24).

[3] For non-interacting particles (an ideal gas) the number of particles in a given volume element will strictly follow a Poisson distribution.

4.4 Free rhodamine and Poisson distributed vesicles

The system to be studied consists of free rhodamine 6G chloride (R6G) molecules, as well as large unilamellar vesicles (LUV) with a fairly well-defined size (approximately 100nm in diameter). As these vesicles will have a distribution of R6G molecules inside, the correlation function for the system becomes

$$\begin{aligned} G(\tau) = & \frac{B_1^2\langle N_{R6G}\rangle}{(B_1\langle N_{R6G}\rangle + \langle B\rangle\langle N_v\rangle)^2}\left[1+\frac{\tau}{\tau_{D,R6G}}\right]^{-1}\left[1+\frac{\tau}{\omega^2\tau_{D,R6G}}\right]^{-1/2} \\ & + \frac{\langle B\rangle^2\langle N_v\rangle(1+B_1/\langle B\rangle)}{(B_1\langle N_{R6G}\rangle + \langle B\rangle\langle N_v\rangle)^2}\left[1+\frac{\tau}{\tau_{D,v}}\right]^{-1}\left[1+\frac{\tau}{\omega^2\tau_{D,v}}\right]^{-1/2} \qquad (46) \\ = & \frac{\langle N_{R6G}\rangle}{(\langle N_{R6G}\rangle + \widetilde{B}\langle N_v\rangle)^2}\left[1+\frac{\tau}{\tau_{D,R6G}}\right]^{-1}\left[1+\frac{\tau}{\omega^2\tau_{D,R6G}}\right]^{-1/2} \\ & + \frac{\widetilde{B}^2\langle N_v\rangle(1+\widetilde{B}^{-1})}{(\langle N_{R6G}\rangle + \widetilde{B}\langle N_v\rangle)^2}\left[1+\frac{\tau}{\tau_{D,v}}\right]^{-1}\left[1+\frac{\tau}{\omega^2\tau_{D,v}}\right]^{-1/2}. \qquad (47) \end{aligned}$$

The fraction $\widetilde{B} \equiv \frac{\langle B\rangle}{B_1}$ can be determined by making two separate measurements. From Eq. (21) it follows that

$$\begin{aligned} \langle F_i(t)\rangle &= \langle B_i\rangle\langle c_i\rangle \int_{all\ space} \Omega(\mathbf{r})d\mathbf{r} \propto \langle B_i\rangle\langle N_i\rangle \quad \Rightarrow & (48) \\ \widetilde{B} &\equiv \frac{\langle B\rangle}{B_1} = \frac{\langle F_v\rangle}{\langle F_{R6G}\rangle}\frac{\langle N_{R6G}\rangle}{\langle N_v\rangle} & (49) \\ &= \frac{\langle F_v\rangle}{\langle F_{R6G}\rangle}\frac{G_v(\tau=0)}{G_{R6G}(\tau=0)}\frac{1}{1+\widetilde{B}^{-1}} \quad \Leftrightarrow & (50) \\ \widetilde{B} &= \frac{\langle F_v\rangle}{\langle F_{R6G}\rangle}\frac{G_v(\tau=0)}{G_{R6G}(\tau=0)} - 1, & (51) \end{aligned}$$

where $\langle F_v\rangle$ is the mean fluorescence of a solution consisting purely of vesicles (with R6G inside), $\langle F_{R6G}\rangle$ is the mean fluorescence of a solution which only contains free R6G, and G_v and G_{R6G} are their respective correlation functions.

4.5 Leaking vesicles

If we consider a system which, at first, consists purely of vesicles with a Poisson distribution of rhodamine inside, and no free rhodamine, the correlation function will change with time as the rhodamine leaks.

If we assume that the probability of a given rhodamine molecule leaking out is independent of the concentration inside the vesicle, then the distribution of the number of rhodamine molecules inside the vesicles will start to deviate from the Poissonian one.

For the sake of convenience, let us assume that the mean number of molecules trapped is large (i.e. $\widetilde{B} \gg 1$), so the Poisson distribution can be approximated by a normal distribution

$$p(B_i) = \frac{e^{-\widetilde{B}}\widetilde{B}^i}{i!} \simeq \frac{1}{\sqrt{2\pi\sigma^2}}\exp\Big(\frac{-(i-\widetilde{B})^2}{2\sigma^2}\Big). \qquad (52)$$

If we let $f(t)$ denote the fraction of the rhodamine molecules which is still trapped inside vesicles[4], and $B_i(t)$ the brightness of a vesicle which *initially* contained i rhodamine molecules, then we have that

$$\widetilde{B}(t) = f(t)\widetilde{B}_0 \qquad \text{and} \qquad \sigma^2 = f^2(t)\widetilde{B}_0 \qquad \text{and} \qquad f(t=0) = 1 \tag{53}$$

where $\widetilde{B}_0$ denotes the initial mean number of rhodamine molecules per vesicle.

Using these definitions and approximating the summations in Eq. (35) by integrals, it follows that

$$\begin{aligned}
\sum_{i=0}^{\infty} B_i^2\langle N_i\rangle &= \langle N_v\rangle B_1^2 \sum_{i=0}^{\infty} i^2 \cdot p(B_i,t) && (54)\\
&\simeq \frac{\langle N_v\rangle B_1^2}{f(t)\sqrt{2\pi\widetilde{B}_0}} \int_0^{\infty} x^2 \exp\left(\frac{-(x-f(t)\widetilde{B}_0)^2}{2f^2(t)\widetilde{B}_0}\right) dx && (55)\\
&= \frac{\langle N_v\rangle B_1^2}{f(t)\sqrt{2\pi\widetilde{B}_0}} \int_{-f(t)\widetilde{B}_0}^{\infty} (f(t)\widetilde{B}_0 + x)^2 \exp\left(\frac{-x^2}{2f^2(t)\widetilde{B}_0}\right) dx && (56)\\
&\simeq \frac{\langle N_v\rangle B_1^2}{f(t)\sqrt{2\pi\widetilde{B}_0}} \int_{-\infty}^{\infty} (f(t)\widetilde{B}_0 + x)^2 \exp\left(\frac{-x^2}{2f^2(t)\widetilde{B}_0}\right) dx && (57)\\
&= f^2(t)\langle N_v\rangle B_1^2\widetilde{B}_0^2 + \frac{\langle N_v\rangle B_1^2}{f(t)\sqrt{2\pi\widetilde{B}_0}} \int_{-\infty}^{\infty} x^2 \exp\left(\frac{-x^2}{2f^2(t)\widetilde{B}_0}\right) dx && (58)\\
&= f^2(t)\langle N_v\rangle B_1^2\widetilde{B}_0^2 + \frac{\langle N_v\rangle B_1^2}{f(t)\sqrt{2\pi\widetilde{B}_0}} \frac{\Gamma(3/2)}{\left(2f^2(t)\widetilde{B}_0\right)^{-3/2}} && (59)\\
&= f^2(t)\langle N_v\rangle B_1^2\widetilde{B}_0^2 + f^2(t)\langle N_v\rangle B_1^2\widetilde{B}_0 && (60)\\
&= f^2(t)\langle N_v\rangle B_1^2\widetilde{B}_0^2\left[1 + \frac{1}{\widetilde{B}_0}\right] && (61)
\end{aligned}$$

The sum in the denominator can be calculated in a similar fashion, yielding

$$\begin{aligned}
\sum_{i=0}^{\infty} B_i\langle N_i\rangle &= \langle N_v\rangle B_1 \sum_{i=0}^{\infty} i \cdot p(B_i,t) && (62)\\
&\simeq \frac{\langle N_v\rangle B_1}{f(t)\sqrt{2\pi\widetilde{B}_0}} \int_0^{\infty} x \cdot \exp\left(\frac{-(x-f(t)\widetilde{B}_0)^2}{2f^2(t)\widetilde{B}_0}\right) dx && (63)\\
&\simeq f(t)\langle N_v\rangle B_1\widetilde{B}_0, && (64)
\end{aligned}$$

The average amount of free rhodamine, $\langle N_{R6G}(t)\rangle$, in the observation volume at a given instant is

$$\langle N_{R6G}(t)\rangle = (1 - f(t))\widetilde{B}_0\langle N_v\rangle, \tag{65}$$

and hence the denominator sum becomes

$$B_1\langle N_{R6G}\rangle + \sum_{i=0}^{\infty} B_i\langle N_i\rangle = B_1(1-f(t))\widetilde{B}_0\langle N_v\rangle + \sum_{i=0}^{\infty} B_i\langle N_i\rangle \tag{66}$$

[4] $f(t)$ will thus also be related to the permeation rate of the lipid membranes via Eq. (18).

$$= \quad B_1 \widetilde{B}_0 \langle N_v \rangle, \tag{67}$$

which is, of course, independent of time.

The correlation function for this system will then be given by

$$G(\tau, t) = \quad \frac{1 - f(t)}{\widetilde{B}_0 \langle N_v \rangle} \left[1 + \frac{\tau}{\tau_{D,R6G}} \right]^{-1} \left[1 + \frac{\tau}{\omega^2 \tau_{D,R6G}} \right]^{-1/2} \tag{68}$$

$$+ \quad \frac{f^2(t)}{\langle N_v \rangle} \left[1 + \frac{1}{\widetilde{B}_0} \right] \left[1 + \frac{\tau}{\tau_{D,v}} \right]^{-1} \left[1 + \frac{\tau}{\omega^2 \tau_{D,v}} \right]^{-1/2}. \tag{69}$$

It's worth noting that most of the parameters are independent of time, and can be therefore – in principle – be determined beforehand or from the initial measurements on the system.

For instance we have that

$$\frac{1}{\langle N_v \rangle} \left[1 + \frac{1}{\widetilde{B}_0} \right] = G(\tau = 0, t = 0), \tag{70}$$

while $\widetilde{B}$, $\langle N_v \rangle$, ω, and the τ_D's can be determined as mentioned earlier.

Thus once we have a series of measurements, the only free parameter will be $f(t)$, which is then easily determined by fitting.

4.6 Tetramethylrhodamine dextran

The characteristic permeation rate will depend strongly on the size of the fluorophore, since a larger fluorophore would diffuse more slowly. Furthermore, the fluorophores will only be able to get through the larger pores (of which there tends to be less due to the large energy cost), reducing the rate even further.

To study this we chose to use labelled dextran, which consists of about 16 glucose residues plus approximately one tetramethylrhodamine group on average. However, the actual number of labels per dextran molecule would – to good approximation – follow a Poisson distribution. As the number of dextran molecules per vesicle also follows a Poisson distribution, the actual number of *labels* per vesicle would be a Poisson distribution of Poisson distributions. This will, of course, influence the correlation function in a somewhat non-trivial way.

First, let us consider a vesicle with a known number of dextran molecules inside. For such vesicle the number of labels (i.e. the "brightness") will also follow a Poisson distribution, as a sum of Poisson distributed random variables will also follow a Poisson distribution, provided that they are independent of each other.

Thus, the probability of finding a vesicle with i labels inside, provided it contains j dextran molecules is:

$$p_j(i) = \frac{e^{-j \cdot L} \cdot (j \cdot L)^i}{i!}, \tag{71}$$

where L is the average number of labels per dextran molecule.

Consequently, the probability of finding a vesicle with i labels, given a Poisson distribution of dextran molecules, is simply the probability of finding a

vesicle with j dextrans times the probability given in Eq. (71), summed over all j's.

$$p_B(i) = \sum_{j=0}^{\infty} \frac{e^{-D} \cdot (D)^j}{j!} \cdot \frac{e^{-j \cdot L} \cdot (j \cdot L)^i}{i!}, \tag{72}$$

where D is the average number of dextran molecules per vesicle.

Using this probability distribution, we can calculate the effect on the correlation function.

First off, we have the average an average brightness of a vesicle (i.e. the average number of labels per vesicle) given by

$$\begin{aligned}
\sum_{i=0}^{\infty} B_i \langle N_i \rangle &= \langle N_v \rangle B_1 \sum_{i=0}^{\infty} i \cdot p_B(i) && (73)\\
&= \langle N_v \rangle B_1 \sum_{j=0}^{\infty} \frac{e^{-D} \cdot D^j}{j!} \sum_{i=0}^{\infty} i \cdot \frac{e^{-j \cdot L} \cdot (jL)^i}{i!} && (74)\\
&= \langle N_v \rangle B_1 \sum_{j=0}^{\infty} \frac{e^{-D} \cdot D^j}{j!} \cdot (jL) && (75)\\
&= \langle N_v \rangle LD \cdot B_1, && (76)
\end{aligned}$$

i.e. the product of the averages, which will probably not surprise anyone.

Less trivial is the average of the brightness squared:

$$\begin{aligned}
\sum_{i=0}^{\infty} B_i^2 \langle N_i \rangle &= \langle N_v \rangle B_1^2 \sum_{i=0}^{\infty} i^2 \cdot p_B(i) && (77)\\
&= \langle N_v \rangle B_1^2 \sum_{j=0}^{\infty} \frac{e^{-D} \cdot D^j}{j!} \sum_{i=0}^{\infty} i^2 \cdot \frac{e^{-j \cdot L} \cdot (jL)^i}{i!} && (78)\\
&= \langle N_v \rangle B_1^2 \sum_{j=0}^{\infty} \frac{e^{-D} \cdot D^j}{j!} \cdot (jL) \cdot (jL+1) && (79)\\
&= \langle N_v \rangle B_1^2 \sum_{j=0}^{\infty} \frac{e^{-D} \cdot D^j}{j!} \cdot (jL) \cdot (jL+1) && (80)\\
&= \langle N_v \rangle B_1^2 \cdot \left(L^2 \sum_{j=0}^{\infty} j^2 \frac{e^{-D} \cdot D^j}{j!} + L \sum_{j=0}^{\infty} j \frac{e^{-D} \cdot (D)^j}{j!} \right) && (81)\\
&= \langle N_v \rangle B_1^2 \cdot (L^2(D^2 + D) + LD) && (82)\\
&= \langle N_v \rangle (LD + L + 1) LD \cdot B_1^2 && (83)
\end{aligned}$$

Thus, the correlation function for this system is:

$$\begin{aligned}
G(\tau) = &\quad \frac{\langle N_{TMRd} \rangle L(L+1)}{(L\langle N_{TMRd} \rangle + LD\langle N_v \rangle)^2} \left[1 + \frac{\tau}{\tau_{D,TMRd}} \right]^{-1} \left[1 + \frac{\tau}{\omega^2 \tau_{D,TMRd}} \right]^{-1/2} \\
+ &\quad \frac{\langle N_v \rangle LD(LD + L + 1)}{(L\langle N_{TMRd} \rangle + LD\langle N_v \rangle)^2} \left[1 + \frac{\tau}{\tau_{D,v}} \right]^{-1} \left[1 + \frac{\tau}{\omega^2 \tau_{D,v}} \right]^{-1/2} \qquad (84)
\end{aligned}$$

As can be seen from Eq. (84), the lower the degree of labelling, L, and the fewer dextrans there are per vesicle, D, the more important it is to take it into account.

5 Computer Simulations

It could be argued that modern physics research can be divided into three areas, namely theoretical, experimental, and computational. The use of computers to mimic physical systems as accurately as possible provides a useful and unique tool to bridge the gap between theory and experiment, as they can provide well-behaved experimental systems.

The range of applicability and accuracy of computer models is only limited by the computational processing power available – a limitation which gets less severe every year, thanks to the continual[5] development of more advanced computer technology.

5.1 The different approaches

There are very few statistical mechanical models that have been solved analytically. Even the famous spin-$\frac{1}{2}$ Ising model for transitions in ferromagnets has only been solved for one and two dimensions, where the latter has only been performed for zero field, in a reputedly mathematical tour de force[6].

However, for the study of lipid melting and the lateral organisation of membranes, one has several options.

5.1.1 Mean-field theory

In the bygone age of slow computers, it was necessary to resort to approximation methods, such as the widely used mean-field theories.

The main idea behind mean-field theory is to focus on one particle and assume that the most important contribution to the interactions with the environment is determined by the mean field of all the other particles. In effect, this will reduce the multi-body problem to a one-body problem. For instance, if one third of the particles are estimated to be in the +1 state (fluid state in the case of lipids) and two thirds in the -1 state (gel state), one can calculate an effective nearest neighbour environment. This will, in turn, give a new and better estimate for how likely it is for a given particle to be in either state, and one can then arrive at a solution by iteration.

One rather severe limitation of mean-field theory is that it does not take fluctuations in the environment into account. As mentioned, each particle is assumed to only interact with the mean state of all the other particles in the system (hence the name). Therefore, mean-field theory does, by its very nature, not provide any information about the microscopic organisation of the system.

In general, this means that mean-field theory is only valid when fluctuations are unimportant, so while mean-field theory has been applied with a fair amount of success in the past[7], these kinds of problems are better handled by using computer simulations nowadays, and their properties are now known in great detail from numerical work.

[5] For a long time the development increased exponentially, – an empirical observation called Moore's Law – though it seems to have slowed down a bit in the recent years.

[6] This feat was performed by the Nobel laureate Lars Onsager in 1944 (Onsager (1944)).

[7] In general they improve as the number of neighbours or the range of interactions increases. They usually give good estimates for the phase diagrams of three-dimensional systems, and it can be shown that the values predicted for critical exponents are correct for systems with more than four dimensions.

5.1.2 Molecular dynamics

Molecular Dynamics simulation is a method that can be used to calculate the structural and dynamical properties of a system. In these kinds of simulations the atoms or particles of the system are treated classically.

Given a set of initial coordinates and velocities for the particles of the system, the time evolution of the system through state space (known as a trajectory) can then be computed by numerically integrating Newton's equation of motion, based on the intermolecular interactions of all the particles.

The accuracy of any Molecular Dynamics simulation will strongly depend on the accuracy of description the potential energy of the system. The interactions are normally described by semi-empirical functions which have been parameterised to represent the interactions between the particles of a real system. In most semi-empirical or effective force fields used to describe molecular systems the potential energy is given by a set of non-bonded (electrostatic and van der Waals forces) and bonded (stretching, torsion and bending) interactions.

From this trajectory many dynamic and thermodynamic properties of the system can be gauged, assuming that the calculated trajectory is representative of the phase space of the system.

While Molecular Dynamics simulations do lead to the most accurate information on membrane structure, they have one rather severe disadvantage: they are painfully slow. At the time of this writing, simulating the time evolution of a patch of membrane containing a few hundred lipids over a couple of hundred nanoseconds will take several months on a high-performance computer cluster.

As many biological processes lie in the microsecond to millisecond regime, such processes are quite beyond what is feasible in the near future.

5.1.3 Coarse grain models

As mentioned above, making Molecular Dynamics simulations of large scale cooperative phenomena is still not realistically possible. Therefore one has to look for other methods. On the opposite end of the detail scale are the so-called coarse grain models, which makes use of reduced representations, i.e. they use "pseudo-atoms" to represent groups of atoms or molecules instead of explicitly representing every atom. Also, an oft-used simplification is to place the molecules on a lattice. Furthermore, for such lattice models, the molecules are usually constrained to interact only with their nearest neighbours, which make the programs significantly less computationally demanding.

The solutions of such models can then be numerically calculated with the help of the powerful Monte Carlo method, which makes it possible to make simulations of systems with thousands of particles on a normal desktop computer. Despite its simplicity, this method can yield solutions for fairly complex problems, and is a powerful tool for describing large scale structures and cooperativity phenomena. However, it should be noted that this method normally only gives information about the equilibrium state and time scales does not play a role. One can to a certain extent circumvent this, though, by carefully choosing how one performs the Monte Carlo steps (Hac et al. (2005)).

Due to the nature of the problem at hand and the limited time frame, a Monte Carlo simulation using a coarse grained lattice model seems to be best suited to tackle the problem.

5.2 The Monte Carlo method

The Monte Carlo method is a particularly powerful and versatile approach which was introduced by Metropolis et al. (1953) at the dawn of the computer age. Monte Carlo simulations encompass a very broad variety of algorithms and variations, from what is generically known as statistical sampling to the more recent Quantum Monte Carlo. It is a universal algorithm that can be applied to a large range of systems, but it is especially useful when studying systems with a large number of coupled degrees of freedom (liquids, disordered materials, polymers, or even economics). In fact, its relative efficiency (when compared to other numerical methods) increases with the dimension of the problem. Monte Carlo simulations – like genetic algorithms and neural networks – are stochastic and they rely heavily on the use of random or pseudo-random numbers to mimic the fluctuations characteristic of finite temperatures.

In short, a Monte Carlo simulation can be thought of as a random walk through state space, where every possible state is accepted with a certain probability[8]. If properly set up, the Monte Carlo simulation will bring the system to its equilibrium state (or rather equilibrium distribution of states), which makes it possible to evaluate thermodynamic averages for the equilibrium state.

This method is fairly straightforward to implement and analyse, making it ideally suited as a first attempt at understanding the cooperative behaviour of a system.

5.2.1 Importance sampling

A common aim in statistical mechanics is to determine the average value of some thermodynamic observable, such as the enthalpy, area or magnetisation, which is a weighted sum over all possible states:

$$\langle X \rangle = \frac{\sum_i X_i W_i}{\sum_j W_j} = \frac{\sum_i X_i e^{-H_i/RT}}{\sum_j e^{-H_j/RT}} \tag{85}$$

For a two-state Ising model on a lattice with N sites, this sum will be over 2^N configurations. So even for a relatively small system this number will be so large that a direct evaluation will be impossible. For instance, if $N = 100$ one would have to sum over $2^{100} \approx 10^{30}$ configurations, which would not be possible to complete within one's lifetime[9].

So for anything but the most conservative system sizes, getting an exact answer by direct evaluation is simply impossible. However, there are two important considerations that make Monte Carlo simulations useful by ensuring that a good estimate can be calculated with high accuracy.

1. Most of the time $\langle X \rangle$ does not contain a lot of information about the substates and will only depend on the average of some quantity. If we have

[8] To be a bit more technical, this is more generally known as Markov chain Monte Carlo. The Markov chain Monte Carlo methods (including the simple random walk Monte Carlo methods), encompasses a class of algorithms for sampling from probability distributions based on constructing a Markov chain that has the desired distribution as its equilibrium distribution. In general, it is fairly simple to construct a Markov Chain with the desired properties. The difficulties consist of generating a procedure which will quickly converge to the equilibrium distribution within an acceptable error.

[9] A modern supercomputer can perform around 10^{15} floating point operations per second, meaning that it would take approximately forty million years to finish!

a representative set of states, S_i, we can get a very accurate estimate for $\langle X \rangle$. For the area $\langle A \rangle$ for example, a system of N lipids can only have $N+1$ different values. Therefore, a representative set for this system will be of order N.

2. Despite the fact that what we are summing is a product of two quantities X_i, W_i in many cases (in statistical physics at least) the weights, W_i, will be finite only in a small region. That is, even if the number of configurations outside this region is very large, if their weight is exponentially small the answer will depend almost exclusively on a tiny fraction of the entire parameter space.

So in other words, if one can find a representative set of configurations to sum over, and picking from these at random, it is possible to get a good estimate for $\langle X \rangle$. Even better, if one can select configurations such that the ones with larger weights are more likely to be chosen, then one can obtain an equally accurate answer by summing over even fewer terms.

5.3 A model for lipid membrane systems

Our model is based on the famous spin$\frac{1}{2}$ Ising model. This model was first proposed by Wilhelm Lenz in 1920 to study the phase transition of ferromagnets at the Curie temperature (Brush (1967)). It was later fully worked out by his pupil Ernst Ising for the one dimensional case (1925), while the two-dimensional case was worked out by Lars Onsager 19 years later (Onsager (1944)).

At its most basic, the Ising Hamiltonian is given by

$$\mathcal{H} = -\frac{\epsilon}{2} \sum_{\langle i,j \rangle} \sigma_i \sigma_j - h \sum_i \sigma_i, \tag{86}$$

where $\sigma_i = \pm 1$ are the two spin states allowed on each lattice site, ϵ is the nearest neighbour interaction parameter (also known as the coupling constant), and h is the magnetic field. Here $\langle i, j \rangle$ denotes that the sum is only over nearest neighbours. The first term in Eq. (86) is responsible for the cooperative behaviour and the possibility of a phase transition.

This simple model is of great importance and has wide applicability, as any two-state system can be mapped onto it with only slight modifications. Examples include β-brass, lattice gas, CuZn mixing, and of course lipid membrane melting.

Another important aspect of the Ising model is that any critical exponent derived for it are universal, i.e. they apply to any model that can be mapped onto the Ising model. Mean-field theory has been used to derive some of these critical exponents, but as previously mentioned, the microscopic details/structure is neglected, leading to slightly wrong numbers (Yeomans (1992)).

The two-state Ising model for the melting of lipid membranes was first proposed by Doniach (1978), and the fundamental assumptions are essentially the following: each lipid molecule can only be in one of two states, namely

- A gel state with low enthalpy H_g and low entropy S_g
- A fluid state with high enthalpy H_f and high entropy S_f

Though more complex lattice models such as the 10-state Pink model have been used in the literature (Pink et al. (1980), Mouritsen et al. (1983)), the added complexity of these models does not significantly alter the overall physical behaviour of the two-state model (Mouritsen et al. (1983)). The reason for this is that the melting transition is a cooperative phenomenon with a length scale much larger than a single lipid, making the modelling of molecular details superfluous. In addition, the two-state model has the advantage that it contains very few parameters, all of which can be determined by calorimetric experiments (Ivanova and Heimburg (2001)).

The interactions between molecules are normally governed by van der Waals and electrostatic forces as well as interchain steric repulsion. However, in our model each lipid will only interact with its nearest neighbours on the lattice. This is, of course, an approximation, as it neglects the lipids' interactions with next-nearest neighbours and the other membrane leaflet.

Lastly, all of the lipids are assumed to be hexagonally packed[10], which means that each lipid has $z = 6$ adjacent lipid neighbours (z is the so-called coordination number). The assumption of a hexagonal packing does not strictly hold in the fluid phase, and will consequently also influence the shape of the domains. Also, this will neglect the contributions to the entropy from the spatial disordering, but since the melting transition is dominated by the chain melting entropy, the effect of this will be minor (Doniach (1973)).

With these approximations it is only necessary to consider three kinds of interactions, namely

- The interaction between two gel lipids ϵ_{gg}
- The interaction between two fluid lipids ϵ_{ff}
- The interaction between a fluid lipid and a gel lipid ϵ_{fg}

If all of the lipids are in the gel state, the Gibbs free energy of the gel phase, G_g, will be given by

$$G_g = N\left[(H_{0,g} - TS_{0,g}) + \frac{z}{2}\epsilon_{gg}\right], \tag{87}$$

where N is the number of lipids, $H_{0,g}$ is the enthalpy per lipid, and $S_{0,g}$ is the entropy per lipid. Correspondingly for the fluid phase we have that

$$G_f = N\left[(H_{0,f} - TS_{0,f}) + \frac{z}{2}\epsilon_{ff}\right]. \tag{88}$$

In general there will be a distribution of fluid and gel lipids, where we have

- N_{fg} contacts between fluid and gel lipids
- $N_{gg} = (zN_g - N_{fg})/2$ contacts between two gel lipids
- $N_{ff} = (zN_f - N_{fg})/2$ contacts between two fluid lipids

[10]This is realised by placing the lipids on a triangular lattice with periodic boundaries, resulting in a topology akin to that of a torus.

where N_f is the number of fluid lipids and $N_g = N - N_f$ the number of gel lipids.

For such a configuration, the total Gibbs free energy will be

$$\begin{aligned} G = & \quad N_g(H_{0,g} - TS_{0,g}) + N_f(H_{0,f} - TS_{0,f}) \\ & + \quad N_{gg}\epsilon_{gg} + N_{fg}\epsilon_{fg} + N_{ff}\epsilon_{ff} \qquad (89) \\ = & \quad N_g(H_{0,g} - TS_{0,g}) + N_f(H_{0,f} - TS_{0,f}) \\ & + \quad \frac{ZN_g - N_{fg}}{2}\epsilon_{gg} + N_{fg}\epsilon_{fg} + \frac{ZN_f - N_{fg}}{2}\epsilon_{ff}. \qquad (90) \end{aligned}$$

So if we define $\Delta H \equiv (H_{0,f} + \frac{Z}{2}\epsilon_{ff}) - (H_{0,g} + \frac{Z}{2}\epsilon_{gg})$ and $\Delta S \equiv S_{0,f} - S_{0,g}$, Eq. (90) reduces to (Sugar et al. (1994))

$$\begin{aligned} G &= G_g + N_f(\Delta H - T\Delta S) + N_{fg}\left(\epsilon_{fg} - \frac{\epsilon_{gg} + \epsilon_{ff}}{2}\right) \qquad (91) \\ &\equiv G_g + N_f(\Delta H - T\Delta S) + N_{fg}\omega_{fg}. \qquad (92) \end{aligned}$$

In this model ω_{fg} is a cooperativity parameter, corresponding to the coupling constant in the spin$\frac{1}{2}$ Ising model. What's more, ω_{fg} is the only free parameter of the model, as both ΔH and ΔS can be obtained from calorimetric measurements.

This model is essentially a two-state Ising model on a triangular lattice with a temperature dependent field. So if we set $\sigma_i = -1$ for lipids in the gel state and $\sigma_i = +1$ for those in the fluid state, the "field" would be $h = (T\Delta S - \Delta H)/2$.

Note that at the transition point $h = 0$, and one can therefore apply some of the analytical results from two-dimensional spin$\frac{1}{2}$ Ising model results. For instance, for a triangular lattice the critical interaction strength is given by (Wannier (1945))

$$\omega = RT_m \frac{\ln 3}{2} = 1434.77 \text{ J/mol}, \qquad (93)$$

for $T_m = 314.15$K.

As mentioned, this model is based on a two-dimensional Ising model which is obviously not correct on molecular scales since it only contains two states of the lipid (compared to the $\sim 10^{14}$ states a DPPC molecule can assume) – which is, of course, a gross approximation. Furthermore, interactions with the other monolayer as well as fluctuations in the third dimension are also ignored. However, the two-dimensional Ising model has its strength in the description of macroscopic fluctuations (Mouritsen et al. (1983)), irrespective of molecular details, and is quite successful despite its apparent simplicity.

5.3.1 Adding complexity

The two-state model described in Sec. (5.3) is as simple as it gets, and has been studied in great detail by a number of people (Doniach (1978), Mouritsen et al. (1983), Mouritsen and Zuckermann (1985), Ivanova and Heimburg (2001), Ivanova et al. (2003), Hac (2003), Seeger (2006), Seeger et al. (2007)).

To simulate the influence of anaesthetics on the system, as well as having the possibility of having pores, Eq. (92) will need to be expanded somewhat.

It is straightforward to show that for a system with pores (p) and anaesthetics (a) the Gibbs free energy of a given sub-state (micro-configuration) is given by

$$\begin{aligned} G = & \quad G_g + N_f(\Delta H - T\Delta S) \\ & + \quad N_{fg}\omega_{fg} + N_{pf}\omega_{hf} + N_{pg}\omega_{pg} \\ & + \quad N_{ap}\omega_{ap} + N_{ag}\omega_{ag} + N_{af}\omega_{af} \end{aligned} \tag{94}$$

where the n_{ij} are the number of contacts between particle of type i and j, and the $\omega_{ij} \equiv \epsilon_{ij} - (\epsilon_{ii} + \epsilon_{jj})/2$ are the associated interaction parameters.

If any of the ω_{ij} are equal to zero, the particles of type i and j will mix ideally.

It should be noted that this model does not take the entropic contribution from pore shape and size fluctuations into account.

5.3.2 Determination of model parameters

As mentioned in Sec. (5.3) there are three parameters which need to be determined if one wants to describe the most basic one-component two-state lipid system, namely the melting enthalpy, ΔH, the melting entropy, ΔS, and the cooperativity parameter, ω_{fg}.

For the more advanced simulations, another five interaction parameters will be needed, namely ω_{af} (anaesthetic/fluid), ω_{ag} (anaesthetic/gel), ω_{ap} (anaesthetic/pore), ω_{pg} (pore/gel), and ω_{pf} (pore/fluid).

Fortunately, the first five parameters can be obtained from calorimetric experiments, while the remaining three will need to be guesstimated from permeation measurements.

Specifically, one can obtain the melting enthalpy and entropy of the lipids from the heat capacity profile of one-component lipid system: the enthalpy change of the transition is obtained by integrating over the heat capacity in the relevant temperature interval, i.e.

$$c_p = \frac{dH}{dT}_p \Rightarrow \Delta H = \int_T^{T+\Delta T} c_p dT. \tag{95}$$

The entropy change can then easily be determined via Eq. (6), as the transition midpoint, T_m, can be read off the heat capacity profile directly.

The cooperativity parameter, ω_{fg}, relates directly to the width of the transition peak, and can consequently be determined by fitting the simulated heat capacity profiles to the experimentally measured one.

The five remaining interaction parameters, ω_{ij}, can be obtained indirectly from various other experiments. The simulation is not particularly sensitive to the values of ω_{ag} and ω_{af}, so a common choice for them is to assume ideal mixing with the fluid phase, i.e. $\omega_{af} = 0$, and less favourably with the gel phase with $\omega_{ag} = \omega_{fg}$ (Ivanova and Heimburg (2001), Ivanova et al. (2003)).

Determining the remaining three parameters (ω_{ap}, ω_{pg} and ω_{pf}) can, in principle, be done by comparing the simulated permeability (basically the average number of pores) to measurements.

Even before doing this, it is possible to predict a number of relations, if we assume that hydrophobic matching is a major determinant of the nearest

neighbour interactions. Firstly, if the added anaesthetic is strongly hydrophobic, it seems reasonable to assume that $\omega_{ap} \gg \omega_{fg}$, as the cooperativity parameter, ω_{fg}, is largely determined by the hydrophobic mismatch between a fluid and gel state lipid.

Similarly, this should mean that $\omega_{ag} > \omega_{af}$ for two reasons: 1) the lipid in the gel state would have a larger part of the hydrophobic chains exposed to the water, and 2) the fluid phase is more loosely packed, meaning that defects and spaces between the lipids (i.e. pores) would be more likely to appear than in the tightly packed gel phase.

5.3.3 Evaluation by Monte Carlo simulations

Sec. (5.3) introduced a statistical mechanical model for the description of pore formation in a system with one species of lipids. As this model is obviously beyond what can be solved analytically, numerical evaluation by means of Monte Carlo simulations was used.

To do this one first has to define the various Monte Carlo steps. At it's most basic (i.e. a one-component system without anaesthetics and no pore formation), only one Monte Carlo step is needed, namely one that allows the lipids to change their state (a "melting step"). As we are using the two-state Ising model as a basis, each lipid is assumed to be in either an ordered (gel) or disordered (fluid) state.

For the more advanced models (multiple lipid species, anaesthetics, pore formation, etc.), it is also necessary to include the possibility for any two particles to swap positions (i.e. a "diffusion step"). In general, allowing a non-physical diffusion step where *any* two particles can be exchanged, and not just neighbouring particles, will tend to make the system equilibrate faster, and will not influence the equilibrium distribution of states.

Lastly, for the simulations to work, it is necessary to include a Monte Carlo step which allows for the creation/sealing of a pore. The details of this step will be described in Sec. (5.6.3).

Whether a given step is accepted or not, depends on difference in the free energy of the old and the new system configuration. However, any step should always have a finite likelihood to be accepted in order to ensure ergodicity – i.e. with the use of these three types of Monte Carlo steps, it must be possible to change the system's configuration to any state.

5.3.4 The transition probability

Having a statistical mechanical model is only half the work – one also has to obtain actual information from it. As very few models are tractable to analytical approaches or direct evaluation, one needs another way to handle this, as described in Sec. (5.2.1).

At the heart of the sampling algorithm is the step where a given substate is either included or rejected.

The purpose of the rejection sampling algorithm is basically to generate a sequence of samples from a probability distribution that is difficult to directly sample from, such that

$$\frac{\sum_i X_i N_i}{\sum_j N_j} \rightarrow \frac{\sum_i X_i W_i}{\sum_j W_j}, \tag{96}$$

where N_i is the number of times the state S_i was summed, and W_i are the Boltzmann weights as in Eq. (85).

The program generates a series of random configurations, which will then be accepted or rejected in the sum according to some probability, which are functions of the weight ratios. Two conditions must be fulfilled for Eq. (96) to hold (Frenkel and Smit (2001)):

1. The probability to accept a state, S_i, must be proportional to its weight, W_i.
2. The random generation of configurations must be ergodic[11], i.e. given sufficient time, all possible configurations must eventually be generated.

The transition probability should, of course, be normalised and also obey detailed balance, i.e.

$$W_i P_{i\to j} = W_j P_{j\to i} \quad \Rightarrow \tag{97}$$

$$\frac{W_i}{W_j} = \frac{P_{j\to i}}{P_{i\to j}} = e^{-(E_i - E_j)/RT} \quad \text{(Boltzmann)} \tag{98}$$

So by defining $P_{i\to j} \equiv F(e^{-\Delta E/RT})$, where $F(x)$ can be any function that fulfils

$$\frac{F(x)}{F(1/x)} = x \tag{99}$$

Though there is (in principle) an infinity of functions that fulfil this, the two most common choices are (Metropolis et al. (1953), Glauber (1963)):

- **The Metropolis algorithm:** $F(x) = min(x, 1)$
- **The Glauber algorithm:** $F(x) = \frac{x}{1+x}$

While both give choices yield the same result after infinitely long time (and usually also finite time), the Metropolis algorithm can be more susceptible to getting stuck in metastable states, as it never rejects a change to a state with a lower free energy.

This can lead to problems near the critical point, so or this reason we chose to use the Glauber algorithm in this project.

It seems physically intuitive that with these choices for the transition probabilities the system will tend asymptotically ($t \to \infty$) to a steady state in which the probability of an arbitrary configuration is proportional to $e^{-E_i/RT}$.

For instance, if we consider N_i systems in a state S_i and N_j in state S_j, and let $E_j < E_i$, it is possible to construct a move such that the a priori probability of moving from state S_i to S_j is the same as that to move from S_j to S_i.

For instance, using the Metropolis algorithm, the number of transitions from S_i to S_j and from S_j to S_i is given by

[11] An ergodic system is a system that will accesses all states of the phase space after infinitely long time. Furthermore, averaging over very long times ($t \to \infty$) will lead to the same statistical average value as the averaging over a very large system ($N \to \infty$). Hence one can also average one single system over long times, instead of averaging over a large number of systems. This is known as the 'ergodic theorem'.

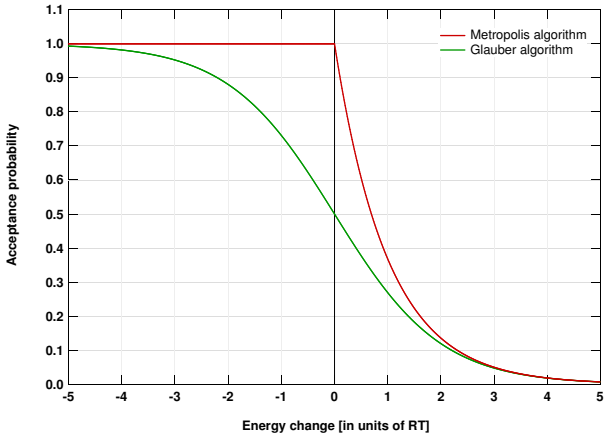

FIG. 11: A comparison of the acceptance probabilities for the Metropolis algorithm and the Glauber algorithm.

$$N_{i\to j} \propto N_i \tag{100}$$
$$N_{j\to i} \propto N_j e^{-(E_i-E_j)/RT}. \tag{101}$$

The net number of transitions will therefore be

$$\Delta N_{i\to j} \propto N_i - N_j e^{-(E_i-E_j)/RT} \tag{102}$$

Alternatively, using the Glauber algorithm, we have that

$$N_{i\to j} \propto N_i \frac{1}{1+e^{-(E_i-E_j)/RT}} \tag{103}$$
$$N_{j\to i} \propto N_j \frac{e^{-(E_i-E_j)/RT}}{1+e^{-(E_i-E_j)/RT}} \tag{104}$$
$$\Rightarrow \Delta N_{i\to j} \propto \frac{N_i - N_j e^{-(E_i-E_j)/RT}}{1+e^{-(E_i-E_j)/RT}} \tag{105}$$

Regardless of the specific choice, the system will converge to a steady state where

$$\Delta N_{i\to j} = 0 \Rightarrow \frac{N_i}{N_j} = \frac{e^{-E_i/RT}}{e^{-E_j/RT}} \tag{106}$$

in accordance with Boltzmann statistics.

5.4 Evaluation of thermodynamic averages

Using the introduced model and evaluating it by means of Monte Carlo simulations one has the possibility of studying different properties of the system.

Once the system has equilibrated, all of the observables will fluctuate around their thermodynamic average value. Some of the observables, such as the average number of pores, or the average fraction of the system in the fluid state, can be obtained directly by simply averaging over many configurations.

Other observables, such as the heat capacity or the area compressibility, can fairly easily be derived from the fluctuations of the system variables. As shown in Eq. (10) and (13), the fluctuations in the enthalpy are directly proportional to the excess heat capacity, while the fluctuations in the system's area are directly proportional to the lateral compressibility.

Thus is straightforward to determine e.g. a heat capacity profile for the model, by repeating the procedure at different temperatures.

The exact temperature dependencies of the various observables are closely related to the cooperativity of the system (ω_{fg}), as the fluctuations at the melting point get larger when ω_{fg} increases. However, at the same time large fluctuations will tend to happen in a narrower temperature range[12], and equilibration will take longer.

It should be mentioned here, that the values obtained are, by the very nature of the method, subjected to statistical errors. Suggestions for how to deal with this will be discussed in Sec. (5.9).

5.4.1 Evaluation of local fluctuations

In contrast to mean field models, Monte Carlo simulations give information about the structural properties of the system, as a direct visualisation of the system configurations is possible. During the simulation the instantaneous configuration of the system can be written to a file making it possible to make a graphical representation of the system by using e.g. a ray tracing program such as POVray (see Fig. (13)).

Furthermore, it is also rather straightforward to determine the strength of the local fluctuations in the lipid states. This can be done by disabling the diffusion and the pore formation/sealing steps at some point during the simulation[13], and then monitoring how often each lipid changes state (averaged over a sufficient number of melting steps per lipid).

Using the state parameter, σ_i, that was introduced in Eq. (86), we can define the local fluctuations of lipid i as the variance of σ_i, i.e.

$$f_i = \langle \sigma_i^2 \rangle - \langle \sigma_i \rangle^2 \tag{107}$$

$$= 1 - \langle \sigma_i \rangle^2, \tag{108}$$

where we have used the usual convention, i.e. $\sigma_i = -1$ for the gel state and $\sigma_i = +1$ for the fluid state. At $T = T_m$ it is, per definition, equally likely to be in either state, meaning that

$$\langle \sigma_i \rangle^2 = 0 \Rightarrow f_i = 1. \tag{109}$$

Far away from the melting point, one of the states will be favoured, so

$$\langle \sigma_i \rangle^2 = 1 \Rightarrow f_i = 0. \tag{110}$$

So the higher f_i is the stronger the fluctuation, which can be visualised by introducing a colour code, as shown in Fig. (13).

[12] In effect, this will mean that the heat capacity profile will get narrower, but its amplitude will increase so as to keep the integral over c_p constant (as the transition enthalpy is independent of the cooperativity).

[13] This can be justified by the fact, that lipid chain conformations change on a time scale several orders of magnitude faster than any lateral diffusion in the system (Holzwarth (1986)).

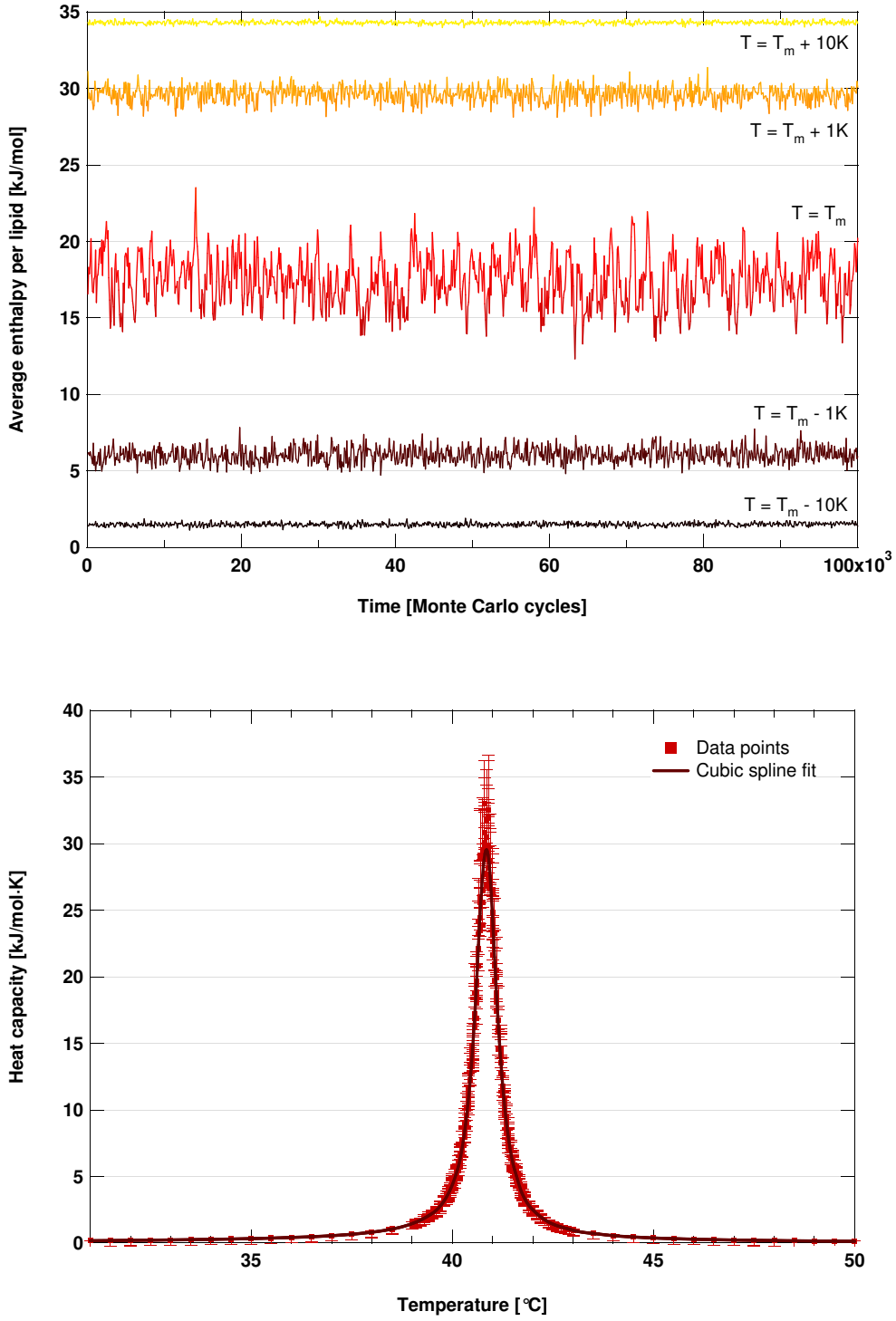

FIG. 12: *Top:* Fluctuations in the enthalpy at different temperatures. *Bottom:* The resulting heat capacity profile.

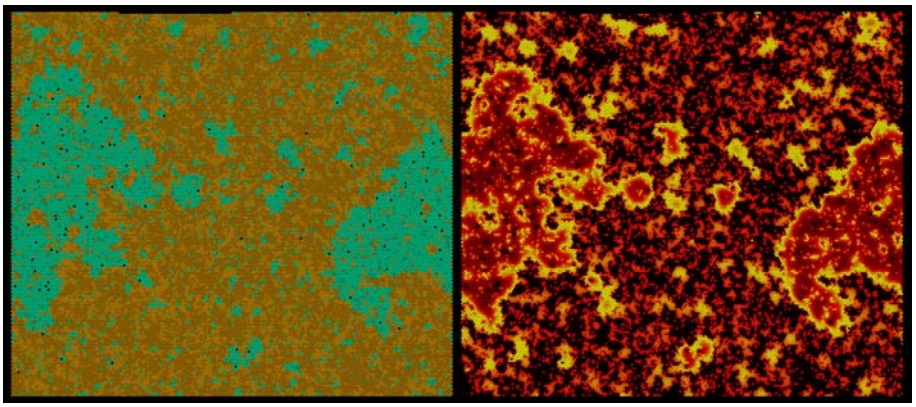

FIG. 13: The local fluctuations of a two-component system in its phase transition. Here the colour code is: black=weak ($f = 0$), red=medium ($f = 0.5$) and yellow=strong fluctuations ($f = 1$).

From these pictures it is immediately obvious that fluctuations are strongest at the interfaces between the domains and the bulk, or in the vicinity of anaesthetics.

5.5 Implementing the Monte Carlo method

The Markov chain[14] is generated in the following way:

1. One starts from the actual system configuration, S_1. Then one of several possible trial moves are performed (see Sec. (5.6) for details), resulting in a new configuration, S_2.
2. Calculate the difference in the free energy of the two configurations, $\Delta G = G(S_2) - G(S_1)$.
3. With this free energy difference one can calculate a Boltzmann factor, i.e. $K(T) = e^{-\Delta G/RT}$, where R is the gas constant and T the temperature.
4. Generate a random number, z, with $z \in [0 : 1]$, and compare it to the acceptance probability, $P_{acc} \equiv \frac{K(T)}{1+K(T)}$.
5. If $z < P_{acc}$ then the new configuration, S_2, is accepted. If $z > P_{acc}$ then the new configuration is discarded, and the system reverts to the old configuration, S_1.

This procedure is the well-established Glauber algorithm (Glauber (1963)) as discussed in Sec. (5.3.4). Alternatively, one can use the Metropolis algorithm, where one sets the probability to $P_{acc} = K(T)$ or $P_{acc} = 1$ if $K(T) > 1$. As both algorithms obey detailed balance, they will lead to the same result[15]. However, in this project we chose to use the Glauber algorithm as the use of the Metropolis

[14] A Markov chain is a series of states of a system which are conditionally independent of the past states (the path of the process).

[15] To be more precise, they will only lead to the same result after sufficiently long runtime as the equilibration times may differ.

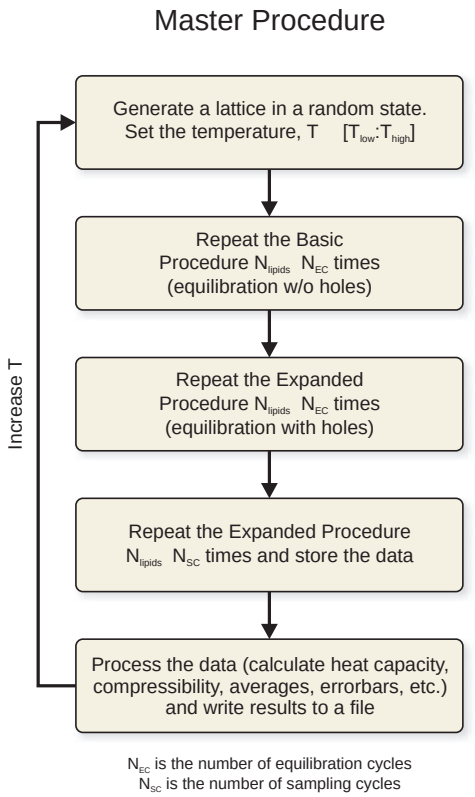

FIG. 14: Flowchart of the program. For the description of the Basic and the Expanded Procedures see Fig. (15).

algorithm can lead to problems near the critical point and metastable states, since a change to a state with a lower free energy is never rejected.

Once we have defined the Monte Carlo steps and a procedure, we can also define a Monte Carlo cycle. In my program, a Monte Carlo cycle is defined as one iteration (on average) of the Basic or Expanded Procedure (see Fig. (15)) per lattice site.

5.6 The Monte Carlo steps

The following sections will outline the general structure of the program. For some of the more technical details of the implementation see Appendix E.

The master architecture of the program is shown in Fig. (14). As can be seen from the flowchart, the program starts from a random state (usually with 50:50 distribution of gels and fluids), which is then allowed to equilibrate allowing only for diffusion and changes in lipid states.

Once equilibrated, the pore formation (and pore sealing) procedure is turned on, and the system evolves until it has found equilibrium. Letting the system equilibrate in two rounds makes the whole equilibration process a lot smoother, as it will reduce the number of pores left over from the initial (and favourable)

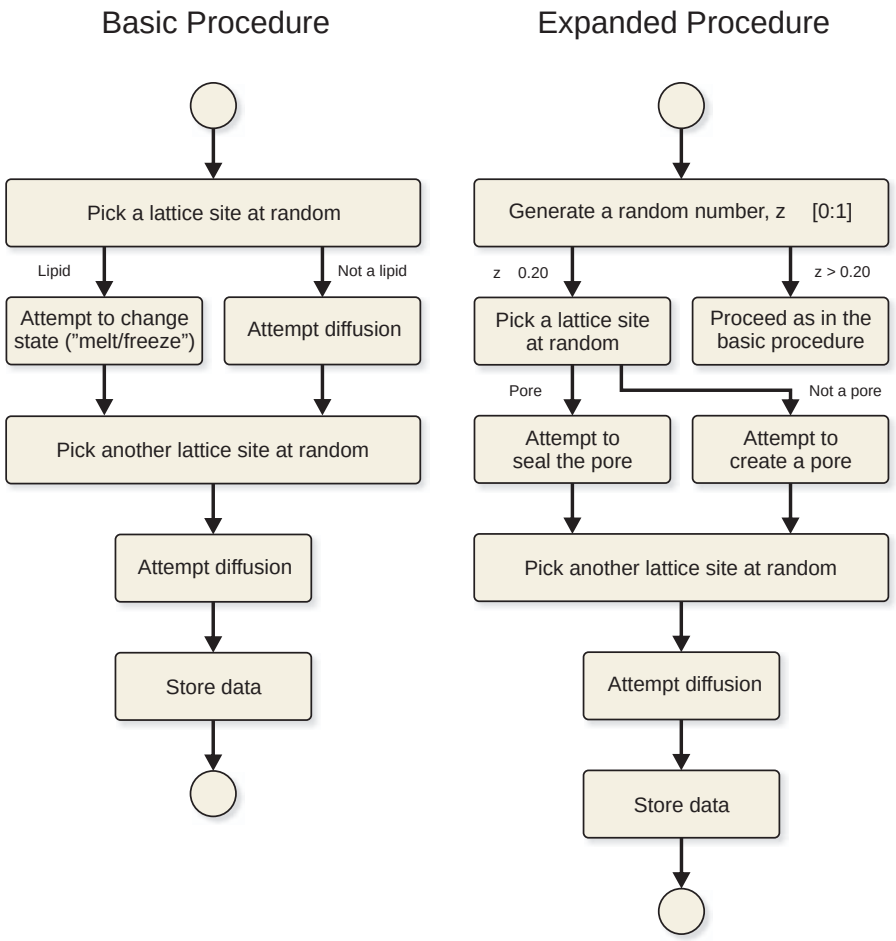

FIG. 15: Flowcharts of the Monte Carlo routines.

system configuration. Once equilibrium has been achieved, the simulation is allowed to run for N_{SC} Monte Carlo cycles.

At the end of the simulation, various averages and thermodynamic quantities (such as the excess heat capacity and the compressibility) are determined by averaging over the simulated distribution of states.

$$\langle X \rangle = \frac{1}{N_{SC}} \sum_{n}^{N_{SC}} X_n. \tag{111}$$

Statistical errors were determined by use of the blocking method (see Appendix F for details), and graphical representations of the system were generated with a raytracer program (POVray).

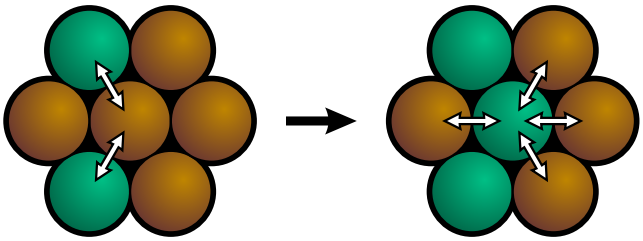

FIG. 16: The "melting" step. Turquoise represents fluid state lipids, while the gels are brownish. In addition to the change in the free energy due to chain ordering/disordering, there is a contribution from the interaction with unlike nearest neighbours. In this example we see that $\Delta N_{fg} = 2$ and ΔH and ΔS are positive numbers.

5.6.1 Melting step

The most oft-used Monte Carlo step is the one that allowed for changes in lipid state from gel to fluid and vice versa ("melting step"):

1. Select a lattice site at random.
2. If an anaesthetic or pore is picked, perform the diffusion step instead as described in Sec. (5.6.2).
3. If a lipid is picked, temporarily change its state (gel $\leftrightarrow$ fluid) and calculate the change in free energy according to Eq. (94), i.e.

$$\begin{aligned}\Delta G = \Delta H - T\Delta S + \Delta N_{fg}\omega_{fg} + \Delta N_{pf}\omega_{pf} + \Delta N_{pg}\omega_{pg} \\ + \Delta N_{ap}\omega_{ap} + \Delta N_{af}\omega_{af} + \Delta N_{ag}\omega_{ag}\end{aligned} \tag{112}$$

4. Calculate the acceptance probability

$$P_{acc} = \frac{K(T)}{1 + K(T)} \quad \text{where} \quad K(T) \equiv e^{-\Delta G/RT} \tag{113}$$

5. Compare P_{acc} to a random number, $z \in [0 : 1]$.
6. Accept the change if $z < P_{acc}$, and otherwise revert the lipid to the original state.
7. Use the final configuration (whether the change was accepted or not) to calculate the value of various thermodynamic observables, X_n.

5.6.2 Diffusion step

After the "melting" step has been performed a "diffusion" step is always attempted. While not strictly necessary in a one-component system (as diffusion is only necessary for the pores and anaesthetics), this step will greatly help the system avoid getting caught in metastable states.

1. Select two lattice sites at random and temporarily swap the two particles.
2. Calculate the resulting change in free energy, ΔG, as in Eq. (112).
3. Calculate the acceptance probability

$$P_{acc} = \frac{K(T)}{1 + K(T)} \quad \text{where} \quad K(T) \equiv e^{-\Delta G/RT} \tag{114}$$

4. Compare P_{acc} to a random number, $z \in [0 : 1]$.
5. Accept the change if $z < P_{acc}$, and otherwise revert the system to the original state.
6. Use the final configuration (whether the change was accepted or not) to calculate the value of various thermodynamic observables, X_n.

5.6.3 Pore step

The two previously described Monte Carlo steps make up the basic steps. Our model has two more possible Monte Carlo steps, namely one that creates pores and one that seals pores.

The basic idea behind these steps is the observation that a lipid changes area by approximately 25% when it goes from the fluid to the gel state. So if three fluids simultaneously change states, one can create a pore which has an area that is equal to a gel state lipid. Thus this step both conserves the number of lipids and also the area as

$$A_{before} = 3A_{fluid} = A_{after} = 3A_{gel} + A_{pore} \tag{115}$$

where a fluid state lipid has been assigned an area of four units, and a gel/pore an area of three units ($3 \cdot 4 = 3 \cdot 3 + 3$).

First pore formation is described. This step can be applied if anything but a pore is picked.

1. If a lipid or an anaesthetic is picked, check the surroundings (nearest neighbours) for lipids in the fluid state. If there are three or more, temporarily create a pore by changing the three fluids into gels, and moving the "central-particle" to the "end" of the lattice, increasing the number of lattice sites by one (see Fig. (17)).
2. Calculate the resulting change in free energy according to Eq. (94), i.e.

$$\begin{aligned}\Delta G = 3(\Delta H - T\Delta S) + \Delta N_{fg}\omega_{fg} + \Delta N_{pf}\omega_{pf} + \Delta N_{pg}\omega_{pg} \\ + \Delta N_{ap}\omega_{ap} + \Delta N_{af}\omega_{af} + \Delta N_{ag}\omega_{ag},\end{aligned} \tag{116}$$

   where ΔH and ΔS refer to the change in enthalpy and entropy of a single lipid.
3. Calculate the acceptance probability

$$P_{acc} = \frac{K(T)}{1 + K(T)} \quad \text{where} \quad K(T) \equiv e^{-\Delta G/RT} \tag{117}$$

4. Compare P_{acc} to a random number, $z \in [0:1]$.
5. Accept the change if $z < P_{acc}$, and otherwise revert the system to the original state.
6. Use the final configuration (whether the change was accepted or not) to calculate the value of various thermodynamic observables, X_n.

In order to obey detailed balance, there must also be a possibility to seal a pore. This could take place if a pore was picked:

1. First, check the surroundings (nearest neighbours) for lipids in the gel state. If there are three or more, temporarily seal the pore by changing the three gels to fluids, and moving the "end-particle" into the pore, thus reducing the number of lattice sites by one (see Fig. (17)).
2. Calculate the resulting change in free energy, ΔG, as in Eq. (116).
3. Calculate the acceptance probability

$$P_{acc} = \frac{K(T)}{1 + K(T)} \quad \text{where} \quad K(T) \equiv e^{-\Delta G/RT} \tag{118}$$

4. Compare P_{acc} to a random number, $z \in [0:1]$.
5. Accept the change if $z < P_{acc}$, and otherwise revert the system to the original state.
6. Use the final configuration (whether the change was accepted or not) to calculate the value of various thermodynamic observables, X_n.

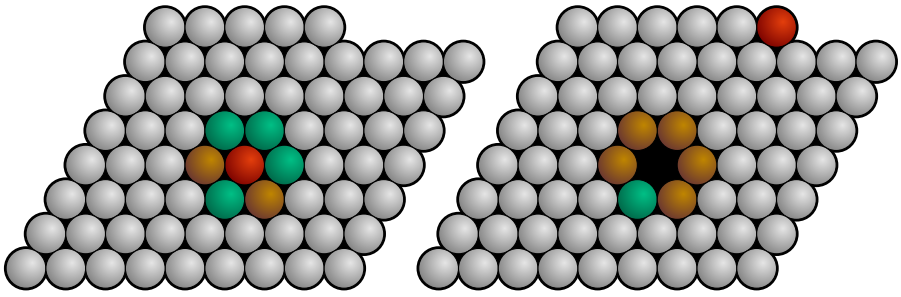

FIG. 17: The pore forming step. Turquoise represents fluid state lipids, while the gels are brownish. The red particle can be either a lipid or an anaesthetic. In this Monte Carlo step three lipids simultaneously change state while the red particle is moved to or from the edge of the lattice. For details on how the neighbourhood of the "last" particle was defined see Appendix E.

5.7 Domain analysis

An important and immediately obvious observation that can be made from Monte Carlo snapshots, is that when the temperature gets close to the transition temperature, T_m, small domains (or clusters) of fluid lipids start to appear in the gel phase (as long as the temperature remains below the transition temperature). The average size and number of these domains increase as the temperature approaches T_m. At T_m the fluid state domains percolate and form a macroscopic phase that coexists with the gel phase. The picture is then reversed when the temperature is above T_m, where domains of gel state lipids appear in the fluid phase.

The temperature range where this occurs strongly depends on the value of the cooperativity parameter, ω_{fg}. Furthermore, the larger the cooperativity parameter, the more compact the domains are at the melting point (see Fig. (42)), as the system will seek to minimise the number of the energetically unfavourable fluid/gel interactions. Only if ω_{fg} gets very large one will find systems that are exclusively in the gel or fluid state (see Appendix G.1), though in general there is no macroscopic phase separation, but rather domains of various size and composition.

The presence of such heterogeneity is the direct result of local thermal density fluctuations. Consequently, they are derived from first principles and are not a consequence of any initial assumptions. Furthermore, these fluctuations are directly related to the lateral compressibility of the system, as shown in Sec. (3.3).

The appearance of such membrane heterogeneities will naturally have a strong impact on the biological function, as it can dramatically alter communication pathways and dynamics.

Monte Carlo simulations can provide information about the microscopic configurations in thermodynamic equilibrium, provided the characteristic length scales are much larger than the atomic level, but still smaller than the system size. For such systems, the statistics of the domain distributions can easily be calculated from these configurations.

Following the definitions in Mouritsen and Zuckermann (1985), we define domains by a nearest neighbour connectivity criterion, so an α-domain ($\alpha = g, f$) is simply defined by the requirement that all lipids must be in the α-state, and that any lipid in the cluster must be connected to any other lipid in the cluster by a series of nearest neighbour bonds on the (triangular and periodic) lattice.

The instantaneous distribution of the domains will then be described by their size distributions, where the size, l^α, of an α-domain is defined as the number lipids in the domain. The number of domains of size l^α is denoted n_l^α. The probability of occurrence, $P^\alpha(l)$, of a domain of size l^α will then be:

$$P^\alpha(l) = \frac{n_l^\alpha}{\sum_l n_l^\alpha}, \quad \text{where} \quad \alpha \equiv g, f. \tag{119}$$

Once the probability distribution has been determined, a number of useful quantities can be calculated, such as the average domain size:

$$\bar{l} = \sum_{l \geq 2} l^\alpha P^\alpha(l), \tag{120}$$

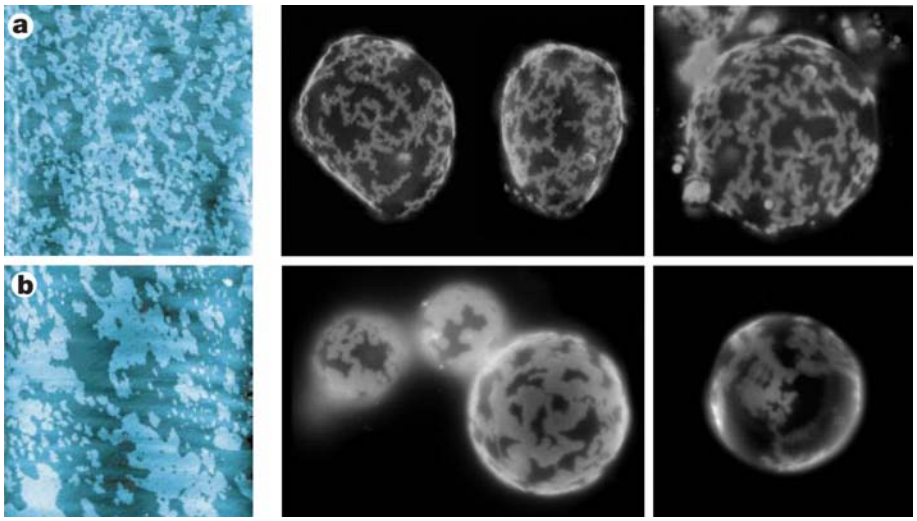

FIG. 18: *Left:* Lipid domains in phospholipid monolayers imaged by atomic force microscopy as a height-difference map. *(a)* Image of DMPC ($25 \times 25\mu\text{m}^2$) and *(b)* DPPC ($20 \times 20\mu\text{m}^2$) monolayers at their respective critical points. Image was taken from Nielsen et al. (2000). *Right:* Lipid domains in giant unilamellar vesicles. *Top:* DMPC/DPPC mixture at $T = 28°\text{C}$. *Bottom:* DLPC/Dipentadecanoylphosphocholine mixture at $T = 26°\text{C}$. Unpublished data from our group (courtesy of Christian Leirer, NBI, University of Copenhagen).

where the sum above has been restricted to only include actual domains, i.e. clusters comprised of at least two lipids.

By averaging $P^\alpha(l)$ over a large number of equilibrium configurations, the thermal ensemble averages of cluster properties can subsequently be obtained.

The existence of large domains near the transition temperature has been verified numerous times, both experimentally (see Fig. (18), Leidy et al. (2001), Hac (2003), Hac et al. (2005), Bagatolli (2006)), as well as by simulation (Mouritsen et al. (1983), Tien and Ottova-Leitmannova (2003), Seeger et al. (2005), Hac et al. (2005), Marrink et al. (2005), Seeger (2006)).

5.8 Multi-component membranes

The Ising model can also be adapted to describe membranes with different lipid species (e.g. DMPC and DSPC). For such systems it is necessary to modify the expression for the free energy, Eq. (92), as the number of different kinds of (non-trivial) nearest neighbour interactions increases as $N_{LS}(2N_{LS} - 1)$, where N_{LS} is the number different lipid species in the system. So for a two-component system we have six nearest neighbour interactions parameters, namely

- Between gel and fluid lipids of species A, ω_{f_A,g_A}
- Between gel and fluid lipids of species B, ω_{f_B,g_B}
- Between gel lipids of species A and B, ω_{g_A,g_B}

- Between fluid lipids of species A and B, ω_{f_A,f_B}
- Between gel species A and fluid species B, ω_{g_A,f_B}
- Between gel species B and fluid species A, ω_{f_A,g_B}

Additionally, each lipid species has a distinct melting enthalpy and entropy, meaning that there are ten(!) parameters to be determined, without even considering the possibility for pore formation or added anaesthetics.

The Gibbs free energy of such a system is then given by

$$\begin{aligned}\Delta G = & \sum_{i}^{N_{LS}} N_{f_i}(\Delta H_i - T\Delta S_i) \\ + & \frac{1}{2}\sum_{\alpha=f,g}\sum_{\beta=f,g}\sum_{i}^{N_{LS}}\sum_{j}^{N_{LS}} N_{\alpha_i,\beta_j}\omega_{\alpha_i,\beta_j}(1-\delta_{\alpha_i,\beta_j})\end{aligned} \tag{121}$$

Apart from the added complexity in the expression for the free energy, Eq. (121), one can proceed exactly as for the one-component system. For a two-component consisting of DMPC and DSPC a series of heat capacity profiles from experiment and Monte Carlo simulations is shown in Fig. (31) and (51). The nearest neighbour interaction parameters $\omega_{\alpha_i,\beta_j}$ are determined by fitting the excess heat capacity profiles to calorimetric measurements.

The details of the microscopic configurations will, of course, also depend on the mixing ratios and on the temperature.

5.9 Considerations in the data analysis

A number of things have to be taken into account when setting up the system and when analysing the data.

5.9.1 Influence of the starting configuration

As the system is initially in a completely random configuration it will most likely not be near the equilibrium during the first iterations of the simulation and should not be included in the final averages.

In general it can be difficult to determine how many iterations should be excluded. This problem becomes even more acute if the simulation is performed near the critical point, as the additional problem of critical slowing down will come into play. As criticality is approached, the range of the correlations increases and the time for relaxation to equilibrium τ will diverge.

Fortunately, the severity of this problem is suppressed in a finite system, as correlations are restricted. Therefore, the smaller the system, the quicker equilibrium can be achieved for a given temperature. However, at the same time finite-size corrections become more apparent, so a balance between these and equilibration times must be struck.

Another problem is that a system can become stuck in a metastable state and feign true thermal equilibrium. The severity of this problem will depend on both the nature of the phase transition (first order or continuous) and the choice of sampling algorithm (Metropolis, Glauber, etc.).

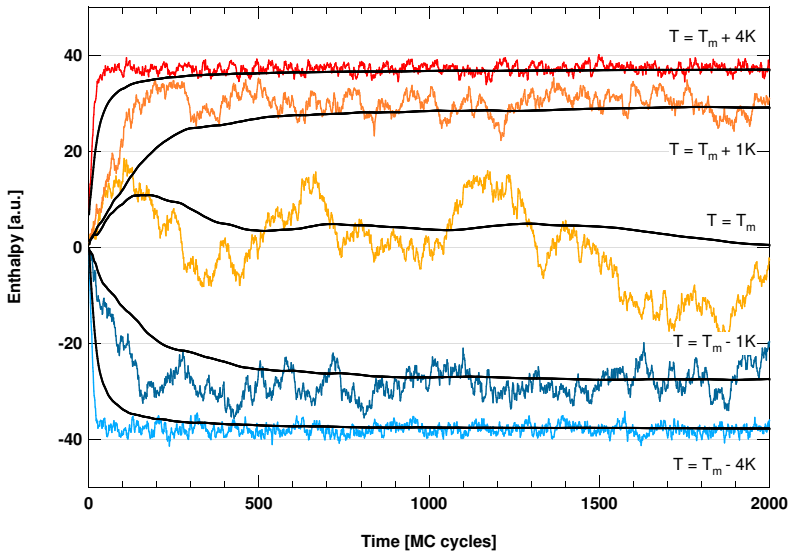

FIG. 19: The approach to equilibrium starting from a completely random configuration. The black lines are the running averages. As can clearly be seen, the closer the temperature is to T_m, the larger the fluctuations and the longer it takes before equilibrium is found (critical slowing down). Also note that even when far away from the transition temperature it takes several hundred MC cycles before the influence of the initial state becomes negligible in the running averages.

Fig. (19) shows an example of the raw data from a simulation, illustrating the approach to equilibrium and the importance of excluding the initial configurations. Note that equilibrium is attained after only a few Monte Carlo cycles for temperatures sufficiently far from the critical point but a slower relaxation and larger fluctuations (both in amplitude and mean lifetime) are observed as T_m is approached.

In general, it is far better to err on the side of throwing away too much data, than it is to be too optimistic, as Fig. (19) clearly shows.

5.9.2 Finite-size effects

Because one is always limited to simulating a finite system, finite-size effects must be taken into account.

Far away from the transition point the correlation length is small compared to the system size, making this effect negligible as the errors due to the limited number of lipids will be small compared to statistical errors.

However, as one approaches the transition the problem will become more pronounced, as the correlation length is limited by the system size. Consequently, any singularities associated with the phase transition will be shifted and rounded.

5.9.3 Statistical errors

One issue that has to be dealt with when making Monte Carlo simulations is the trade-off between having good sampling and computation time. Furthermore, to obtain a reliable estimate for the equilibrium value of an observable, $\langle X \rangle$, the average must be taken over a time significantly longer than that over which the Monte Carlo states are correlated. As with everything else, this becomes more difficult near the phase transition or if the system has metastable states.

There are several possibilities for estimating the statistical error. The simplest way is to average over several independent simulations. However, this method has the disadvantage that the system must be equilibrated anew for each set of data.

Another way is to divide the equilibrium configurations into independent blocks and calculating $\overline{X}$ for each block. This gives a set of (essentially) independent estimates of $\langle X \rangle$, and standard data analysis can be applied to determine the statistical error. The problem is to know how long the block of states must be, so that the different blocks can indeed be considered independent of each other. One method is to perform the analysis using several different block sizes. When the blocks are long enough the variance becomes independent of the block size. More advanced methods are discussed in Appendix F.

Part III
Experiments

This section presents both the numerical and the experimental results, as well as the techniques used. These techniques are mainly Fluorescence Correlation Spectroscopy (FCS) and Monte Carlo simulations, though Differential Scanning Calorimetry (DSC) and Dynamic Light Scattering (DLS) was also used.

6 Materials and Methods

This section describes the sample preparation as well as the experimental methods and considerations. The results are shown and discussed in Sec. (7).

6.1 Preparation of vesicles

The sample preparation is a somewhat involved affair. The procedures are described below in some detail, but for step-by-step descriptions see the Appendices.

6.1.1 Extrusion

For the FCS experiments large unilamellar lipid vesicles (LUV) of DPPC (Avanti Polar Lipids, Birmingham/AL, USA) with 5mol% DPPG were used.

The sample was prepared by dissolving each of the lipid components separately in organic solvent (dichloromethane:methanol 2:1), after which the two components were mixed in the desired ratio.

This mixture was then dried by heating while exposing it to an air stream. The remaining organic solvent was removed by placing the sample in a high vacuum desiccator over night.

Multilamellar lipid vesicles (MLV) containing dye were then prepared by adding the dye solution (50μM rhodamine 6G and 200mM NaCl in Millipore water) to the dry lipids and heating it to about 10K above the melting temperature while stirring it for about an hour. The solution was also vortexed a couple of times during the stirring process.

This process results in multilamellar lipid vesicles, which must then be extruded to give unilamellar vesicles. The extruder (Avestin Europe GmbH, Mannheim, Germany) consists of two mechanised syringes pressing the solution through a polycarbonate filter with a pore size of 100nm. The extruder was placed in a brass block which could be heated by a heat bath, so the system would be above the melting temperature of the lipid membranes ($T = 49.6°$C) while being extruded (so as to make the membranes softer and easier to extrude).

Before starting the extruder setup, 1ml of the lipid solution was transferred to one of the two syringes, after which the syringes were put back into the extruder block and kept there for 15 minutes to ensure that the sample and extruder had a constant temperature.

The extrusion was carried out very slowly (about 1.5 minutes to empty a syringe) so that the filter would not break, and repeated dozens of times to ensure that the vesicles had a narrow size distribution.

After the extrusion process the LUV solution was taken from the syringe which was initially empty, as this ensures that all lipid vesicles have been through the polycarbonate filter at least once.

For a more thorough description of the extrusion procedure, see Appendix A.

To check the quality of the extruded vesicles some dynamic light scattering measurements were also performed. The measurements were performed at 25°C (and hence in the gel state of the vesicles), and the results can be seen in Fig. (20). The distribution were obtained by making a regularised least squares fit (using a smoothness constraint) of a sum of 200 exponential functions to the measured autocorrelation functions. The resulting distribution is consequently the widest and most featureless distribution that is still consistent with the measurements, so the actual distribution is therefore likely to be much narrower. What is clear is that it is a monomodal distribution, indicating that there seems to be no strong aggregation going on. Having a monomodal distribution also makes it possible to do a second order cumulant analysis. This gave an average hydrodynamic radius of $r = 54.6 \pm 0.3$nm, with a polydispersity factor of 0.03. For comparison, the instrument gave a polydispersity factor of ≈ 0.02 for a known mono-disperse solution, indicating that the vesicle distribution was very narrow, thus justifying the use of the equations derived in Sec. (4).

Taken together with the good agreement of the theoretical fits obtained from the FCS measurements, it can be concluded that the solution was close to being mono-disperse, with the scatterers (vesicles) having an average diameter of ≈ 100nm in the gel state. The $\approx 33\%$ increase in lipid area when going from gel state to fluid state (Heimburg (1998)) means that the vesicles' diameter would increase by $\approx 15\%$.

6.1.2 Chromatography

After the vesicles have been prepared by extrusion it is necessary to separate the vesicles from the free dye in order to have concentration gradients in the system. This was done by size exclusion chromatography.

Before the actual separation could be performed, the gel column needed to be prepared and equilibrated. This step is crucial to get decent results. The full details can be found in Appendix B, but is also illustrated in Fig. (22).

The chromatography procedure was as follows: Set up a clean disposable glass Pasteur pipettes (the longer the better) with a small piece of sterile glass wool plugged in the neck. Clamp the column in a vertical position, and add some Millipore water and the G50 Sephadex gel. Thereafter, let a minimum of three column volumes of a NaCl solution run through the column to block all non-specific binding sites.

Once the gel column had been prepared, the sample was poured in and collected again in five or six fractions of varying concentration and separation.

On a general note, make sure that the ambient temperature is at least 10K below the phase transition temperature to prevent unnecessary dye leakage during the separation procedure.

The prepared samples were stored in a refrigerator to prevent leakage, and a fresh batch was prepared if the sample got more than two weeks old. When used for the actual FCS measurements, the sample was usually diluted by a factor of 50-100 with a 200mM NaCl solution, so as to have 1-2 vesicles in the confocal volume on average.

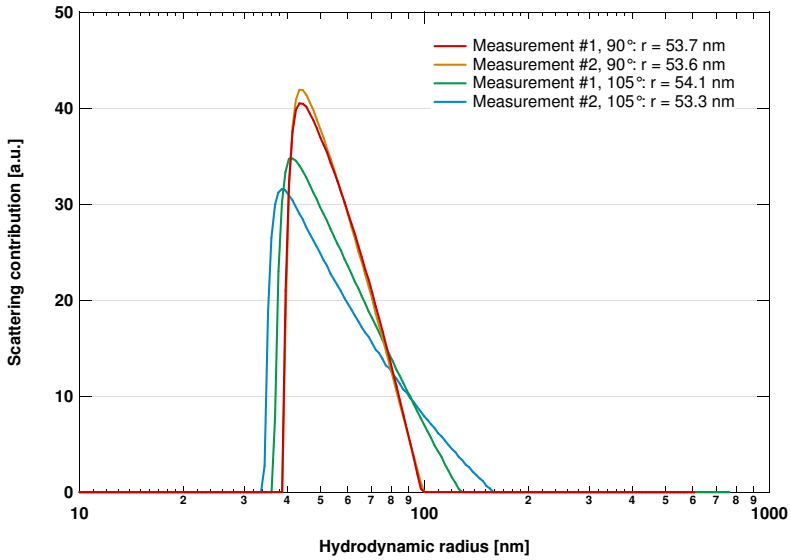

FIG. 20: Distribution of the scattering contributions obtained from dynamic light scattering. The average hydrodynamic radius for each of the distributions is listed in the upper right corner.

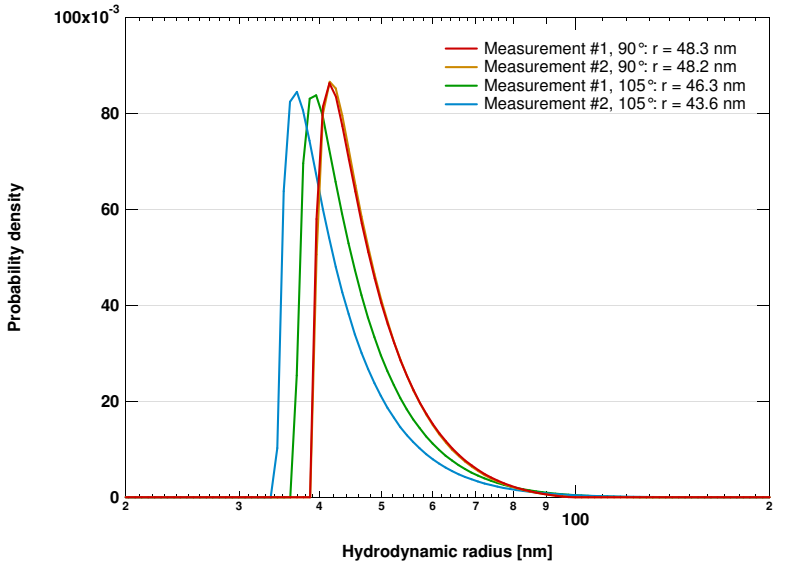

FIG. 21: The resulting distribution of vesicle sizes, as obtained from Fig. (20). The scattering amplitude of a scatterer is proportional to its molar mass squared, so $A(r) \propto n_r \mathcal{M}_r^2 \propto n_r r^4$, where $A(r)$ is the scattering amplitude, r the radius, and $\mathcal{M}_r$ and n_r are the molar mass and the number of scatterers with radius r. The average hydrodynamic radius for each of the distributions is listed in the upper right corner.

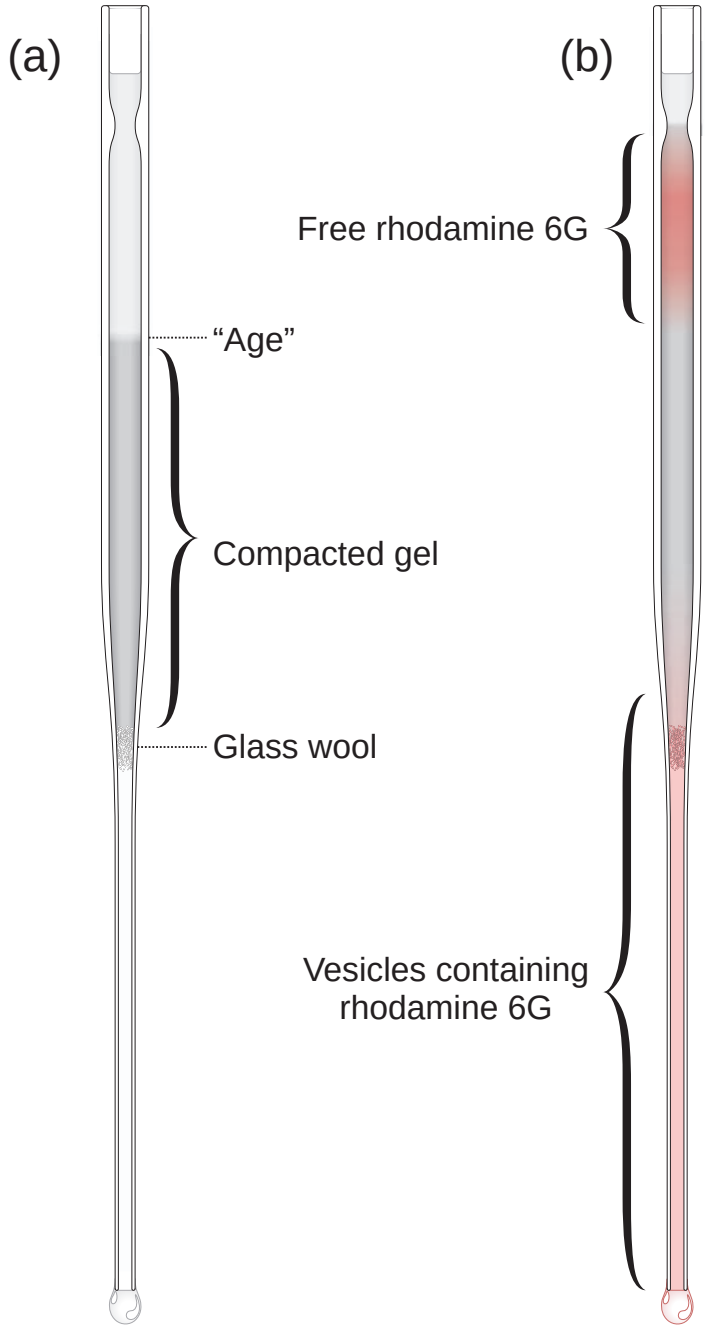

FIG. 22: Chromatography procedure. *(a)* Preparation of gel column. *(b)* Separation of vesicles and free rhodamine.

6.2 Fluorescence correlation spectroscopy measurements

Fluorescence Correlation Spectroscopy (FCS) uses fluctuations in the fluorescence signal to get information about diffusion processes. The necessary theory is derived in Sec. (4).

For a step-by-step description of the measuring procedure see Appendix C.

6.2.1 Experimental setup

In order to see large fluctuations, one needs a small confocal volume. This was realised through a confocal setup which is schematically shown in Fig. (23).

The confocal fluorescence setup used consists of a Nd:Yag laser (LASER 2000, Reno/NV, USA) with an emission maximum at a wave length of 532nm (green) emitting coherent, linearly polarised light (power 5mW, beam diameter 0.36mm). The laser power could be adjusted by inserting optical density filters (OWIS, Staufen, Germany) into the light path. Typically the laser power was reduced by a factor of 400 (OD 2.6) in order to minimise the photobleaching[16] of the fluorophores inside the slow moving vesicles. To further reduce the effect of photobleaching, a computer controlled shutter was used to block the light path when data wasn't being collected.

The first (and rather sensitive) part of the setup was a $\times 20$ telescope (two lenses with focal lengths of 5mm and 100mm) that magnifies the beam diameter to 7.2mm, so that the laser beam will properly fill the back of the objective.

The laser light is then reflected by a dichroic mirror (reflecting light with a wavelength shorter than 537nm, while transmitting light with a longer wave length) into a water immersion objective[17] (Olympus Optical Com, Hamburg, Germany; UPLAPO 60×W; N.A. 1.20; W.D. 0.25mm); F.N. 26.5; C.C. 0.13-0.21 μm; objective focal length 3mm).

When the fluorophores in the sample are hit by the laser light, they are excited to a higher energy level followed by an immediate decay whereby a photon is released with a wave length longer than the excitation wave length (see Sec. (6.5)). Some of the fluorescence light then re-enter the objective and is transmitted back towards the dichroic mirror. The wave length of the fluorescence light is chosen so that the dichroic mirror will transmit instead of reflect.

The signal is then further filtered as the light passes through a bandpass filter. This filter cuts off the background signal originating from the Raman scattering of the water in the sample, as well as residual reflected light from the laser.

After being filtered, the fluorescence signal passes through a small pinhole (OWIS, with a diameter of 30μm, 50μm or 100μm) which is crucial for defining the detected confocal volume of the setup. Changing its size results in a bigger or smaller detection volume (see Fig. (24)). Typically a 100μm pinhole was used, creating a ellipsoidal detection volume of approximately 0.8μm $\times$ 2.5μm.

[16] Photobleaching is when a fluorophore permanently loses the ability to fluoresce due to photon-induced chemical damage and covalent modification. The bleaching rate increases markedly if the excitation irradiance is larger than $\approx 10^3 \mathrm{W/m}^3$ (Eggeling et al. (1998)).

[17] By placing a drop of water between the objective and the coverglass, one gets much greater light collection efficiency due to the high refractive index of the water. It does, however, also mean that there is strong thermal contact between the objective and the sample, which can cause complications as discussed in Sec. (6.3.1).

Thereafter, the light is split into parallel and perpendicularly polarised light by the polarising beam splitter (Linos; SBB/450-1100nm). Two avalanche photodiodes (SPCM-AQR-13, Perkin Elmer, Boston/MA, USA), which allow single photon counting, register the fluorescence signals of the parallel or the perpendicular polarised light. These signals were then correlated by a hardware Flex5000 correlator card from Correlator.com (Bridgewater/NY, USA).

The setup used was built by Agnieszka Hac, so for a more thorough description of the setup see Hac (2003).

6.3 FCS complications

While performing these experiments, a number of difficulties were encountered.

6.3.1 Temperature control

Heating the sample homogeneously turned out to be a major issue, as the heating jacket tended to get substantially hotter (as much as 10K) than the heated objective (which also had good thermal contact with the sample due to the water drop in between) if the ambient temperature was significantly lower than the desired temperature. In addition to having an ill defined temperature measure of the sample, this also resulted in convection. While such directed motion distorts the correlation curves, this can be taken into account in the analytical expression (Schwille and Haustein (2002)). More importantly, the convection led to an exchange of sub- and super-transition vesicles which made it next to impossible to extract a meaningful measure for the permeation rate at high temperatures. Increasing the ambient temperature to about 40°C by placing a simple hot air heater beneath the optical table as well as wrapping the objective and its heater in cotton and aluminium foil, did alleviate this problem somewhat, but a complete control of the temperature was not possible with the current setup. The precision of the temperature measurements was estimated to be about 0.5K at best.

6.3.2 Vesicle leakage

It also turned out to be difficult to heat the sample quick enough to avoid having most of the dyes leak out while heating it. This meant that the permeation rates calculated for the experiments above the phase transition temperature were problematic to determine with any reliability. Simply preheating the sample just prior to the measurements was not sufficient, nor did diluting a high concentration sample in a preheated solution help. To solve this problem, we also tried using tetramethylrhodamine dextran (3000 MW, anionic) for the measurements above the phase transition, as a larger fluorophore would have a lower permeation rate, thus making it possible to heat up the sample without severe leakage before the actual measurements. This, however, had its own issues as discussed in Sec. (7.3).

6.3.3 Electrostatic interactions

Having a positively charged dye (rhodamine 6G chloride) and negatively charged lipid head groups (1,2-Dipalmitoyl-sn-Glycero-3-[Phospho-rac-(1-glycerol)] (sodium salt), a.k.a. DPPG), also caused complications, as the electrostatic at-

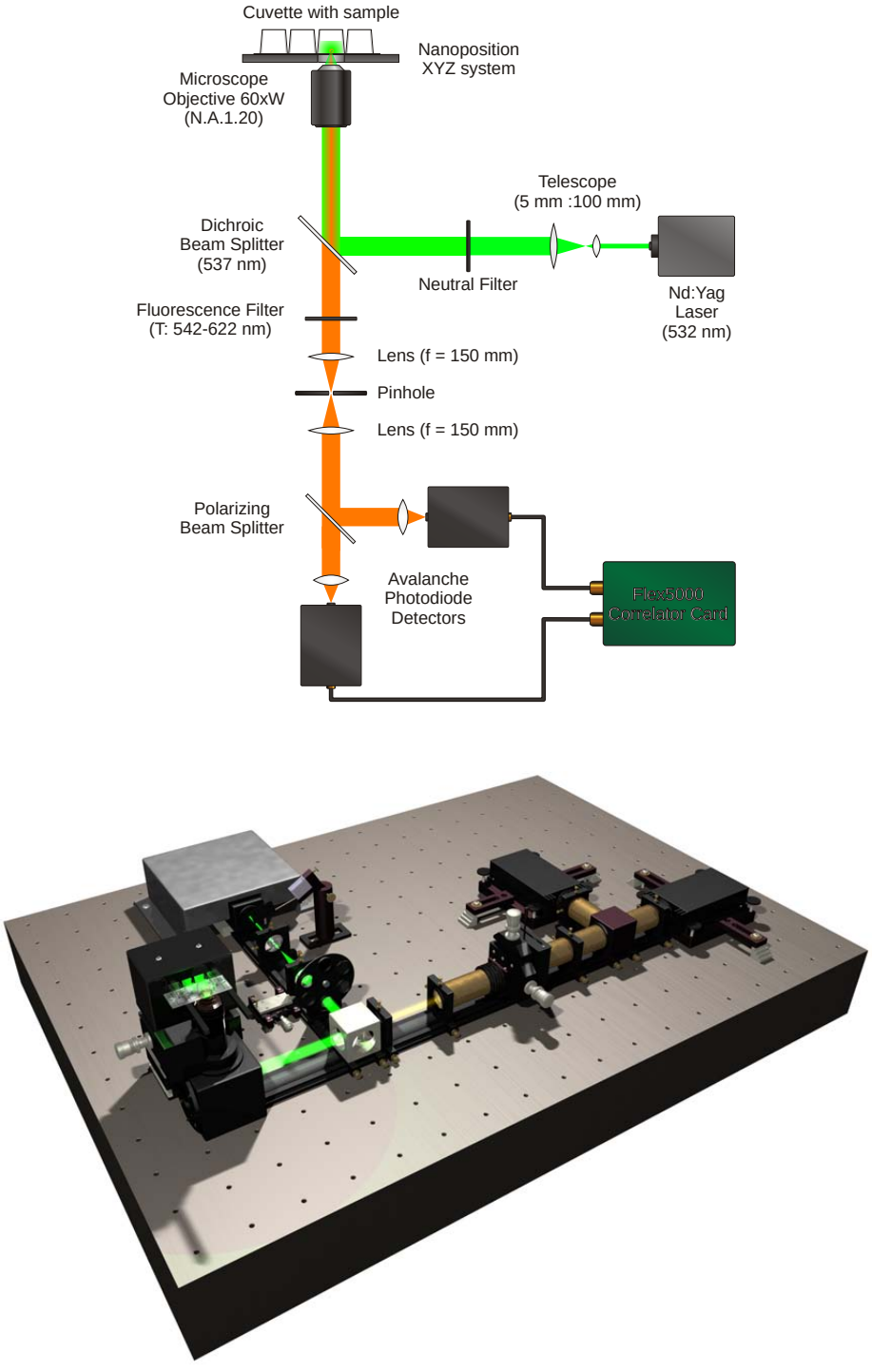

FIG. 23: The FCS setup. *Top:* A schematic illustration of the setup. *Bottom:* A raytraced image of the setup.

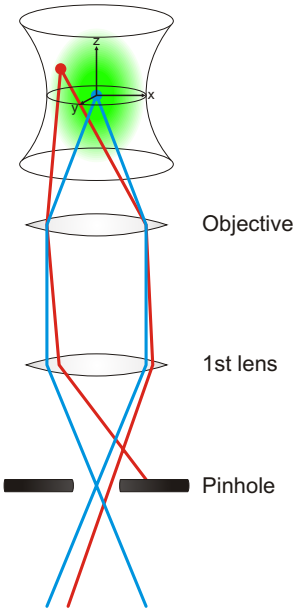

FIG. 24: The basic principle of the pinhole. Light reaching the first pinhole lens from the centre of the focal plane of the sample will travel parallel to the axis of symmetry, and is thereby focused exactly on the pinhole. The further from the focal plane centre, the less parallel the light will be when it reaches the pinhole lens. In effect the pinhole will block any fluorescence light that does not originate from the focal region, and thus provides axial resolution. The size of the pinhole must be greater than the diffraction limit, but too large a pinhole will defeat its purpose.

traction prevented leakage, and caused the free rhodamine molecules to stick to the surface of the vesicles. Simply adding 200mM NaCl reduced this interaction as the ions screened the charges significantly, reducing the Debye length to less than 1nm.

6.3.4 Evaporation

The high temperatures caused the water drop between the objective and the cover glass to evaporate, which meant that as time went by, the light collection efficiency decreased as drop got smaller. Replacing the drop was of course possible and necessary, but it did disturb the sample somewhat, which would show up in the measured signal. Evaporation of the sample itself was also an issue, as this caused the concentrations to change with time as well as cooling the surface. This, however, could be prevented by sealing the cuvette well with Parafilm.

6.3.5 Count rates for rhodamine

As the entire setup was heated by about 20K meant that the thermal expansion of the system was quite significant, and could at times ruin the calibration. As the exact alignment of the cover glass, differences in the background signal, etc. also changed things a bit, it turned out to be next to impossible to get an exact measure for the count rate per rhodamine molecule. Typically the uncertainty was on the order of 10–20%.

6.3.6 Air bubbles

Small air bubbles often formed on the cover glass, which could completely ruin a data series. Degassing the sample prior to the measurements did alleviate this problem somewhat, but did not completely eliminate it.

6.3.7 Adding an anaesthetic

When adding an anaesthetic to the sample, a number of things has to be taken into account. Firstly, it is fairly difficult to find exact and reliable numbers for the partition coefficient, β, which also apply to the system under consideration.

When calculating the concentration of the anaesthetic in the membranes, the general expression can easily be derived, giving

$$\beta \equiv \frac{C_{mem}}{C_{buffer}} \quad \Rightarrow \tag{122}$$

$$C_{mem} = \frac{\beta n_{anae}}{\beta V_{mem} + V_{buffer}}, \tag{123}$$

where β is the partition coefficient, C_{mem} is the concentration of anaesthetics in the membranes, C_{buffer} is the concentration of anaesthetics in the buffer, V_{mem} is the volume of the membranes, and V_{buffer} is the volume of the buffer, and n_{anae} is the amount of anaesthetic added to the system (in moles).

Due to various uncertainties in the preparation of the sample (such as extrusion and the chromatography procedure, as well as the usual uncertainties in weighing, etc.), the exact amount of lipid in the system is hard to determine. However, if the amount of lipids in the system is very low (i.e. $\beta V_{mem} \ll V_{buffer}$), the Eq. (123) can be approximated by

$$C_{mem} \approx \beta \frac{n_{anae}}{V_{buffer}}, \tag{124}$$

i.e. it is linear in the partition coefficient. So any inaccuracy in the value of the partition coefficient will result in an equally inaccurate determination of the concentration of the anaesthetic in the membranes.

In this project the following values for the partition coefficients were used (values taken from Firestone et al. (1986)):

- Octanol (DPPC/water): $\beta = 387$
- Halothane (DPPC/water): $\beta = 50$

Secondly, actually adding the anaesthetic requires some care, as it has to be mixed with the entire sample almost instantaneously, to avoid having a certain fraction of the vesicles becoming completely saturated, while others are

left nearly untouched. Furthermore, as the anaesthetics used tend to be almost water insoluble, there is always the risk of having tiny droplets forming in the sample, which can severely disrupt the signal as they scatter the laser light. Lastly, one should also take care not to add so large amounts that some of the vesicles are completely destroyed (dissolved) by it, which will cause an instantaneous release of dye.

6.4 Fitting the data

Once a correlation curve has been measured, it is, of course, necessary to fit the analytical expressions that were derived in Sec. (4) to the data. However, there is a slight problem in doing this, as the correlation curve for this system can only give five parameters (the two step amplitudes, the two time scales and the shape of the tail as shown in Fig. (25)), while we actually have at least six free parameters (average number of free fluorophores, average number of vesicles, average number of fluorophores per vesicle, the two time scales, and the ratio of the longitudinal and radial dimensions of the focus. If using TMR dextran, there's also the average number of labels per dextran).

For a system where the number of fluorophores is conserved, there are no free parameters and Eq. (51) can be used. Unfortunately, rhodamine 6G has a strong tendency to stick to the cuvette walls, making it necessary to find an alternative approach.

This problem was handled by making a measurement on free fluorophores beforehand. Here, there will only by three to four variables to fit (average number of fluorophores, time scale, ratio of the longitudinal and radial dimensions of the focus, and possibly the average number of labels per dextran), which is fittable from the amplitude, the position of the half-height, and the shape of the tail. Also, from the average intensity of the signal, and signal per fluorophore can be determined, which in turn can be used to determine the total (average) number of fluorophores in the focus in the two-component system.

Normally, the degree of labelling (i.e. the average number of labels per dextran) is provided by the manufacturer, giving us one less variable to worry about. Also, the ratio of the longitudinal and radial dimensions of the focus is setup-dependent, and will therefore just need to be determined once and for all.

While the characteristic diffusion time scales depend on temperature, these can also just be determined beforehand, though better fits might be obtained, if these are fitted each time as they are subjected to statistical variations. This leaves us with just three parameters, namely the average number of free fluorophores, $\langle N_{R6G} \rangle$, average number of vesicles, $\langle N_v \rangle$, and the average number of fluorophores per vesicle, $\tilde{B}$, which can be determined from the two amplitudes and the total number of fluorophores in focus.

Written in a more concise form, we have that:

$$\begin{aligned} G(\tau) = 1 \quad &+ \quad A_{R6G}\left[1+\frac{\tau}{\tau_{D,R6G}}\right]^{-1}\left[1+\frac{\tau}{\omega^2\tau_{D,R6G}}\right]^{-1/2} \\ &+ \quad A_v\left[1+\frac{\tau}{\tau_{D,v}}\right]^{-1}\left[1+\frac{\tau}{\omega^2\tau_{D,v}}\right]^{-1/2}, \end{aligned} \tag{125}$$

where

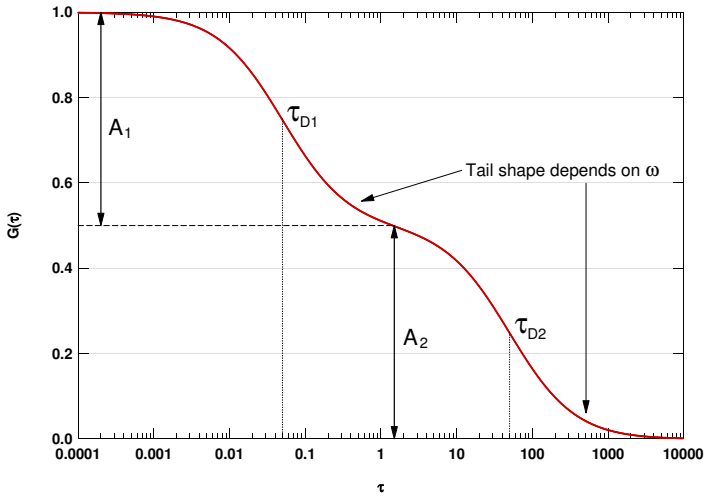

FIG. 25: Correlation function for a two component system. For the sake of clarity the time scales are a factor of 1000 apart, whereas the vesicles and free rhodamine only differ by a factor of about 200.

$$A_{R6G} \equiv \frac{\langle N_{R6G}\rangle}{N_{tot}^2} \quad \text{and} \quad A_v \equiv \frac{\langle N_v\rangle \tilde{B}^2}{N_{tot}^2}\Big(1+\frac{1}{\tilde{B}_0}\Big). \tag{126}$$

Here we have also introduced N_{tot}, which is the total number of fluorophores that is in the confocal volume on average

$$N_{tot} \equiv \langle N_{R6G}\rangle + \tilde{B}\langle N_v\rangle \tag{127}$$

$$= \frac{\langle F_{total}\rangle}{F_{one\ fluorophore}} \tag{128}$$

Fitting to the two amplitudes, A_{R6G} and A_v, gives much more numerically fits than trying to fit directly to the N_i's, which would otherwise be an issue when there is very little rhodamine in free solution.

All fits and data analysis were performed using self-made IGOR Pro routines.

6.5 Dye spectra

The dye used in most of the experiments was rhodamine 6G chloride (Xanthylium, 9-(2-(ethoxycarbonyl)phenyl)-3,6- bis(ethylamino)-2,7-dimethyl, chloride; MW 479.02). This laser dye is pumped by the 2nd (532 nm) harmonic from a Nd:Yag laser, and it has a remarkably high photostability, high quantum yield, low cost, and close proximity to the absorption maximum, making it well suited for FCS studies.

A few of the experiments made use of labelled dextran (D3307; dextran-tetramethylrhodamine, MW 3000, anionic), which consists of about 16 sucrose molecules, plus 0.3–0.7 tetramethylrhodamine groups per dextran.

The absorption and emission spectra for rhodamine 6G chloride and tetramethylrhodamine are shown in Fig. (27). The maxima in the absorption and emission spectra are at 528nm and 551nm for rhodamine 6G, while they are located at 555nm and 580nm for tetramethylrhodamine.

6.6 Differential Scanning Calorimetry

Differential Scanning Calorimetry (DSC) is a powerful thermoanalytical technique by which one measure a number of characteristic properties of a sample, such as fusion, melting, crystallisation, as well as certain chemical reactions. This method has also been used to study of melting processes in artificial or biological membrane systems for than three decades now (see e.g. Hinz and Sturtevant (1972)).

In short, one measures the difference in the amount of heat required to increase the temperature of a sample and a reference as a function of temperature. Depending on the nature of the process (exothermic or endothermic), more or less heat must flow to the sample. For instance, as a gel state lipid membrane melts (an endothermic phase transition) it will require more heat flowing to the sample in order to increase its temperature at the same rate as the reference.

The basic principle of DSC instrument is shown in Fig. (28). The DSC consists of two cells that are enclosed by an adiabatic shield to prevent uncontrolled heat leakage. One cell is filled with sample (e.g. a lipid/buffer solution) and the other with a reference solution (usually a buffer).

The temperature of the cells is then increased linearly as a function of time while keeping the temperature difference between the two cells at zero.

If an exothermic or endothermic process takes place within the sample, there will be a significant deviation in the difference between the two heat flows ($\Delta P = P_{sample} - P_{reference} \neq 0$), and a peak will show up in the DSC curve.

By integrating the excess power, ΔP, with respect to time, the excess heat flow to the sample is consequently

$$\Delta Q = \int_t^{t+\Delta t} \Delta P(t')dt' \simeq \Delta P \cdot \Delta t \tag{129}$$

The heat capacity is given by the energy needed, ΔQ, to heat the system ΔT at constant pressure, i.e.

$$\Delta c_p = \left(\frac{\Delta Q}{\Delta T}\right)_p = \frac{\Delta P}{\Delta T/\Delta t} \tag{130}$$

where $\Delta T/\Delta t$ is known as the scan rate.

So by simply monitoring the power difference of the two cells one has a direct measure of the excess heat capacity of the sample substance, from which one can easily derive the transition enthalpy and entropy (see Sec. (5.3.2)).

The heat capacity profiles in this thesis were all recorded using a VP-DSC, produced by Microcal (Northhampton/MA, USA). In all the experiments the pressure in the calorimeter was approximately 50psi = 3.4atm (above atmospheric pressure), and the scan rate was 5K/hour.

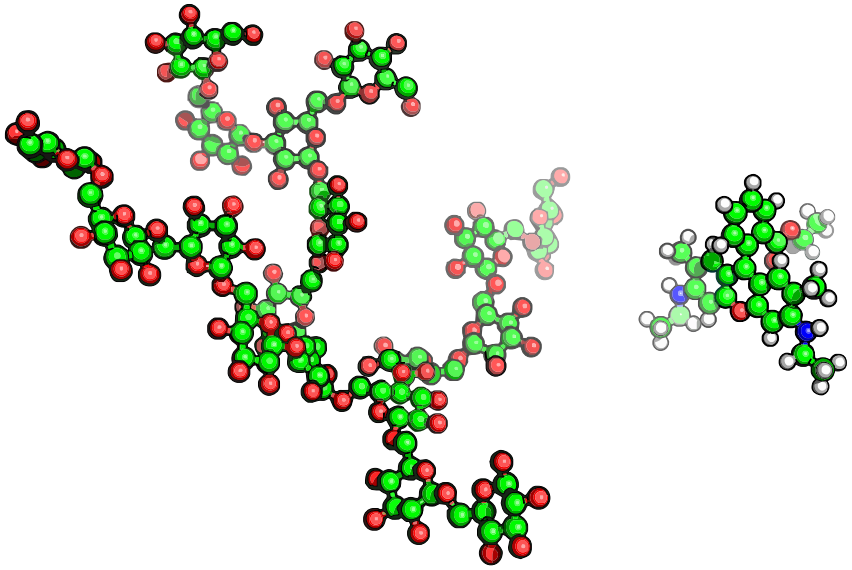

FIG. 26: *Left:* Example of a dextran molecule (tetramethylrhodamine group and hydrogens not shown). Dextran is a complex, branched polysaccharide made from glucose residues. This example consists of 18 residues, but the TMR dextran purchased had distribution going from ≈ 10–20. *Right:* Molecular structure of rhodamine 6G chloride. For a schematic representation of the dyes, see Fig. (56) in the Appendix.

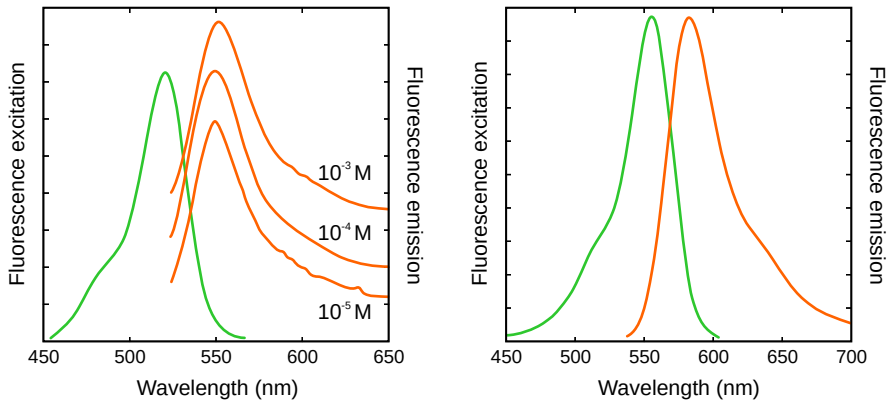

FIG. 27: *Left:* Absorption and emission spectra for rhodamine 6G chloride at different concentrations. Figure was adapted from Zondervan et al. (2003). *Right:* Absorption and emission spectra for tetramethylrhodamine at pH 7.0. Figure was adapted from `www.invitrogen.com`.

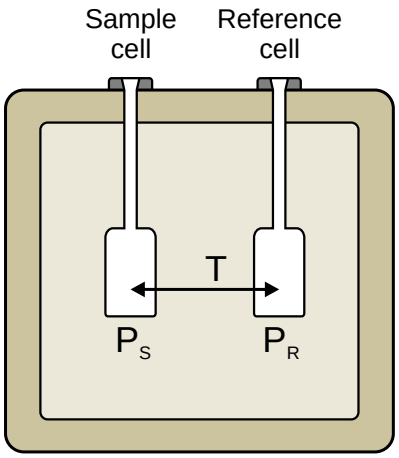

FIG. 28: A schematic drawing of a Differential Scanning Calorimeter. A sample and a reference cell are isolated from the outer environment by an adiabatic shield. The temperature difference between the two cells, ΔT, is kept zero. The difference between the heat flows to each of the cells, ΔP, is proportional to the excess heat capacity.

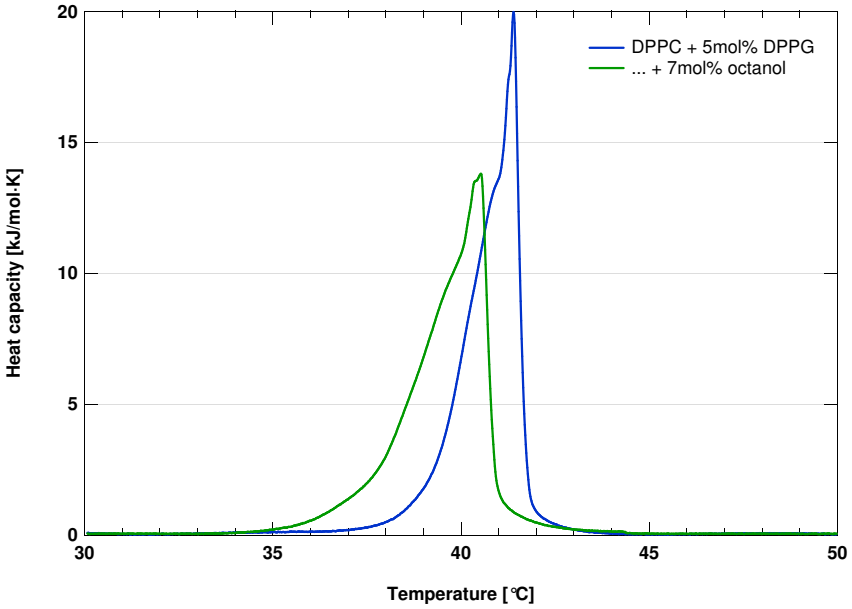

FIG. 29: DSC measurement of the excess heat capacity profile for the system under study. The blue curve is large unilamellar vesicles of DPPC with 5mol% of DPPG in 200mM NaCl and nanomolar concentrations of rhodamine 6G. The green curve also has approximately 7mol% 1-octanol in the membranes.

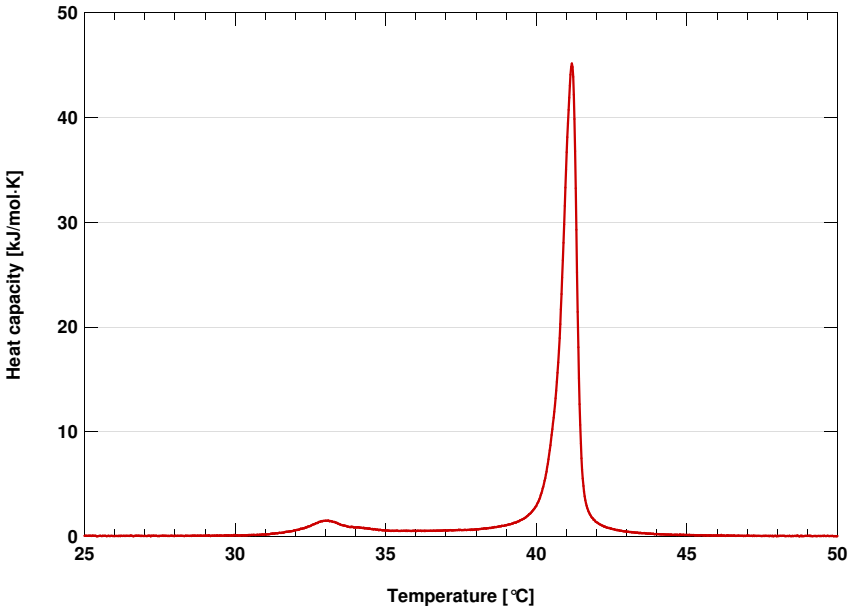

FIG. 30: The excess heat capacity profile for large unilamellar DPPC vesicles determined by DSC. The peak at 33°C is called the pre-transition, and is thought to be due to ripple formation (Heimburg (2000)). The peak at 41°C is the chain-melting transition. This data was provided by Thomas Heimburg, NBI, University of Copenhagen.

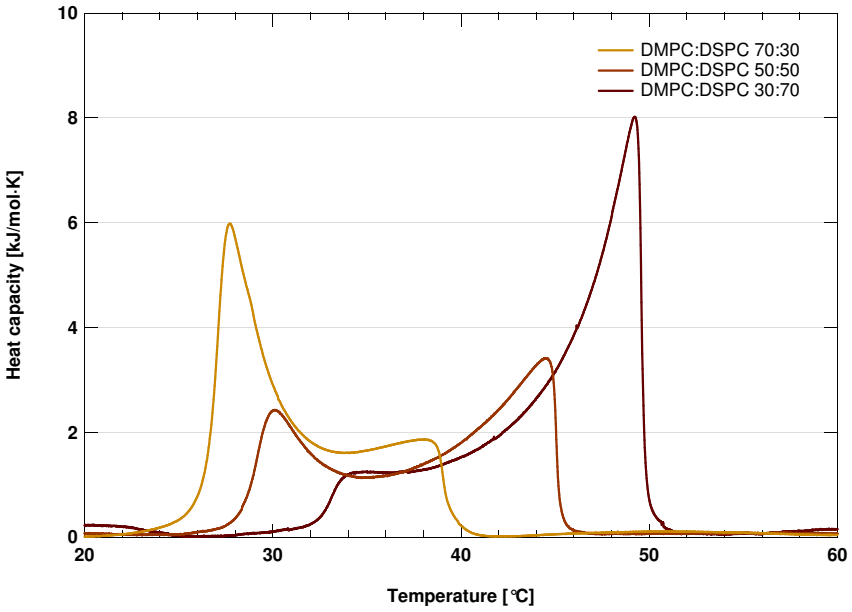

FIG. 31: The excess heat capacity for multilamellar vesicles of DMPC and DSPC. Note that the baseline subtraction was not perfect, resulting in a somewhat uneven baseline. This data was provided by Thomas Heimburg, NBI, University of Copenhagen.

7 Experimental Results

This section presents all of the results from the FCS experiments.

7.1 Fluorescence correlation spectroscopy

The primary focus of the experimental work was the study of permeation rates through synthetic phospholipid membranes, with the use of fluorescence correlation spectroscopy.

While other methods can (and have been) used to measure permeation rates, no-one has successfully used FCS to do this and published it.

The basic idea behind these measurements is that the characteristic permeation rates of the lipid membranes can be determined by analysing the time evolution of the measured correlation curves (see Fig. (32)).

From such curves one can obtain the average number of dyes trapped per vesicle, $B(t)$, which will follow an exponential decay to zero, provided the concentrations are sufficiently low to neglect dyes reentering the vesicles (see Fig. (33)).

If the leakage is less than total (e.g. due to dyes sticking to the vesicles or aggregating inside them), the $B(t)$ curve will go to some constant, non-zero value.

7.2 Rhodamine 6G permeation

The majority of the FCS studies were on the permeation rates of rhodamine 6G chloride out of large unilamellar vesicles made from DPPC and slight amounts of DPPG (a negatively charged lipid, which was used to prevent the vesicles from aggregating or fusing together).

7.2.1 Control by temperature

A systematic series of measurements of permeability rates, k_p, as a function of temperature was carried out. The results are shown in Fig. (34) and proved to be in accordance with the previous findings (see Papahadjopoulos et al. (1973), Corvera et al. (1992) and Heimburg (2007)).

What is not shown in the figure is that the characteristic permeation time scale was on the order of weeks or even months when the system was at 5°C, and on the order of days when at 25°C. The fastest time scale shown is approximately 100 seconds, but is quite likely to be faster as this was on the border of what could be reliably measured. It was estimated that the fastest time scale was on the order of tens of seconds or even faster, so by changing the temperature by $\approx 13\%$ (from 5°C to 41°C), the permeation rate could be changed by more than six orders of magnitude.

However, making measurements close to or above the phase transition turned out to be troublesome. This was due to the very fast permeation rate in the phase transition, which was on a time scale of less than a minute. This made it impossible to make reliable measurements, as everything had leaked out before the system had settled enough (turbulence, convection, and rhodamine sticking to the cuvette walls, tended to disrupt the measurements for the first couple of minutes) to record reliable correlation curves.

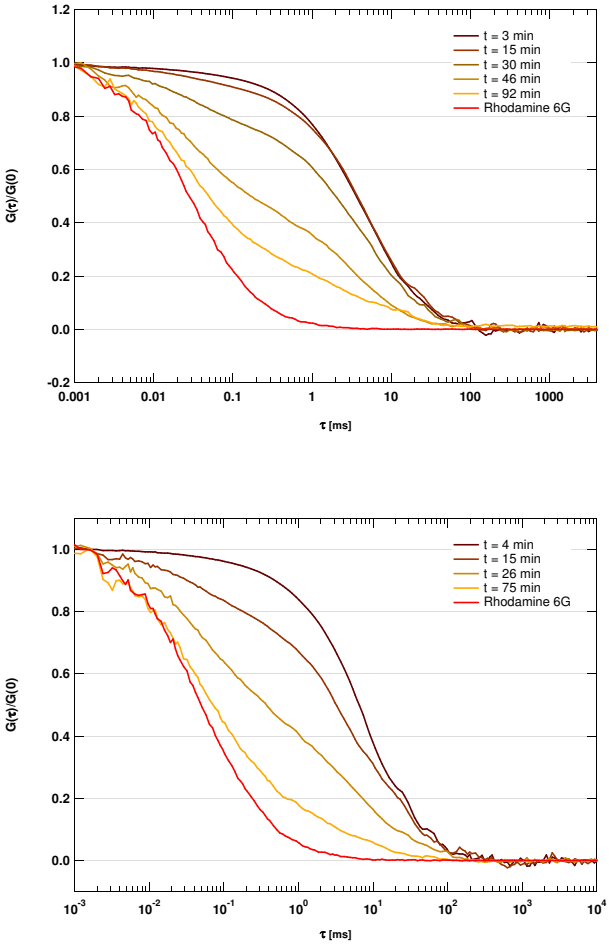

FIG. 32: The observed evolution of the correlation curve, $G(\tau)$. As time goes by, dye leaks out of the vesicles and this fast diffusing population appears as a second bump on the measured correlation curves. In an ideal experiment all of the dyes would be released, making the end result a normal correlation curve of the dye in free solution. The red correlation curve for the rhodamine was not part of this data series, but is simply shown as a reference. *Top:* 38.4°C. *Bottom:* 39.3°C.

The few permeation rates above the phase transition were obtained by disregarding an initial quick permeation time (caused by the finite time it took to heat the sample through the transition), and only fitting to the slowly decaying tail of the $B(t)$ curves. Consequently, there is an inherent uncertainty in these numbers as the permeation rates were a combination of several permeation rates.

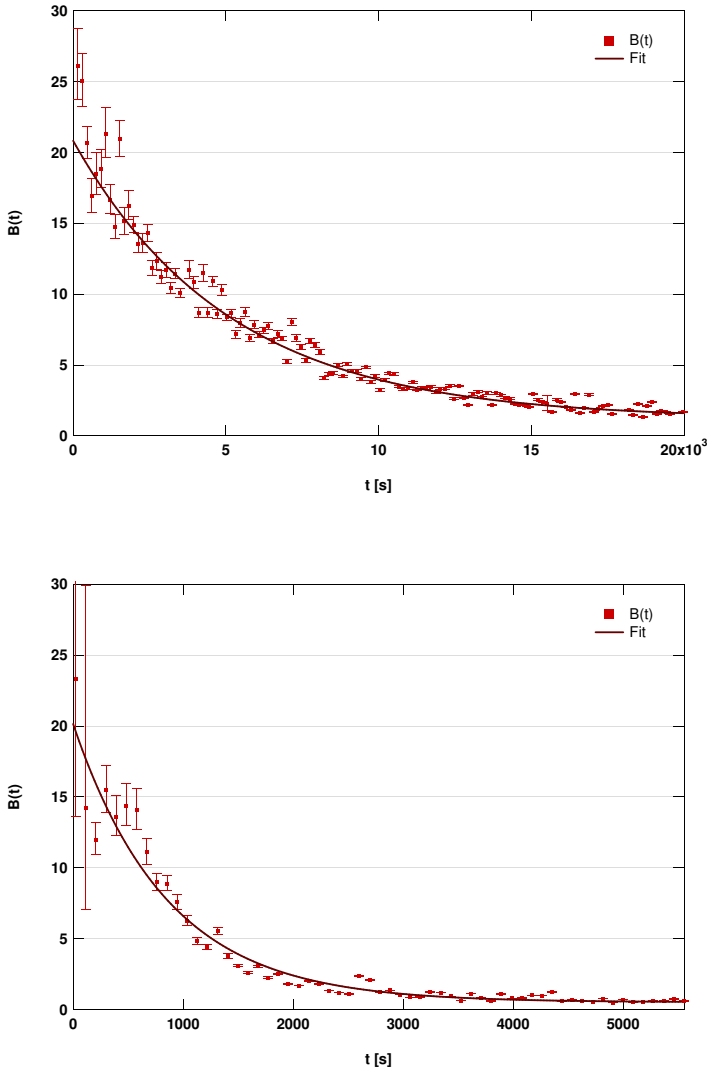

FIG. 33: The evolution of the average number of rhodamine molecules per vesicle, $B(t)$, at two different temperatures. The solid lines are least squares fit of an exponential function with an offset. *Top:* 37.1°C. $\tau_p = k_p^{-1} = 4.8 \cdot 10^3$ sec. *Bottom:* 38.4°C. $\tau_p = k_p^{-1} = 1.2 \cdot 10^3$ sec.

7.2.2 Control by anaesthetics

A number of experiments at constant temperature were also performed. Both of the thermodynamic theories predict that the transmembrane permeability is determined strongly coupled to the thermodynamic state of the membrane, so a change in any of the membrane variables should influence the observed permeation rate. To demonstrate this effect we chose to alter the state of the system by adding of one of two kinds of general anaesthetics, namely 1-octanol

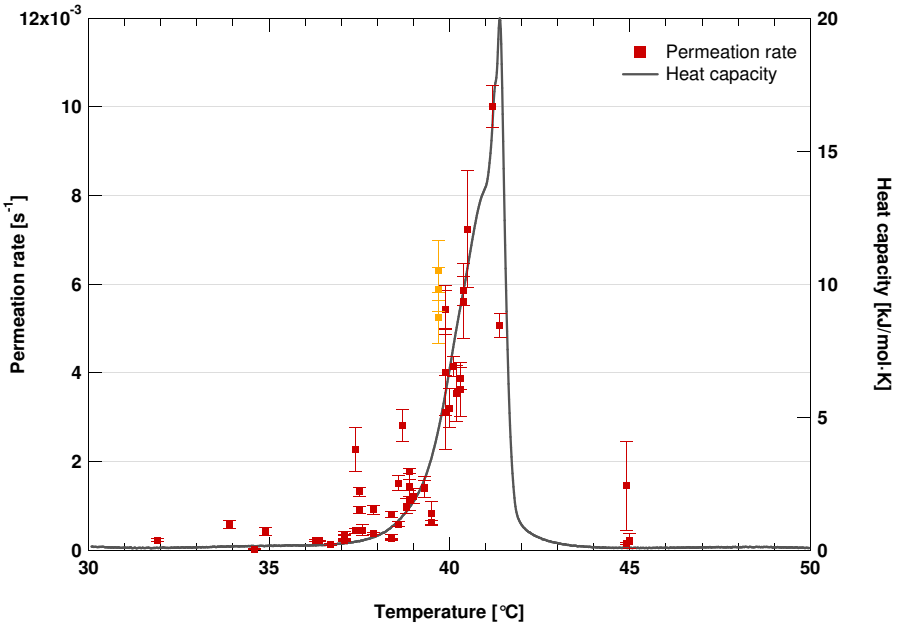

FIG. 34: The measured permeability rates, k_p, and the excess heat capacity, c_p, as functions of temperature. The error bars show the uncertainties in the least squares fit to the $B(t)$ curves, and do not take into account any of the other sources of error. The uncertainty in the temperature is about ± 0.5K. The three yellow data points were obtained on the same day, without new temperature measurements being made between the experiments. Thus if the temperature measurement was off, all three points should be shifted together. Lastly, the three data points above the phase transition are a whole lot more uncertain than their error bars indicate (see text).

and halothane (see Fig. (4)).

From the heat capacity profiles (Fig. (29)) one would expect a significant increase in the permeation rate at temperatures close to (but below) the transition temperature, as the increase in the lateral compressibility will be proportional to the increase in the heat capacity. Similarly, the interfacial area of the domains also increases dramatically when an anaesthetic is added.

As can be seen from Fig. (36) and (35), there was a large increase in the permeation rates, in good agreement with what one would expect from the thermodynamic data (Fig. (29)).

Additionally, a few experiments of a slightly different character were also performed. Here the temperature was also kept constant at a temperature several degrees below the transition. Then after approximately one hour, the state of the system was changed "instantaneously" by either adding octanol to the sample, or by increasing the temperature to $\approx 45°$C as quickly as possible. Both changes caused an abrupt shift in the permeation rate as can be seen from Fig. (37).

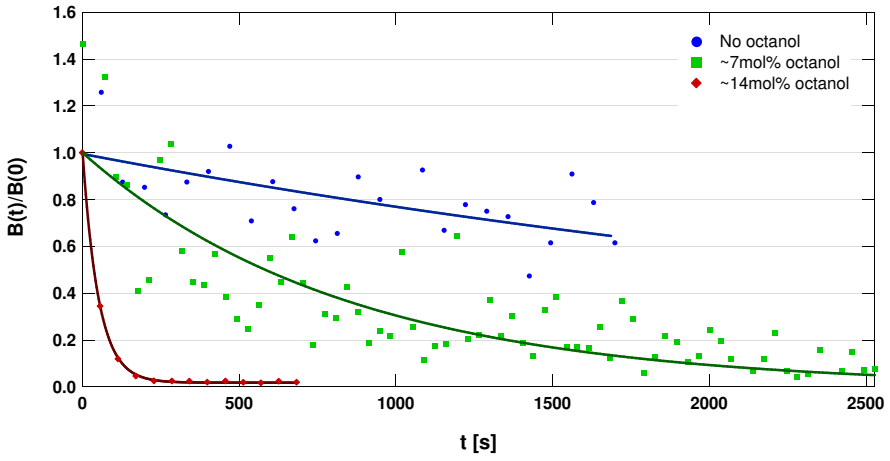

FIG. 35: Measured $B(t)$ with varying amounts of 1-octanol in the membranes at $T = 37.6°C$. The solid lines are least squares fit of an exponential function with an offset.

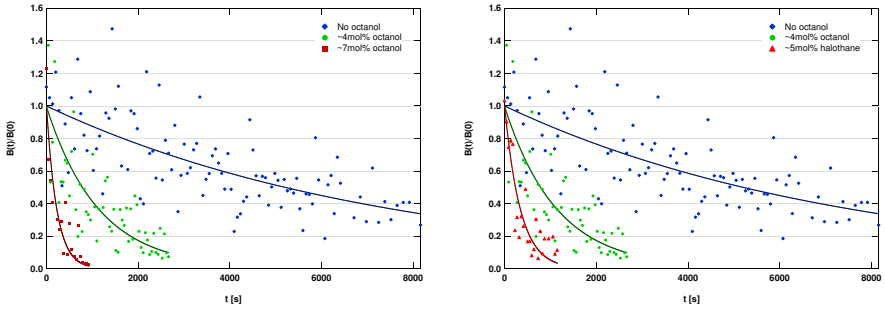

FIG. 36: Measured $B(t)$ with varying amounts of anaesthetics in the membranes at $T = 36.3°C$. The solid lines are least squares fit of an exponential function with an offset.

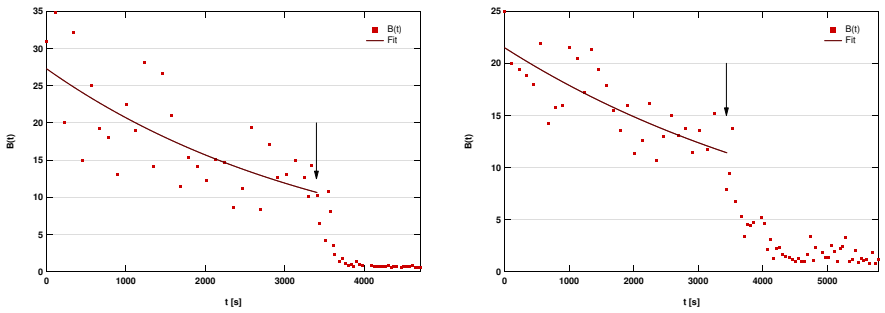

FIG. 37: Measured $B(t)$ at $T = 37.1°C$. *Left:* Sudden increase in temperature. *Right:* Sudden addition of 1-octanol. The arrows indicate when the changes were made.

7.3 Tetramethylrhodamine dextran permeation

As mentioned above, the permeation rates of rhodamine 6G chloride seems to be on the order of seconds or tens of seconds in the phase transition, which made it next to impossible to make reliable measurements above the phase transition, as everything had been released during the heating of the sample.

To circumvent this problem, we tried to repeat the experiment with tetramethylrhodamine dextran (approx. 3000 g/mol) instead of rhodamine 6G chloride (479.02 g/mol), as the larger molecule diffuse more slowly and would only be likely to leak through very large (and thus less probable) pores.

Unfortunately, the time scale of the permeation at the transition midpoint turned out to be on the order of days (see Fig. (38)). Consequently, these measurements were aborted after a few days, as this was too impractical to be of use.

The stability of these measurements did, however, provide one critical piece of information, namely that the vesicles did not break apart or fuse together when in the phase transition or when repeatedly heated and cooled.

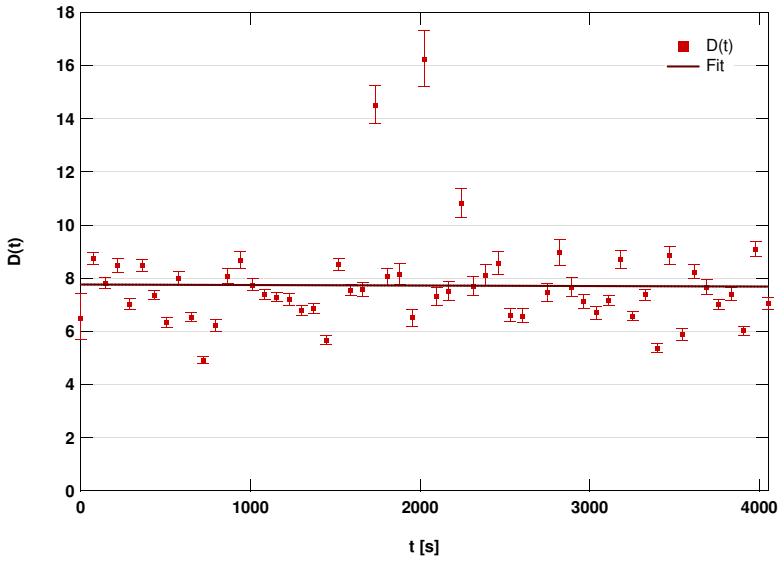

FIG. 38: The average number of dextran molecules per vesicle, $D(t)$, as a function of time at $T = 41.1°\mathrm{C}$. As can be seen, no leakage could be detected after one hour. Repeated heating and cooling through the transition did not alter $D(t)$ noticeably.

8 Simulation Results

As explained earlier, a major aim of the project was to compare Monte Carlo simulations with experiment. One of the great strengths of such simulations is that they can give information about the spatial structure of the membrane, making it possible to visualise membrane heterogeneity and domain formation directly.

Unless otherwise noted, all simulations were performed on $100 \times 100 + 30$ lattices, where the incomplete row with 30 lipids was there to minimise the influence of the lattice oddity (described in Appendix E).

The typical simulation was allowed to equilibrate for $N_{EC} = 2 \cdot 10^4$ to 10^5 Monte Carlo cycles two times, first without pores involved, and then again with pore formation allowed. The actual sampling was then done over another $N_{SC} = 10^5$ to $5 \cdot 10^5$ cycles. Most of the calculated curves presented in this thesis were in addition averaged over several independent runs.

8.1 One-component system

The main focus of the numerical work was on simulation of a one-component system mimicking a DPPC membrane.

The parameter values used in the simulations are shown in Table (1). The values for ΔH, ΔS and ω_{fg} are identical to those used in Ivanova et al. (2003). The choice that $\omega_{af} = 0$ (i.e. ideal mixing with the fluid phase) and $\omega_{ag} = \omega_{fg}$ is based on the considerations made in the same article and in Ivanova and Heimburg (2001).

The results from these simulations were in good qualitative agreement with the experiments, in that they show a pronounced peak in the phase transition. While the program does include a number of free parameters (namely the interaction parameters between pores and lipids), a number of insights can be derived from the output.

Fig. (41) and Fig. (42) shows how the permeability (number of pores) of the system depends on the cooperativity, ω_{fg}. As can be seen, a lowering of the cooperativity results in a higher number of fluid/gel interactions (i.e. more ramified domains), but is also seen to reduce the maximum heat capacity (and consequently the lateral compressibility). This clearly shows that in this model the permeability of the system is strongly coupled to the lateral compressibility and not the interfacial area of the domains (which is closely related to the number of fluid/gel interactions in the system).

Typical microscopic configurations for different temperatures are shown in Fig. (40). Domains on all scales – from pairs to cluster on a similar scale as the system – can be observed. Naturally, a given cluster fluctuates in size as time goes by, as expected.

A couple of difficulties were encountered when these simulations were made. Firstly, black lipid membrane experiments have shown that the density of pores in a DPPC bilayer is only around 50 pores per mm^2 of membrane surface, even at the transition point (Antonov et al. (2005)). As this area is more than eight orders of magnitude larger than a typical simulations ($\approx 5 \cdot 10^5 \text{Å}^2$) there should only be a pore around one out of every four million time steps. This, of course, will require that the simulation runs for a ludicrously long time, in order to get anything resembling decent statistics. Therefore, it was decided to

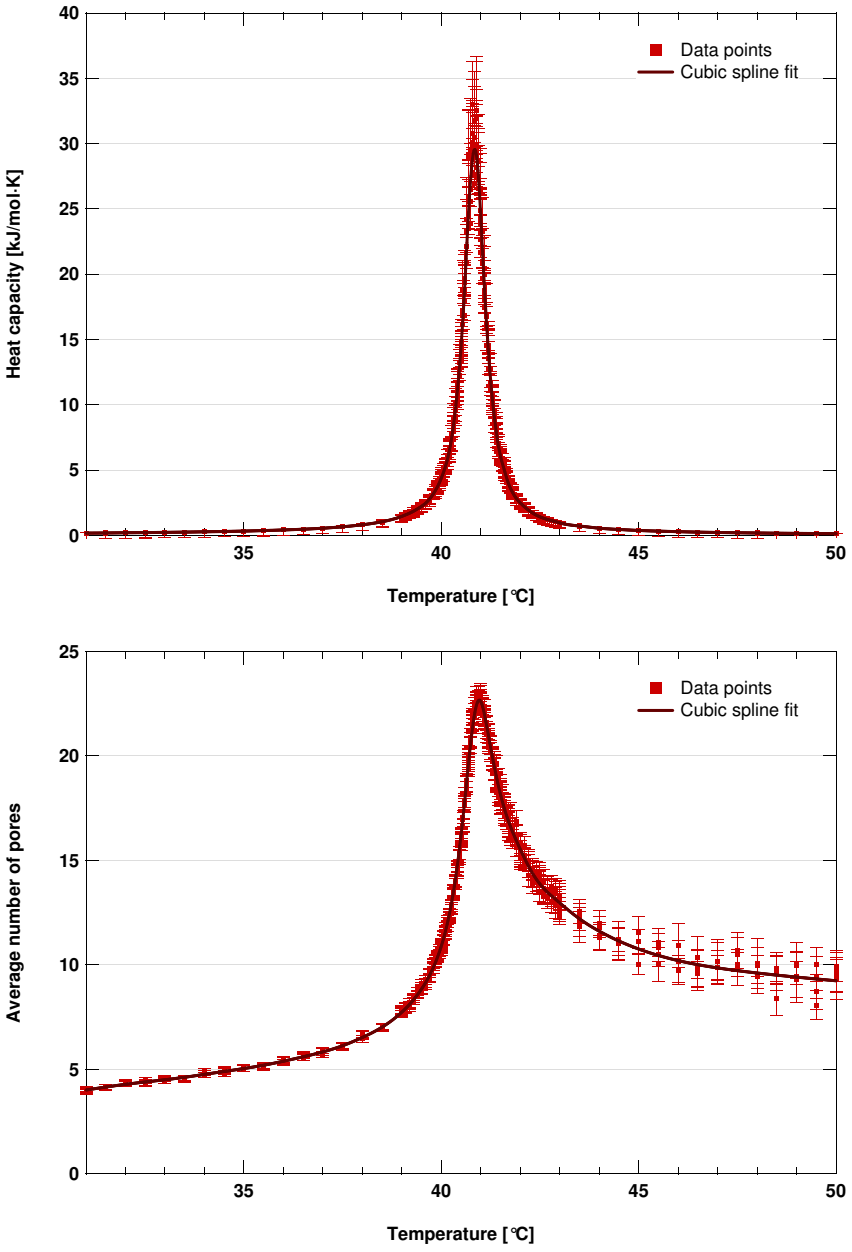

FIG. 39: Simulated one-component system (DPPC) with error bars calculated via the blocking method described in Appendix F. The solid line is a cubic spline fit. *Top:* Simulated excess heat capacity. *Bottom:* Simulated permeability profile (i.e. the average number of pores, which is assumed to be proportional to the probability of crossing, $P(T)$).

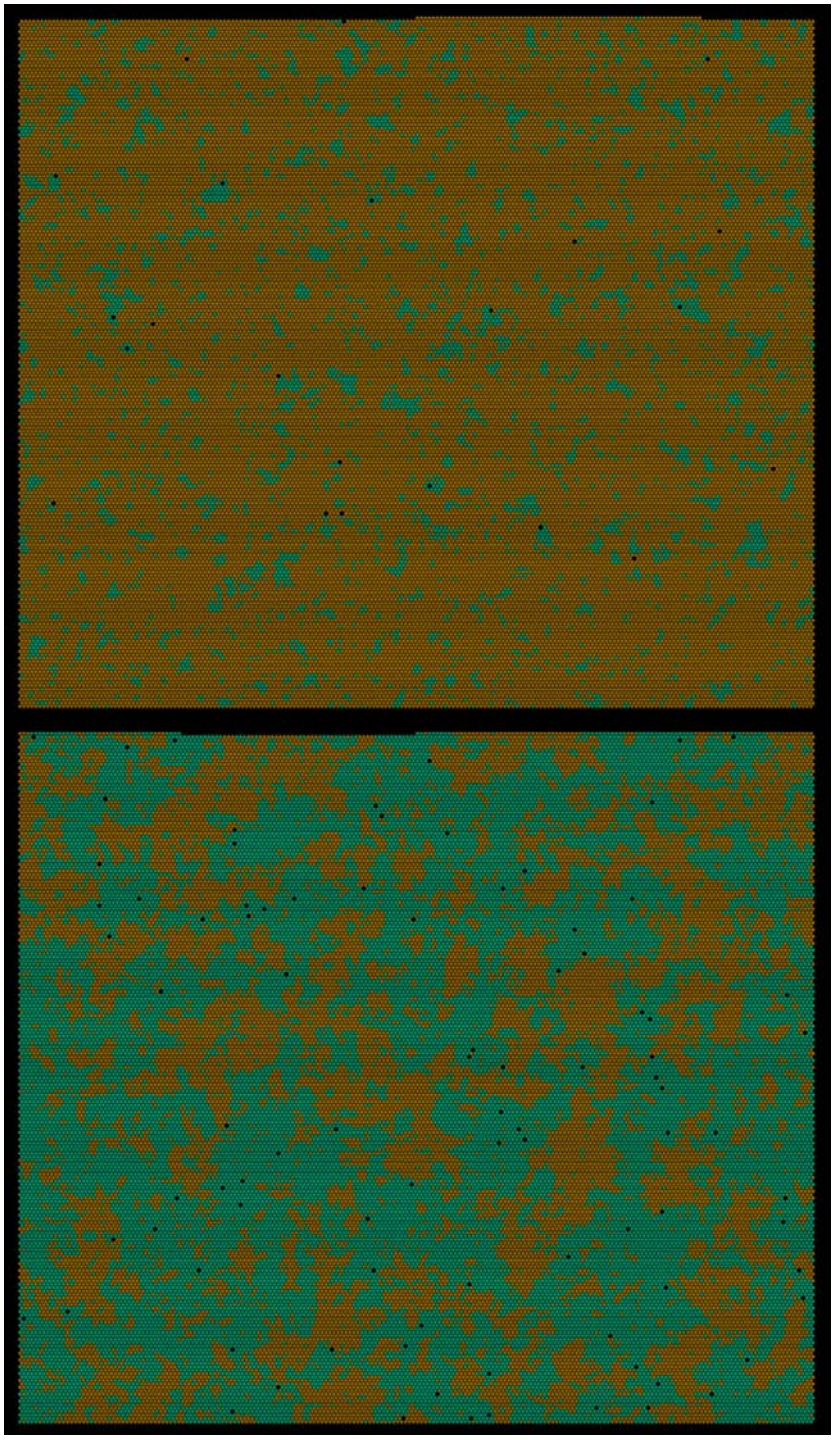

FIG. 40: Snapshots of the system at two different temperatures (*top:* $T = 39°\mathrm{C}$, *bottom:* $T = 41°\mathrm{C}$). Gel state lipids are brownish, fluid state turquoise, and pores black.

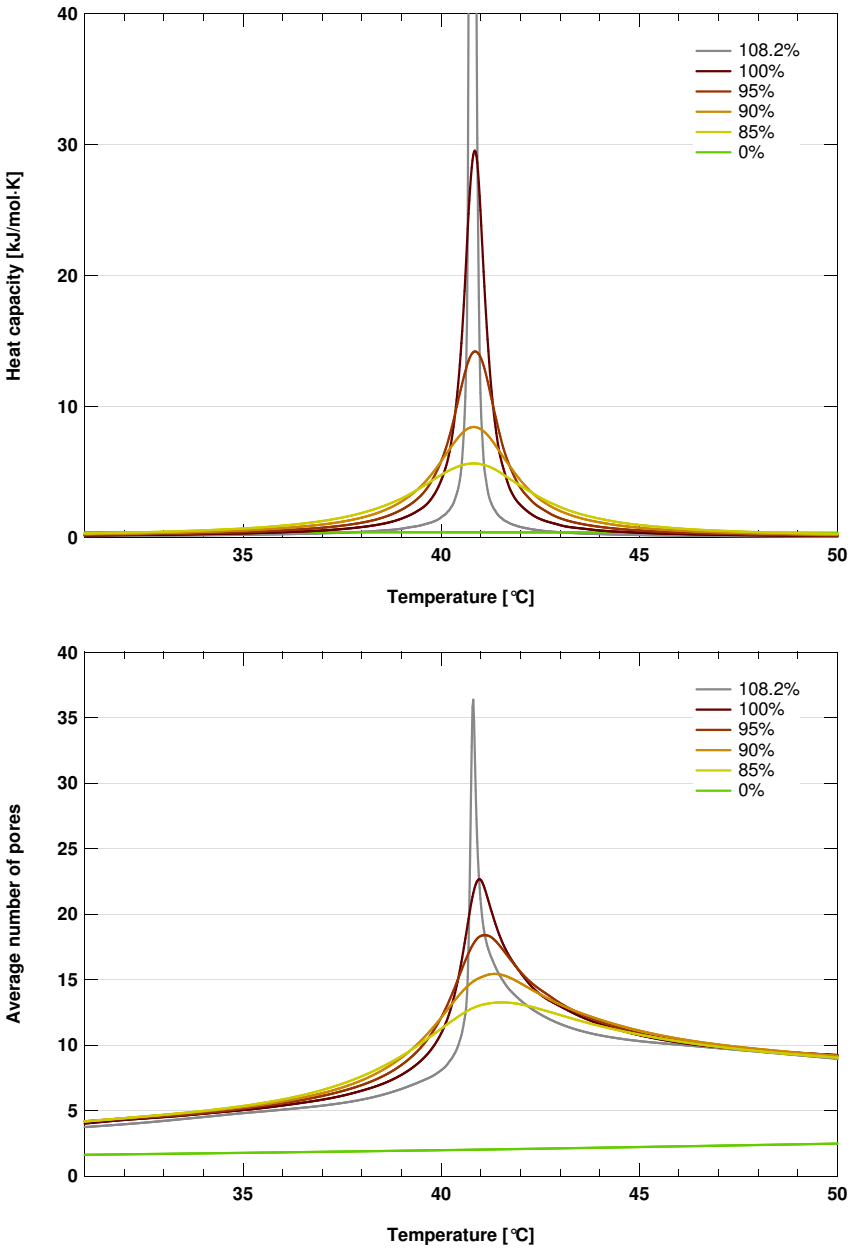

FIG. 41: Simulated one-component system (DPPC) with varying cooperativity. The reference value (100%) is $\omega_{fg} = 1326$J/mol. The 108.2% corresponds to $\omega_{fg} = 1434.77$J/mol, i.e. the critical value from Eq. (93). *Top:* The simulated excess heat capacities. *Bottom:* The average number of pores in a system with 10030 lipids. The slight shifts in the locations of the maxima are caused by the differences in the average number of pores.

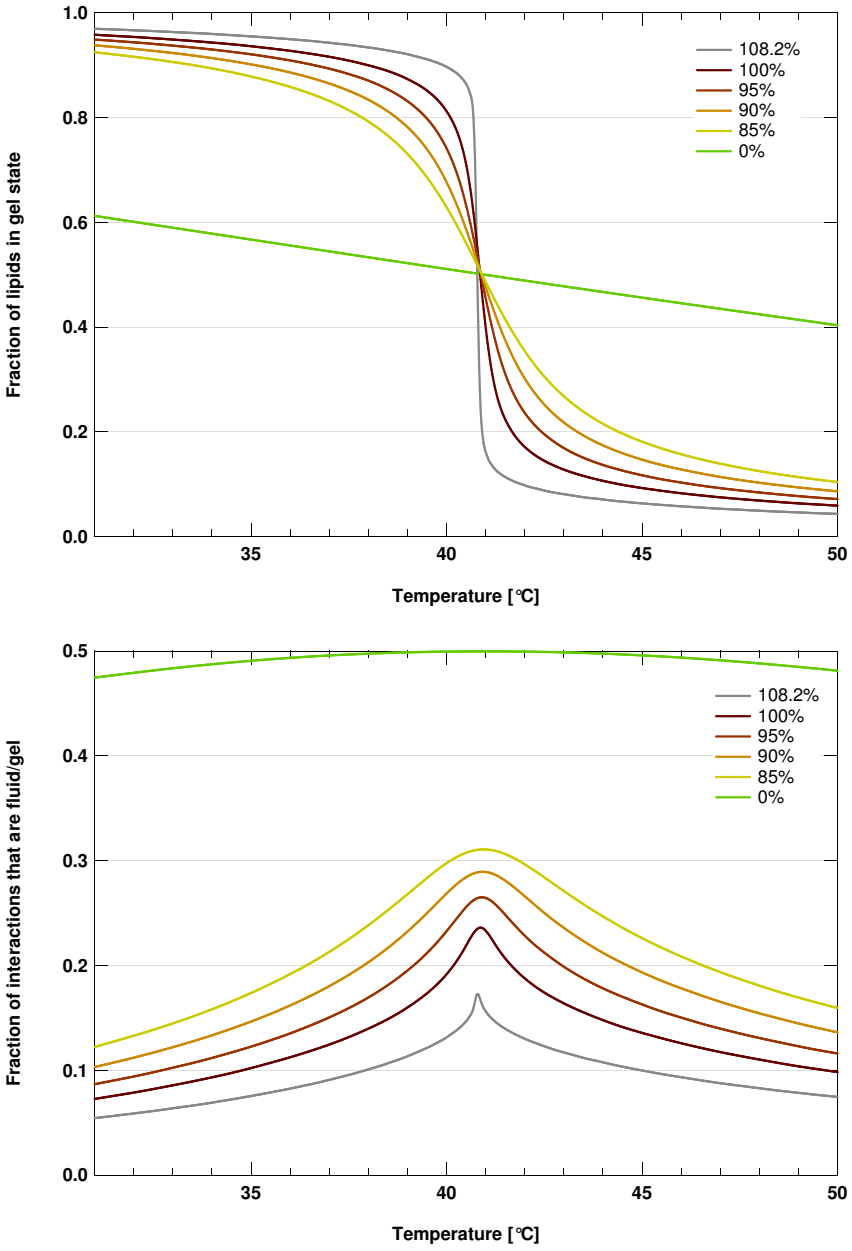

FIG. 42: *Top:* Fraction of the lipids that are in the gel state. *Bottom:* Fraction of the nearest neighbour interactions that are fluid/gel interactions. As can be seen from this figure, lipids tend to have neighbours in the same state for $\omega_{fg} > 0$ as expected. In other words, the higher the cooperativity, the lower the degree of ramification of the domains. Shown for different values of the cooperativity parameter as in Fig. (41).

Parameter	Value used [J/mol]
ΔH	36400
ΔS	115.87 K^{-1}
ω_{fg}	1326.0
ω_{pf}	2254.4
ω_{pg}	4508.0
ω_{pa}	13260.0
ω_{af}	0.0
ω_{ag}	1326.0

TABLE 1: Parameter values used in the simulations of DPPC, unless otherwise noted. Note that ω_{fg} is close to the critical value given in Eq. (93).

lower the energy cost of forming a pore, in order to have a few dozen pores in the membrane in the phase transition. This, however, caused other problems, as the interaction between pores and lipids was still very unfavourable, which means that the pores would tend to aggregate. This sometimes led to runaway aggregation, which would take system out of equilibrium and cause the program to crash. Lowering the interaction energies sufficiently to alleviate this problem would in turn result in very large numbers of pores, which would then distort the heat capacity profile significantly, which was not acceptable either.

In the end, I opted for a set of parameters (see Table (1)) which allowed for enough pores to give decent statistics, but still low enough to not influence the heat capacity of the system significantly (see Fig. (43)). The "runaway aggregation problem" was circumvented by disallowing pore-pore interactions. While unphysical and inelegant, the effect on the results should be negligible, as the pore density was so low as to make pore-pore interactions insignificant (as they seem to be in real membranes).

8.1.1 Lateral compressibility

As can be seen from Fig. (44), the simulated heat capacity is proportional to the lateral compressibility near the phase transition, as expected from experiments (Ebel et al. (2001)). For a two-state model this is hardly surprising, as the enthalpy fluctuations are dominated by the changes in the chain enthalpy ($\approx$ 36kJ/mol), and not the nearest neighbour interactions ($\leq 6 \cdot 1326 \approx$ 8kJ/mol).

8.1.2 Pore formation

The exact appearance of the pores vs. temperature profiles will of course depend on the choice of parameters (see Fig. (45)). However, for a large range of interaction values, the permeability profile shows a strong peak at the phase transition temperature, and the position of this peak was found to always follow the peak of the heat capacity profile.

As can be seen from Fig. (46) the distribution of pores at a given temperature is governed by a Poisson distribution, which shows the following two things: 1) the probability of forming a pore is very small, and 2) the pores form independently of each other, as required to follow such a probability distribution.

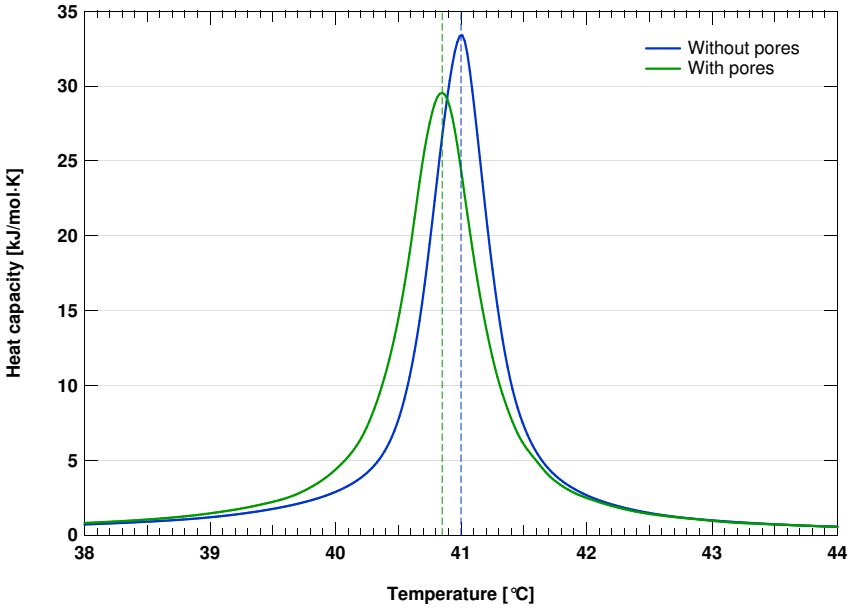

FIG. 43: Comparison of the calculated heat capacity profiles for simulations with and without pore formation involved. As can be seen from the figure, there is a shift of about -0.15K in the transition temperature as well as a slight broadening of the profile. This is due to the difference in the pore interaction energies with fluids and gels.

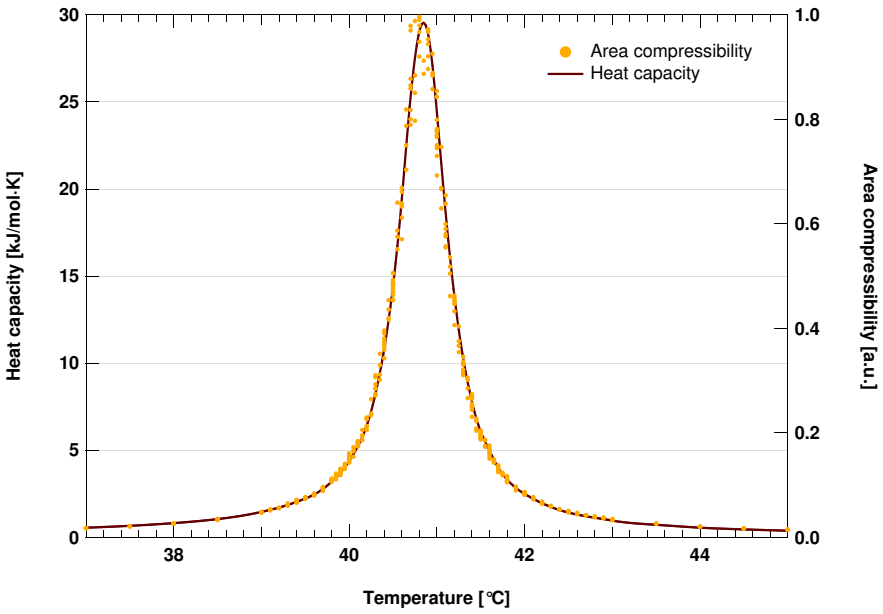

FIG. 44: Comparison of the heat capacity and area compressibility from the simulations of DPPC.

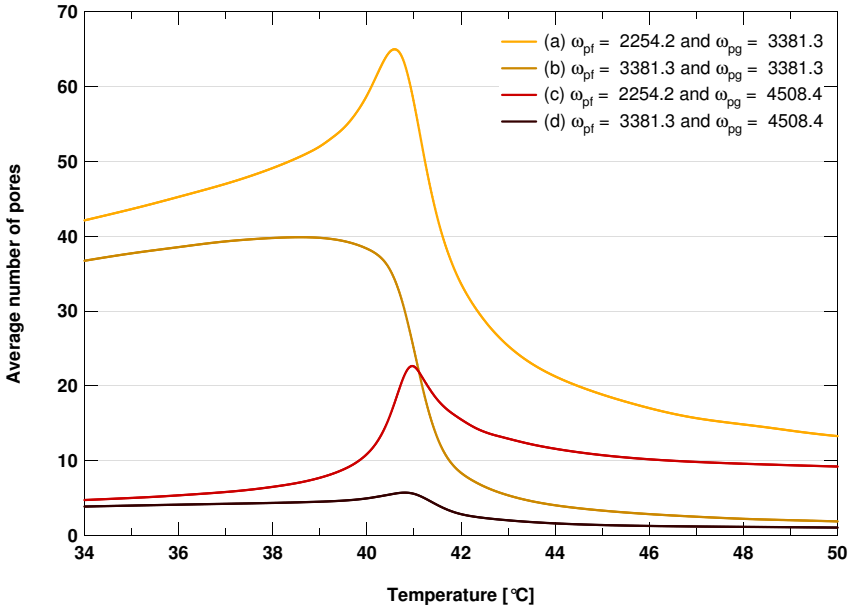

FIG. 45: Comparison of the permeability curves different values of the interaction parameters between lipids and pores. All values are in J/mol. Curve *(c)* was the normal choice for the simulations.

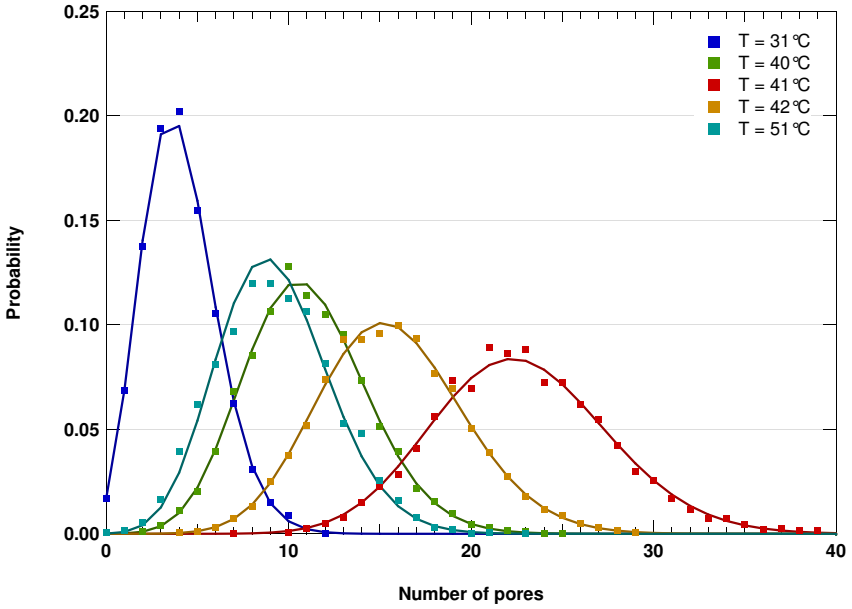

FIG. 46: Distribution of pores at different temperatures in a simulation of DPPC. The squares are the observed distributions, while the solid lines are Poisson distributions.

8.1.3 Influence of anaesthetics

Including a non-melting species in the system (an "anaesthetic") provided further insights into the mechanisms at work, and could be compared to the experimental findings.

The anaesthetics that are located at the interfaces between domains and bulk will lower the overall line tension, and causes a broadening of the heat capacity, and – depending on how well it mixes with either phase – a melting point depression (Ivanova and Heimburg (2001)).

As can be seen from Fig. (48) the permeability curve follows the heat capacity profiles, being both shifted and broadened in a similar fashion.

These results are consistent with the experimental finding, that the permeability at sub-transition temperatures can be significantly enhanced by addition of an anaesthetic. The data also supports the idea that it is the fluctuations of the whole system that determines the likelihood of the formation of a pore.

The interactions between the pores and the anaesthetics were set to be extremely unfavourable (as would be the case for a strongly hydrophobic molecule), so as to not have the anaesthetics serve as nucleation points for pore formation. For less unfavourable interactions between the pores and the anaesthetics this was actually the case, as can be seen from the bottom most graph in Fig. (48).

8.2 Beyond one-component systems

In addition to the simulations of the DPPC membranes, a couple of Monte Carlo simulations of a two-component system were also performed. The results are shown in Fig. (50) and (51).

Determining a good set of values for the interaction parameters can be a very time-consuming process, so I settled for something that gave the same qualitative behaviour as a mixture of DMPC and DSPC. As can be seen from Fig. (31) and (51), the simulated results are fair, but not in perfect agreement with the DSC measurements. However, they are close enough to give some confidence in the numerical results. Also, it should be noted that the experimental heat capacity profiles were obtained from a multilamellar system, which influences the exact shape somewhat. In particular, the onset and termination of the phase transition are sharper in a multilamellar system than in a unilamellar one.

Due to the limited time frame of the project, these simulations were not optimised and studied to the same extent as the one-component ones, and should therefore only be seen as a proof of concept.

As can be seen from the figures, the two-component system qualitatively follows the same behaviour as the one-component one, with a significant increase in the average number of pores in the phase transition. The sharp peaks in the heat capacity profile do not seem to appear in the permeability profile, though that could simply be a matter of adjusting the interaction parameters.

As mentioned in Sec. (5.4.1) the simulations of two-component system can also provide information about the local fluctuations of the system[18]. It is immediately obvious from Fig. (52) that the local fluctuations are strongest

[18] Actually, it is also possible to do this with one-component systems, though it requires more care as the domains are not stable entities in such systems. Therefore one is limited to averaging over time scales much shorter than the typical lifetime of a domain.

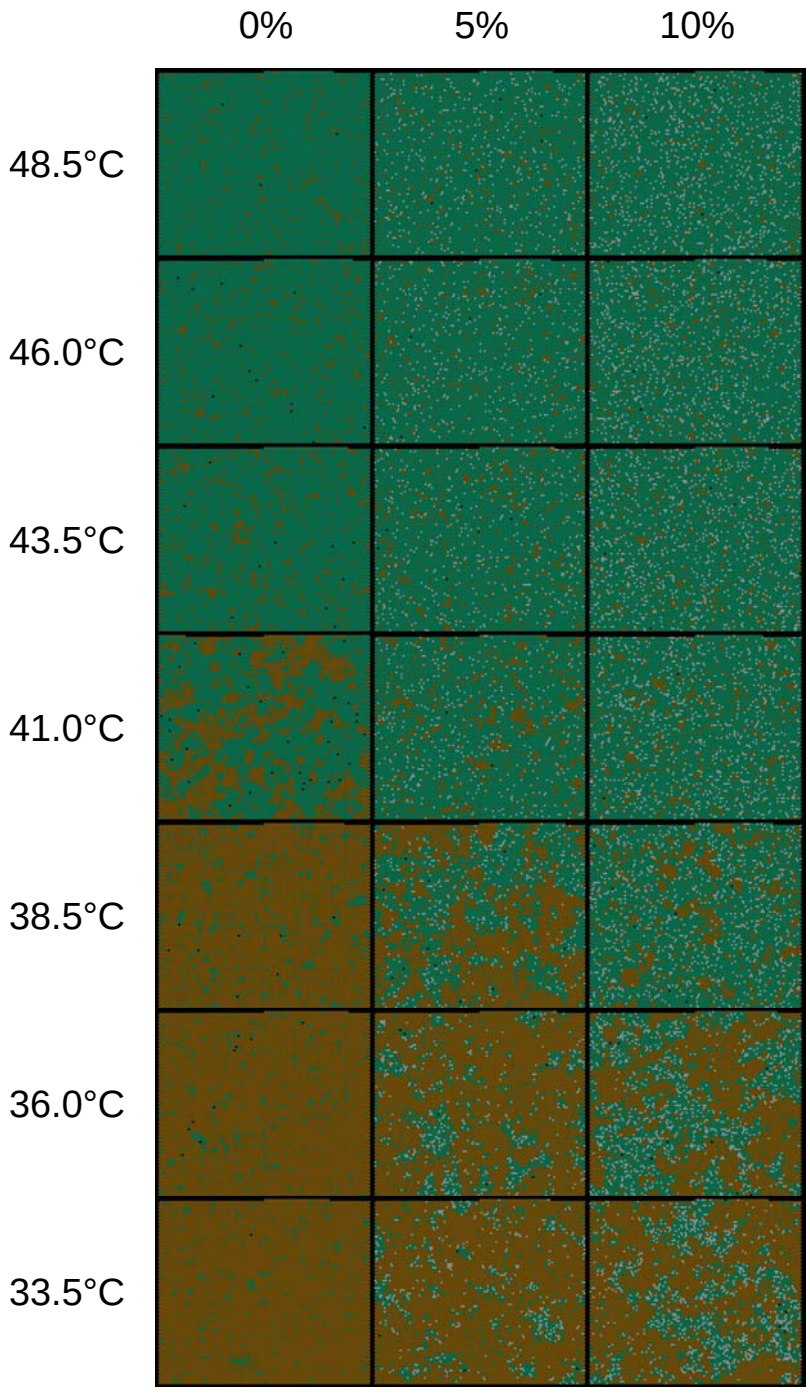

FIG. 47: Snapshots of the system at different temperatures and anaesthetic concentrations. Gel state lipids are brownish, fluid state turquoise, anaesthetics white, and pores black. Note how the onset of domain formation is influenced by the anaesthetics.

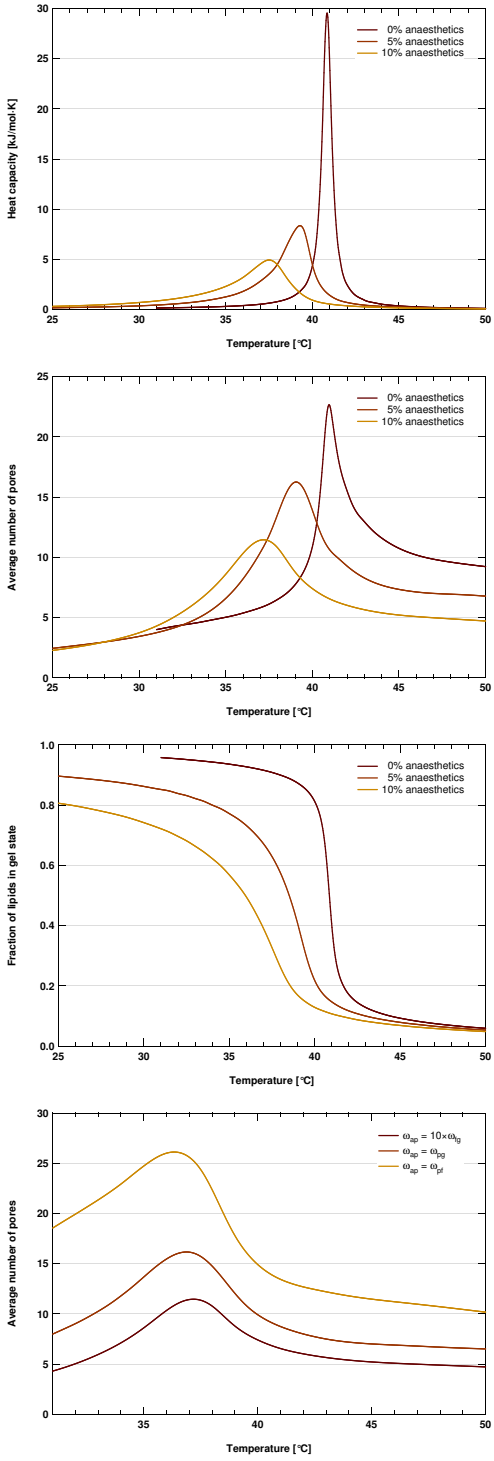

FIG. 48: Simulated one-component system (DPPC) where varying amounts (0%, 5%, and 10%) of the lipids have been replaced by unmeltable particles (”anaesthetics”).

Parameter	Value used [J/mol]
ΔH_1	26330
ΔH_2	50740
ΔS_1	88.61 K^{-1}
ΔS_2	154.72 K^{-1}
$\omega_{f_1 g_1}$	1353.0
$\omega_{f_2 g_2}$	1474.0
$\omega_{f_1 f_2}$	414.15
$\omega_{g_1 g_2}$	940.85
$\omega_{f_1 g_2}$	1887.6
$\omega_{f_2 g_1}$	1702.8
$\omega_{p f_1}$	2254.2
$\omega_{p g_1}$	4508.4
$\omega_{p f_2}$	2254.2
$\omega_{p g_2}$	4508.4

TABLE 2: Unless otherwise noted, these were the parameter values used in the Monte Carlo simulations of the two-component system. The values for the melting enthalpies and entropies were taken from Seeger (2006).

near the domain boundaries, which means that one would expect pore formation to occur close to such interfaces. Similarly, it has been shown that peptides and proteins (and other membrane-soluble molecules) strongly affect the fluctuations in their immediate environment and thereby the local compressibility (and thus also the permeability), elastic constants and relaxation times (Ivanova and Heimburg (2001)). In effect this means that the role of such molecules need not be exclusive defined by their intrinsic function, but also by their influence on the physical properties of their immediate environment.

8.2.1 Biological complexity

Simulation of a system closer to the complexity of a biological membrane was also carried out (see Fig. (54)). Here, thirteen different lipid species were used (in equal amounts), and all interactions were based purely on the hydrophobic matching of the lipids, using the values from the DPPC simulations as a guideline. This was of course a necessity, as fitting to experimental data would be daunting prospect, since there are 325 different interactions to determine for a system with just 13 lipid species!

A few simulations of a 13-component system which also included a fraction of unsaturated lipids were also performed. This was modelled by reducing the melting points of the unsaturated lipids by 50K, but keeping the interactions as for the saturated lipids (data not shown).

A detailed analysis of these simulations is quite beyond the scope of this thesis, but the results seems promising in that the system shows large scale domain formation and exhibits a broad phase transition, not unlike what has found for biological membranes. Pore formation was not implemented in these simulations due to lack of time.

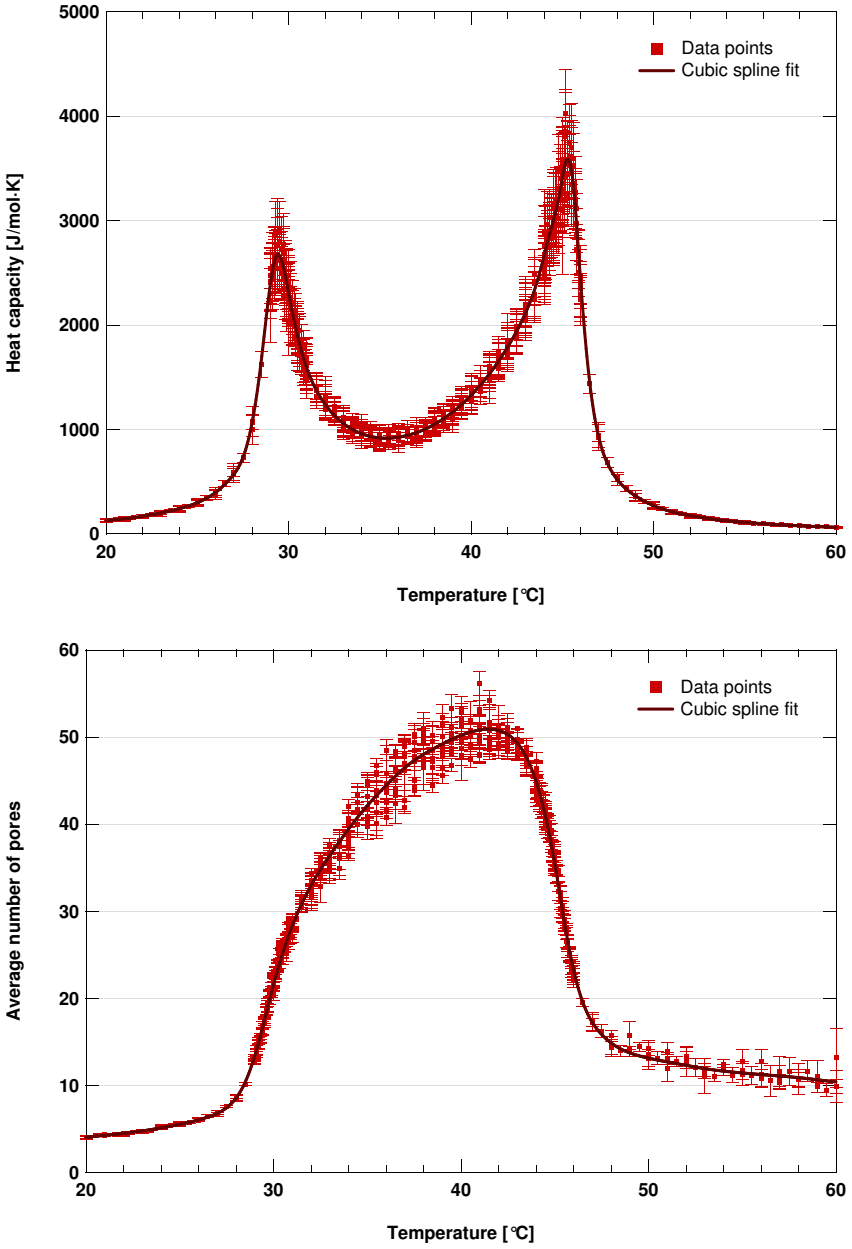

FIG. 49: Simulated two-component system (50:50) with error bars calculated via the blocking method described in Appendix F. The solid lines are cubic spline fits.

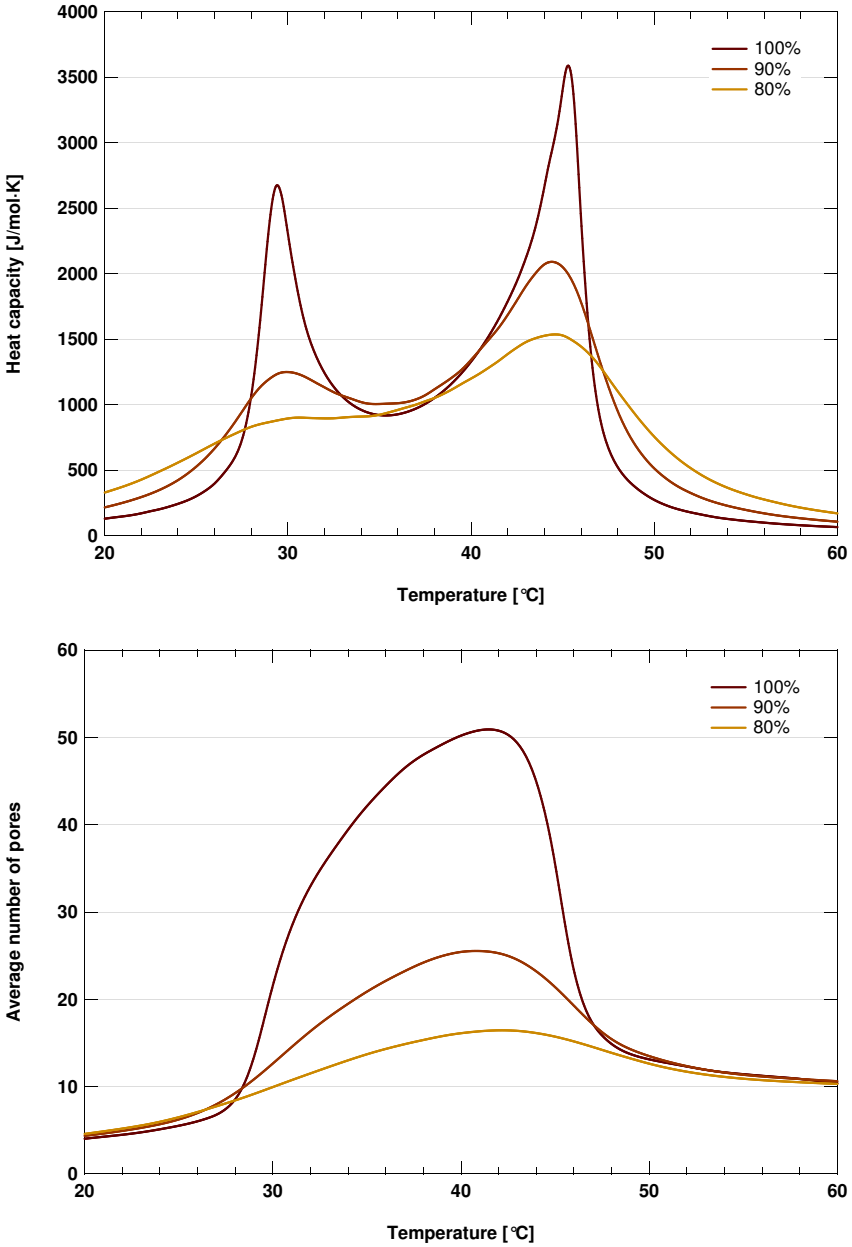

FIG. 50: Simulated two-component system (50:50) with varying values for the fluid/gel interaction parameters. The 100% are the values given in Table (2). As can be seen the average number of pores qualitatively follows changes in the heat capacity profile.

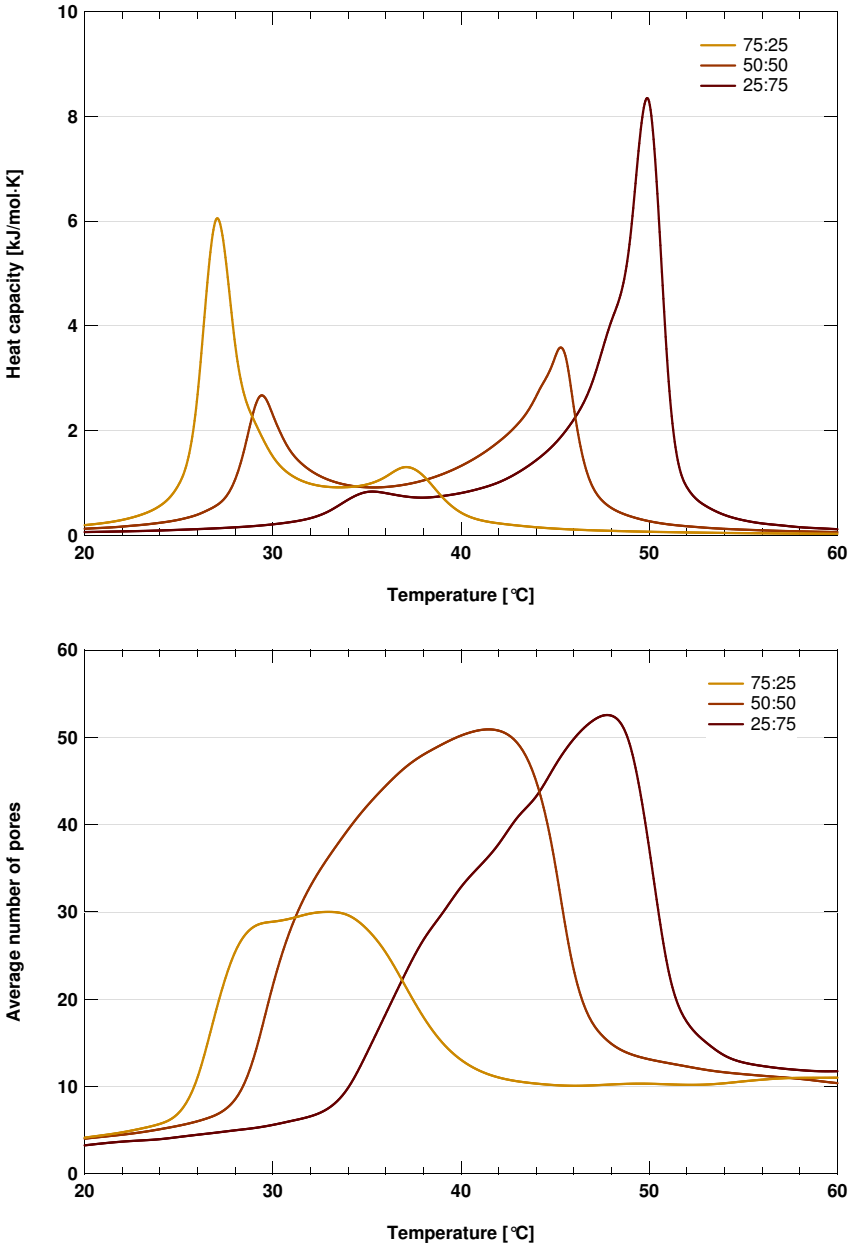

FIG. 51: Simulated two-component system with various mixing ratios. As can be seen the increase in the permeability follows the shifts in the heat capacity profile.

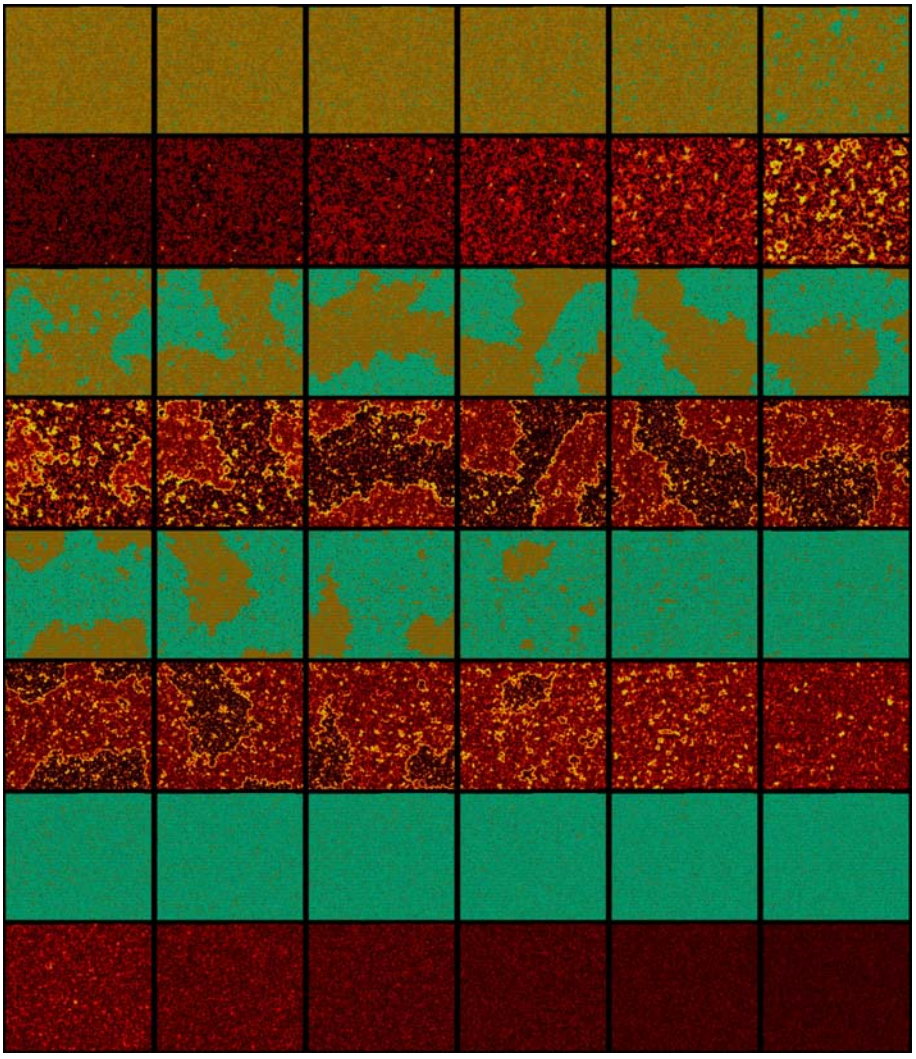

FIG. 52: Domain formation and local fluctuations of a two-component system at different temperatures. The temperature increases linearly from $T = 20°\mathrm{C}$ *(upper left)* to $T = 60°\mathrm{C}$ *(lower right)*. Notice how the fluctuations are strongest in the phase transition and at the interfaces between domains and the bulk.

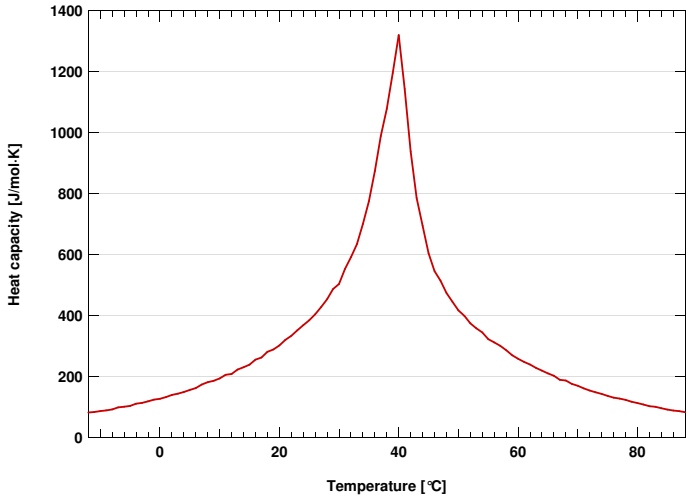

FIG. 53: Simulated heat capacity of a system comprised of 13 different lipid species (equal amounts; chain lengths varying from 10–22). Interactions between lipids were based solely on their hydrophobic matching.

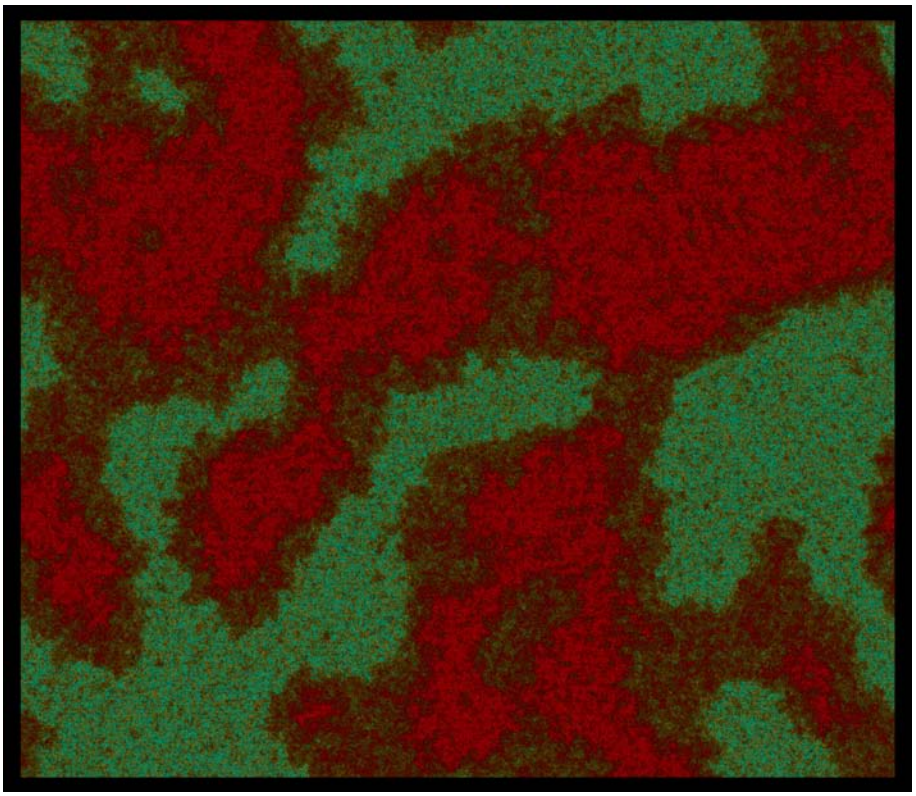

FIG. 54: Snapshot of a 13-component system with 1000×1000 lipids at $T = 1°\mathrm{C}$. Red and brown nuances are gel state lipids, while green and turquoise are fluid state lipids. Notice the broadness and the pronounced wings of the transition.

Part IV
Conclusions and Perspectives

9 Conclusions

The primary aim of this thesis was to gain a better understanding of how the melting transition influences the transmembrane permeability of artificial membranes through both experiments and simulations.

It was shown by use of fluorescence correlation spectroscopy that the permeability of unmodified phospholipid membranes depends strongly on the thermodynamic state of the system, exhibiting a pronounced peak in the transition regime in agreement with previous studies (Papahadjopoulos et al. (1973), Georgallas et al. (1987), Corvera et al. (1992), Heimburg (2007)). This behaviour is likely to be a direct consequence of the enhanced lateral compressibility of the membranes, which leads to spontaneous pore formation.

While there were some experimental difficulties in obtaining a clear-cut permeation rate profile for high temperatures, two central facts were established:

- The characteristic permeation times (inverse rates) for rhodamine 6G chloride through DPPC bilayers could be changed by more than six orders of magnitude by increasing the temperature by only 10%. The observed time scales were on the order of weeks at 5°C, days at $\approx$ 25°C, hours at $\approx$ 35°C, minutes at $\approx$ 40°C, and seconds at $\approx$ 41°C. Above the transition point, the rate was seen to decrease again.

- The permeation rates could similarly be strongly influenced by adjusting another of the intensive thermodynamic variables of the membrane. Here two different membrane-soluble drugs were tested, namely halothane and 1-octanol – both of which are known to be general anaesthetics. While these two drugs are structurally quite different, they had similar effect on the permeation rates, indicating that the enhanced permeability was not due to some special pore forming property of the drug, but rather a more general effect.

Assuming that the numerical simulations contain the essential physics of the system, it was shown that the permeability (i.e. the number of pores in the system) curves seem to qualitatively follow the heat capacity (and hence the lateral compressibility), being both shifted and broadened to a similar degree. This behaviour was demonstrated for a variety of circumstances, such as for different cooperativities, in the presence of anaesthetics, and for two-component systems at various mixing ratios. Within this model, this finding speaks strongly in favour of the compressibility theory.

Taken together with the experimental results and similar studies by other groups, it is expected that any phospholipid bilayer will exhibit a pronounced anomaly in the permeation rates at the chain-melting transition where the thermodynamic fluctuations in the lateral density (area) are strongest.

In conclusion, the findings in this thesis support the notion that the thermodynamic state and fluctuations of the membranes are of critical importance

to their functional properties. It provides a mechanism for regulating the transmembrane transport which is based on the physics of the membrane as a thermodynamic system rather than on single molecule properties.

10 Perspectives

10.1 Future research

While it was found that temperature is a variable that is notoriously difficult to control, the theoretical framework that was developed for the FCS studies is – as demonstrated – by no means limited to such studies. In fact, a number of other membrane variables (e.g. pH, pCa, different membrane-soluble substances, etc.) could be systematically tested with very few or no changes to the experimental procedure. In particular, future studies could focus on determining which mechanism for the permeation (line defects or pore formation) is the dominant one for different molecules. The two mechanisms can, in principle, be distinguished as they give different predictions. For instance, at the transition point a lowered cooperativity would according to the line defect model increase the permeation rate, whereas the pore model predicts a decrease.

Likewise, studies on different lipid mixtures and even biological membranes should present no additional problems, and could provide definite evidence for the relevance of this phenomenon for biological systems. In particular, it could be interesting to additionally investigate pore formation in a "biological" system (a membrane with a dozen or more lipid species) by Monte Carlo simulation, and how the dynamics and statistics of the pore formation would change if local perturbations were made.

Given the numerous experimental difficulties involved in using FCS to measure permeability rates, a different approach might also be worth investigating.

One possible method would be to use labelled lipids such as TRITC DHPE along with a suitable dye quencher, and then simply measure how the overall count rate decays as the quencher leaks into the vesicles. This way, it would be possible to heat and equilibrate the sample *before* adding the quencher, thus avoiding the problems with dye leakage while the vesicles are heated through the phase transition. However, one should take care to avoid quenchers that interact strongly with the membranes themselves, as this could change the dynamics of the system in undesirable ways.

In addition, with this method it wouldn't be necessary to perform chromatography (always a somewhat tricky affair), and the size (and size distribution) of the vesicles wouldn't matter either, as long as their curvature is sufficiently low to have a negligible influence on the phase transition.

In effect this method should have none of the difficulties of the correlation spectroscopy and does not require as large a number of assumptions when analysing the data. In particular, the measurements would not be affected by convection or vibrations.

Finally, these findings could also be of more technological interest, as it could be used for controlling drug delivery, for instance (Davidsen et al. (2002)). It could also be used to carry out controlled biochemical reactions between few or even single molecules, by having reactants in small vesicles that are in turn enclosed by giant vesicles that have been immobilised on a surface. One can

then systematically release the reactants by increasing the temperature to the transition temperature of the enclosed vesicles, while still staying below that of the giant vesicles (Christensen and Stamou (2007)).

10.2 Implications for biology

The underlying premise of this thesis is that thermodynamics of the membrane itself is of major biological relevance.

As previously mentioned, biological membranes are known to have transition temperatures close to the organism's temperature, regardless of the temperature, hydrostatic pressure, or salinity of the environment. What's more, it is well known that organisms will adapt the lipid composition of their membranes if subjected to prolonged changes in their environment (homeoviscous adaptation). This suggests that there must be a specific reason for having the membranes in a certain, well-defined thermodynamic state which is quite sensitive to small changes in the environment (Hazel and Williams (1990)).

In addition to the changes in the transmembrane permeability, it is known that both elastic constants, bending moduli, relaxation timescales and even the function of certain proteins depend strongly on the thermodynamic state and fluctuations of the membrane. Thus a likely explanation would be that is favourable for the system to be in a state where the strength of the membrane fluctuations can be easily controlled *in vivo* by simply varying any of the intensive thermodynamic variable in such a way that the corresponding susceptibility increase or decrease as needed (Kaufmann et al. (1989)).

For example, it has been found that certain drugs (such as neurotransmitters, antibiotics, and – as demonstrated – general anaesthetics) influence the heat capacity profile significantly and thus also the membrane permeability. Thus the release of e.g. neurotransmitters would – in addition to their specific binding – give rise to a brief permeability change in nearby membranes. This would in turn result in an ion flow that alters the membrane potential of the cell.

It is already known that certain membranes change resting potential in response to a short-term change in temperature (see MacDonald (1990) and the references therein).

Changes in the pH due to e.g. enzyme activity leads to a protonation of lipid head groups, which will induce a change in phase behaviour. Thus, such activity can lead to higher fluctuations locally, and can therefore indirectly induce pore formation (Kaufmann (1977), Kaufmann and Silman (1983a,b)). In fact, it has been shown that in the presence of acetylcholine acetyholinesterase induces ion channel properties (Kaufmann and Silman (1980)). The hydrolysis of acetylcholine by acetylcholinesterase is known to be of great importance during synaptic transmission.

On a similar note, it is known that the local fluctuations and elastic constants are strongly influenced near peptides (Ivanova et al. (2003), Oliynyk et al. (2007)), thus making it possible for peptides that do not form pores to influence the transmembrane permeability.

In summary, a deep understanding of the thermodynamics of the system is of great importance for a complete description of the physiology of biological systems, as the state (and thus properties) of the membranes are easily and locally alterable by varying membrane variables such as the pH, salt concentrations, or transmembrane electrical fields (e.g. an action potential). This

approach serves to create a more holistic picture of how the thermodynamic properties of biological membranes can be used for physiological control. In particular, the thermal fluctuations can provide a physical mechanism for the control of the permeability, and should therefore be important for the description and understanding of any process which involves passive transport through the membrane, such as osmotic regulation, electrical excitability of cells, release of enzymes or chemical transmitters (e.g. calcium or neurotransmitters), and the absorption and secretion of salts and nutrients to name but a few (Giocondi and Le Grimellec (1991), Alberts et al. (1994)).

10.3 Anaesthetics

A wide variety of chemically diverse substances (e.g. nitrous oxide, octanol, chloroform, procaine, and even the noble gas xenon!) can act as general anaesthetics. The fact that general anaesthetics are additive and lack of any characteristic structure would seem to indicate a non-specific interaction. Hence, it seems reasonable to speculate that the anaesthetic action is related to changes in the properties of the lipid membranes, and not to specific interaction with proteins. This project has irrefutably shown that changes in the thermodynamic state of the membrane by addition of anaesthetics can have a significant influence on the membrane's permeability and therefore its ability to maintain concentration gradients.

Even though the use of anaesthetics was introduced into clinical practise more than one and a half century ago, the molecular mechanism behind it still remains unclear. Current theories favour the notion of anaesthetics that bind to ligand-gated ion-channels, thereby restricting their function. However, there are several competing theories. It has been proposed that the conformational changes of the embedded proteins are indirect, as they stem from changes in the transverse pressure profile of the membrane caused by the presence of anaesthetics in the membrane (Cantor (1997a,b)).

In a recent paper by Heimburg and Jackson (2005) it was proposed that the nerve pulse is actually a propagating soliton, i.e. an electromechanical rather than purely electrical phenomenon. In this model, a lowering of the melting temperature would result in an increase of the free energy threshold of soliton propagation. Part of this theory was inspired by the more than 100 year old Meyer-Overton rule which states that the anaesthetic potency of a substance is almost linearly correlated with its solubility in olive oil (Heimburg and Jackson (2007a)). This model is radically different from the accepted one by Hodgkin and Huxley (1952), but it provides a quantitative explanation of a large number of seemingly unrelated phenomena, such as the pressure reversal of anaesthesia and why inflammation and the addition of divalent cations reduce the effectiveness of anaesthetics (Heimburg and Jackson (2007a,b)).

In the soliton model the lipid membrane is forced by about 85% through the melting transition by the soliton (Heimburg and Jackson (2007b)). One would consequently expect an increase in the nerve membrane permeability due to the enhanced thermal fluctuations. In fact, it is well known that permeability increases during an action potential (Hodgkin and Huxley (1952)). However, this increase in the permeability of the nerve membrane during an action potential is normally attributed to the opening of ion-selective protein channels. As mentioned in Sec. (2) single channel currents of membranes show discrete

conductance steps, even in the absence of protein-channels (see Fig. (55)). Especially the work by Antonov et al. (2005) verifies that the phase transition and the enhancement of fluctuations is closely related to the appearance of quantised currents. In all cases – membranes both with and without proteins or peptides – one additionally finds ion selectivity, i.e. that different ions have different permeation rates. Interestingly, it has been found that the effect of selectivity is most pronounced in the transition regime of the membrane (Georgallas et al. (1987)). This means that one should be careful when interpreting ion channel data, since conductances may be due to lipid pores and not necessarily protein channels.

In general, a disruption of the system by some membrane-soluble substance (general anaesthetics, neurotransmitters or antibiotics, for instance) can severely influence the dynamics of the system (domain formation and structure, protein diffusion and clustering, signal cascades, pore formation, budding events, pulse propagation, etc.), which could account for the influence of general anaesthetics (Seeger et al. (2007), Heimburg and Jackson (2007a)).

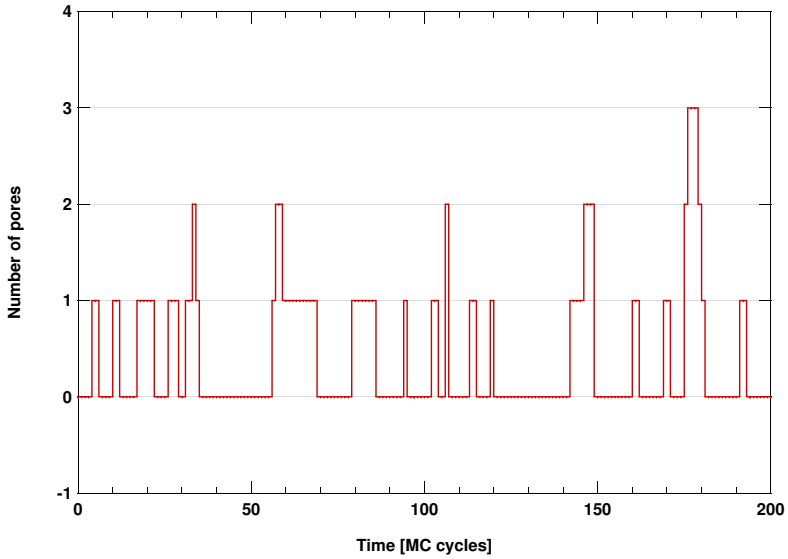

FIG. 55: Example of a trace of the number of pores as a function of Monte Carlo time in a 50×50 system. Though the stepwise nature of the trace is a direct consequence of the model, the pores obey statistics that are not unlike what is observed for real systems (see Fig. (5)). It should be mentioned that the reason for this stepwise nature of the current traces of real membranes is still not fully understood (Heimburg (2007)).

References

Alberts et al. (1994): Alberts, B.; Bray, D.; Lewis, J.; Raff, M.; Roberts, K; Watson, J. D. 1994. Molecular Biology of the Cell. *Garland Publishing, 3rd Edition (in particular Chapter 11).*

Aloia and Raison (1989): Aloia, R. C.; Raison, J. K. 1989. Membrane function in mammalian hibernation. *Biochimica et Biophysica Acta - Reviews on Biomembranes, Volume 988, Issue 1, pp. 123-146.*

Antonov et al. (1980): Antonov, V. F.; Petrov, V. V.; Molnar, A. A.; Predvoditelev, D. A.; Ivanov, A. S. 1980. The appearance of single-ion channels in unmodified lipid bilayer membranes at the phase transition temperature. *Nature, Volume 283, pp. 585-586.*

Antonov et al. (1985): Antonov, V. F.; Shevchenko, E. V.; Kozhomkulov, E. T.; Mol'nar, A. A.; Smirnova, E. Y. 1985. Capacitive and ionic currents in BLM from phosphatidic acid in Ca^{2+}-induced phase transition. *Biochemical and Biophysical Research Communications, Volume 133, pp. 1098-1103.*

Antonov et al. (2005): Antonov, V. F.; Anosov, A. A.; Norik, V. P.; Smirnova, E. Y. 2005. Soft perforation of planar bilayer lipid membranes of dipalmitoylphophatidylcholine at the temperature of the phase transition from the liquid crystalline to the gel state. *European Biophysical Journal, Volume 34, pp. 155-162.*

Bagatolli (2006): Bagatolli, L. A. 2006. To see or not to see: Lateral organization of biological membranes and fluorescence microscopy. *Biochimica et Biophysica Acta, Volume 1758, pp. 1541-1556.*

Benedetti et al. (1987): Benedetti, A.; Birarelli, A. M.; Brunelli, E.; Curatola, G.; Ferretti, G.; Del Prete, U.; Jezequel, A. M.; Orlandi, F. 1987. Modification of lipid composition of erythrocyte membranes in chronic alcoholism. *Pharmacological Research Communications, Volume 19, Issue 10, pp. 651-662.*

Boheim et al. (1980): Boheim, G.; Hankey, W.; Eibl, H. 1980. Lipid phase transition in planar bilayer membrane and its effect on carrier and pore mediated ion transport. *Proc. Nat. Acad. Sci. USA, Volume 77, pp. 3402-3408.*

Brush (1967): Brush, S. G. 1967. History of the Lenz-Ising Model. *Reviews of Modern Physics, Volume 39, Issue 4, pp. 883-893.*

Cannon et al. (2003): Cannon, B.; Hermansson, M.; Györke, S.; Somerharju, P.; Virtanen, J. A. 2003. Regulation of Calcium Channel Activity by Lipid Domain Formation in Planar Lipid Bilayers. *Biophysical Journal, Volume 85, pp. 933-942.*

Cantor (1997a): Cantor, R. S. 1997. Lateral pressures in cell membranes: a mechanism for modulation of protein function. *Journal of Physical Chemistry B, Volume 101, pp. 1723-1725.*

Cantor (1997b): Cantor, R. S. 1997. The Lateral Pressure Profile in Membranes: A Physical Mechanism of General Anesthesia. *Biochemistry, Volume 36, Issue 9, pp. 2339-2344.*

Charrier and Thibaudau (2005): Charrier, A.; Thibaudau, F. 2005. Main Phase Transition in Supported Lipid Single-Bilayer. *Biophysical Journal, Volume 89, pp. 1094-1101.*

Christensen and Stamou (2007): Christensen, S. M.; Stamou, D. 2007. Surface-based lipid vesicle reactor systems: fabrication and applications. *Soft Matter, Volume 3, pp. 828-836.*

Corvera et al. (1992): Corvera, E.; Mouritsen, O. G.; Singer, M. A.; Zuckermann, M. J. 1992. The permeability and the effect of acyl-chain length for phospholipid bilayers containing cholesterol: theory and experiment. *Biochimica et Biophysica Acta, Volume 1107, Issue 2, pp. 261-270.*

Cruzeiro-Hansson and Mouritsen (1988): Cruzeiro-Hansson, L.; Mouritsen O. G. 1988. Passive ion permeability of lipid membranes modelled via lipid-domain interfacial area. *Biochimica et Biophysica Acta, Volume 944, Issue 1, pp. 63-72.*

Danielli and Davson (1935): Danielli, J. F.; Davson, H. 1935. A contribution to the theory of permeability of thin films. *Journal of Cellular and Comparative Physiology, Volume 5, Issue 4, pp. 495-508.*

Davidsen et al. (2002): Davidsen, J.; Mouritsen, O. G.; Jørgensen, K. 2002. Synergistic permeability enhancing effect of lysophospholipids and fatty acids on lipid membranes. *Biochimica et Biophysica Acta, Volume 1564, pp. 256-262.*

Doniach (1978): Doniach, S. 1978. Thermodynamic fluctuations in phospholipid bilayers. *The Journal of Chemical Physics, Volume 68, Issue 11, pp. 4912-4916.*

Ebel et al. (2001): Ebel, H.; Grabitz, P.; Heimburg, T. 2001. Enthalpy and volume changes in lipid membranes I. The proportionality of heat and volume changes in the lipid melting transition and its implication for the elastic constants. *Journal of Physical Chemistry B, Volume 105, pp. 7353-7360.*

Efron and Tibshirani (1994): Efron, B.; Tibshirani, R. J. 1994. An Introduction to the Bootstrap (Monographs on Statistics and Applied Probability). *Chapman & Hall/CRC.*

Eggeling et al. (1998): Eggeling, C.; Widengren, J.; Rigler, R.; C. A. M. Seidel, C. A. M. 1998. Photobleaching of Fluorescent Dyes under Conditions Used for Single-Molecule Detection: Evidence of Two-Step Photolysis. *Anal. Chem, Volume 70, pp. 2651-2659.*

Eisenberg and McLaughlin (1976): Eisenberg, M.; McLaughlin, S. 1976. Lipid Bilayers as Models of Biological Membranes. *BioScience, Volume 26, Issue 7, pp. 436-443.*

Firestone et al. (1986): Firestone, L. L.; Miller, J. C.; Miller, K. W. 1986. Appendix: Tables of physical and pharmacological properties of anesthetics, Molecular and Cellular Mechanisms of Anesthetics. Edited by Roth SH, Miller KW. *Plenum Medical Book Co., pp. 455-470.*

Flyvbjerg and Petersen (1989): Flyvbjerg, H.; Petersen, H. G. 1989. Error estimates on averages of correlated data. *The Journal of Chemical Physics, Volume 91, Issue 1, pp. 461-466.*

Fox (1972): Fox, C. F. 1972. The structure of cell membranes. *Scientific American, Volume 226, pp. 30-38*

Frenkel and Smit (2001): Frenkel, D.; Smit, B. 2001. Understanding Molecular Simulation (Computational Science Series, Vol 1) *Academic Press, 2nd Edition.*

Gennis (1989): Gennis, R. B. 1989. Biomembranes. Molecular Structure and Function. *Springer.*

Georgallas et al. (1987): Georgallas, A.; MacArthur, J. D.; Ma, X.-P.; Nguyen, C. V.; Palmer, G. R. 1987. The diffusion of small ions through phospholipid bilayers. *Journal of Chemical Physics, Volume 86, Issue 12, pp. 7218-7226.*

Giocondi and Le Grimellec (1991): Giocondi, M.-C.; Le Grimellec, C. 1991. Water permeation in Madin-Darby canine kidney cells is modulated by membrane fluidity. *Biochimica et Biophysica Acta, Volume 1064, pp. 315-320.*

Glauber (1963): Glauber, R. J. 1963. Time-Dependent Statistics of the Ising Model. *The Journal of Mathematical Physics, Volume 4, Issue 2, pp. 294-307.*

Gorter and Grendel (1925): Gorter, E. M. D.; Grendel, F. 1925. On bimolecular layers of lipoids on the chromocytes of the blood. *The Journal of Experimental Medicine, Volume 41, pp. 439-443.*

Grabitz et al. (2002): Grabitz, P.; Ivanova, V. P.; Heimburg, T. 2002. Relaxation kinetics of lipid membranes and its relation to the heat capacity. *Biophysical Journal, Volume 82, pp. 299-309.*

Hac (2003): Hac, A. 2003. Diffusion Processes in Membranes Containing Coexisting Domains Investigated by Fluorescence Correlation Spectroscopy. *Ph.D. Thesis.*

Hac et al. (2005): Hac, A.; Seeger, H.; Fidorra, M.; Heimburg, T. 2005. Diffusion in two-component lipid membranes - A Fluorescence Correlation Spectroscopy and Monte-Carlo simulation study. *Biophysical Journal, Volume 88, pp. 317-333.*

Hazel and Williams (1990): Hazel, J. R.; Williams, E. E. 1990. The role of alterations in membrane lipid composition in enabling physiological adaptation of organisms to their physical environment. *Progress in Lipid Research, Volume 29, Issue 3, pp. 167-227.*

Heimburg and Biltonen (1994): Heimburg, T.; Biltonen, R. L. 1994. Thermotropic Behaviour of Dimyristoylphosphatidylglycerol and Its Interaction with Cytochrome C. *Biochemistry, Volume 33, pp. 9477-9488.*

Heimburg (1998): Heimburg, T. 1998. Mechanical aspects of membrane thermodynamics. Estimation of the mechanical properties of lipid membranes close to the chain melting transition from calorimetry. *Biochimica et Biophysica Acta, Volume 1415, Issue 1, pp. 147-162.*

Heimburg (2000): Heimburg, T. 2000. A Model for the Lipid Pretransition: Coupling of Ripple Formation with the Chain-Melting Transition. *Biophysical Journal, Volume 78, pp. 1154-1165.*

Heimburg and Jackson (2005): Heimburg, T.; Jackson, A. D. 2005. On soliton propagation in biomembranes and nerves. *Proc. Nat. Acad. Sci. USA, Volume 102, pp. 9790-9795.*

Heimburg and Jackson (2007a): Heimburg, T.; Jackson, A. D. 2007. The thermodynamics of general anesthesia. *Biophysical Journal, Volume 92, pp. 3159-3165.*

Heimburg and Jackson (2007b): Heimburg, T.; Jackson, A. D. 2007. On the action potential as a propagating density pulse and the role of anesthetics. *Biophysical Review Letters, Volume 2, pp. 57-78.*

Heimburg (2007): Heimburg, T. 2007. Thermal Biophysics of Membranes. *Wiley-VCH, 1st Edition.*

Hilgemann (2003): Hilgemann, D. W. 2003. Getting Ready for the Decade of the Lipids. *Annual Review of Physiology, Volume 65, pp. 697-700.*

Hill (1962): Hill, T. 1962. Introduction to Statistical Thermodynamics. *Addison-Wesley, 2nd Edition.*

Hille (2001): Hille, B. 2001. Ion Channels of Excitable Membranes. *Sinauer Associates, 3rd Edition.*

Hinz and Sturtevant (1972): Hinz, H.-J.; Sturtevant, J. M. 1972. Calorimetric Studies of Dilute Aqueous Suspensions of Bilayers Formed from Synthetic l-α-Lecithins. *Journal of Biological Chemistry, Volume 247, pp. 6071-6075.*

Hodgkin and Huxley (1952): Hodgkin, A. L.; Huxley, A. F. 1952. A quantitative description of membrane current and its application to conduction and excitation in nerve. *Journal of Physiology, Volume 117, pp. 500-544.*

Holzwarth (1986): Holzwarth, J. F. 1986. Dynamics of the phase transition in phospholipid vesicles from nanoseconds to seconds. *Faraday Discussions, Volume 81, pp. 348-363.*

Ipsen et al. (1990): Ipsen, J. H.; Jørgensen, K.; Mouritsen, O. G. 1990. Density fluctuations in saturated phospholipid bilayers increase as the acyl-chain length decreases. *Biophysical Journal, Volume 58, pp. 1099-1107.*

Ivanova and Heimburg (2001): Ivanova, V. P.; Heimburg, T. 2001. A histogram method to obtain heat capacities in lipid monolayers, curved bilayers and membranes containing peptides. *Physical Review E, Volume 63, pp. 1914-1925.*

Ivanova et al. (2003): Ivanova, V. P.; Makarov, I. M.; Schäffer, T. E.; Heimburg, T. 2003. Analyzing Heat Capacity Profiles of Peptide-Containing Membranes: Cluster Formation of Gramicidin A. *Biophysical Journal, Volume 84, pp. 2427-2439.*

Jacobsen et al. (1995): Jacobsen, K; Sheets, E. D.; Simson, R. 1995. Revisiting the Fluid Mosaic Model of Membranes. *Science, New Series, Volume 268, Issue 5216, pp. 1441-1442.*

Jensen and Prentø (1994): Jensen, P. V.; Prentø, P. 1994. Cellebiologi: Teori og Metoder. *Cellebiologisk-Anatomisk Laboratorium, Zoologisk Institut, Københavns Universitet.*

Kaufmann (1977): Kaufmann, K. 1977. Fast Kinetics of Acetylcholine at Synaptic Membranes. *International Journal of Quantum Chemistry, Volume XII, Supplement 2, pp. 169-178.*

Kaufmann and Silman (1980): Kaufmann, K.; Silman, I. 1980. The Induction of Ion Channels Through Excitable Membranes by Acetylcholinesterase. *Naturwissenschaften, Volume 67, pp. 608-610.*

Kaufmann and Silman (1983a): Kaufmann, K.; Silman, I. 1983. Proton-Induced Ion Channels Through Lipid Bilayer Membranes. *Naturwissenschaften, Volume 70, pp. 147-149.*

Kaufmann and Silman (1983b): Kaufmann, K.; Silman, I. 1983. The induction by protons of ion channels through lipid bilayer membranes. *Biophysical Chemistry, Volume 18, pp. 89-99.*

Kaufmann et al. (1989): Kaufmann, K.; Hanke, W.; Corcia, A. 1989. Ion Channel Fluctuations in Pure Lipid Bilayer Membranes: Control by Voltage. *Book 3. Can be found at* `www.membranes.nbi.dk/Kaufmann`.

Koynova and MacDonald (2003): Koynova, R.; MacDonald, R. C. 2003. Mixtures of Cationic Lipid *O*-Ethylphosphatidylcholine with Membrane Lipids and DNA: Phase Diagrams. *Biophysical Journal, Volume 85, pp. 2449-2465.*

Lee (2006): Lee, A. G. 2006. A paddle in oil. *Nature, Volume 444, pp. 697.*

Leidy et al. (2001): Leidy, C.; Wolkers, W. F.; Jørgensen, K.; Mouritsen, O. G.; Crowe, J. H. 2001. Lateral Organization and Domain Formation in a Two-Component Lipid Membrane System. *Biophysical Journal, Volume 80, pp. 1891-1828.*

Leontiadou et al. (2004): Leontiadou, H.; Mark, A. E.; Marrink, S. J. 2004. Molecular Dynamics Simulations of Hydrophilic Pores in Lipid Bilayers. *Biophysical Journal, Volume 86, pp. 2156-2164.*

Linden et al. (1973): Linden, C. D.; Wright, K. L.; McConnell, H. M.; Fox, C. F. 1973. Lateral Phase Separations in Membrane Lipids and the Mechanism of Sugar Transport in Escherichia coli. *Proc. Nat. Acad. Sci. USA, Volume 70, Issue 8, pp. 2271-2275.*

Logue et al. (2000): Logue, J. A.; De Vries, A. L.; Fodor, E.; Cossins, A. R. 2000. Lipid compositional correlates of temperature-adaptive interspecific differences in membrane physical structure. *Journal of Experimental Biology, Volume 203, pp. 2105-2115.*

MacDonald (1988): MacDonald, A. G. 1988. Application of the theory of homeoviscous adaptation to exitable membranes: pre-synaptic processes. *Biochemical Journal, Volume 256, pp. 313-327.*

MacDonald (1990): MacDonald, A. G. 1990. The homeoviscous theory of adaptation applied to excitable membranes: A critical evaluation. *Biochimica et Biophysica Acta - Reviews on Biomembranes, Volume 1031, Issue 3, pp 291-310.*

Magde et al. (1972): Magde, D.; Elson, E.; Webb, W. W. 1972. Thermodynamic Fluctuations in a Reacting System-Measurement by Fluorescence Correlation Spectroscopy. *Physical Review Letters, Volume 29, Issue 11, pp. 705-708.*

Margineanu et al. (2004): Margineanu, A.; Hofkens, J.; Cotlet, M.; Habuchi, S.; Stefan, A.; Qu, J.; Kohl, C.; Müllen, K.; Vercammen, J.; Engelborghs, Y.; Gensch, T.; Schryver, F. C. D. 2004. Photophysics of a Water-Soluble Rylene Dye: Comparison with Other Fluorescent Molecules for Biological Applications. *Journal of Physical Chemistry B, Volume 108, pp. 12242-12251.*

Marr and Ingraham (1962): Marr, A. G.; Ingraham, J. L. 1962. Effect of temperature on the composition of fatty acids in Escherichia Coli. *Journal of Bacteriology, Volume 84, Issue 6, pp. 1260-1267.*

Marrink et al. (2005): Marrink, S. J.; Risselada, J.; Mark, A. E. 2005. Simulation of gel phase formation and melting in lipid bilayers using a coarse grained model. *Chemistry and Physics of Lipids, Volume 135, pp. 223-244.*

Maynard et al. (1985): Maynard, V. M.; Magin, R. L.; Dunn, F. 1985. Ultrasonic absorption and permeability for liposomes near phase transition. *Chemistry and Physics of Lipids, Volume 37, pp. 1-12.*

Metropolis et al. (1953): Metropolis, N.; Rosenbluth, A. W.; Rosenbluth, M. N.; Teller, A. H. 1953. Equation of State Calculations by Fast Computing Machines. *The Journal of Chemical Physics, Volume 21, Issue 6, pp.1087-1092.*

Mouritsen et al. (1983): Mouritsen, O. G.; Boothroyd, A.; Harris, R.; Jan, N.; Lookman, T.; MacDonald, L.; Pink, D. A.; Zuckermann, M. J. 1983. Computer simulation of the main gel-fluid phase transition of lipid bilayers. *The Journal of Chemical Physics, Volume 79, Issue 4, pp. 2027-2041.*

Mouritsen and Bloom (1984): Mouritsen, O. G.; Bloom, M. 1984. Mattress model of lipid-protein interactions in membranes. *Biophysical Journal, Volume 46, pp. 141-153.*

Mouritsen and Zuckermann (1985): Mouritsen, O. G.; Zuckermann, M. J. 1985. Softening of lipid bilayers. *European Biophysics Journal, Volume 12, Issue 2, pp. 75-86.*

Nagle and Scott (1978): Nagle, J. F.; Scott, H. L. 1978. Lateral compressibility of lipid mono- and bilayers: Theory of membrane permeability. *Biochimica et Biophysica Acta, Volume 513, pp. 236-243.*

Neher and Sakmann (1976): Neher, E.; Sakmann, B. 1976. Single-channel currents recorded from membrane of denervated frog muscle fibres. *Nature, Volume 260, pp. 799-801.*

Nielsen et al. (2000): Nielsen, L. K.; Bjørnholm, T.; Mouritsen, O. G. 2000a. Fluctuations caught in the act. *Nature, Volume 404, pp. 352.*

Oliynyk et al. (2007): Oliynyk, V.; Kaatze, U.; Heimburg, T. 2007. Pore formation of lytic peptides in lipid membranes and their influence on the thermodynamic properties of the pore environment. *Biochimica et Biophysica Acta, Volume 1768, pp. 236-245*

Onsager (1944): Onsager, L. 1944. Crystal Statistics. I. A Two-Dimensional Model with an Order-Disorder Transition. *Physical Review 65, Issue 3-4, pp. 117-149.*

Overton (1899): Overton, E. 1899. On the general osmotic properties of the cell, their probable origin, and their significance for physiology. *Vierteljahrschrift der Naturforschende Gesselschaft (Zurich), Volume 44, pp. 88-135.*

Papahadjopoulos et al. (1973): Papahadjopoulos, D.; K. Jacobsen, S. Nir; Isac, T. 1973. Phase transition in phospholipid vesicles. Fluorescence polarization and permeability measurements concerning the effect of temperature and cholesterol. *Biochimica et Biophysica Acta, Volume 311, pp. 330-348.*

Parmahamsa et al. (2004): Parmahamsa, M.; Rameswara Reddy, K.; Varadacharyulu, N. 2004. Changes in composition and properties of erythrocyte membrane in chronic alcoholics. *Alcohol & Alcoholism, Volume 39, Issue 2, pp. 110-112.*

Paula et al. (1998): Paula, S.; Volkov, A. G.; Deamer, D. W. 1998. Permeation of halide anions through phospholipid bilayers occurs by the solubility-diffusion mechanism. *Biophysical Journal, Volume 74, Issue 1, pp. 319-327.*

Petrache et al. (2000): Petrache, H. I.; Dodd, S. W.; Brown, M. F. 2000. Area per Lipid and Acyl Length Distributions in Fluid Phosphatidylcholines Determined by ^{2}H NMR Spectroscopy. *Biophysical Journal, Volume 79, pp. 3172-3192.*

Petrov (2005): Petrov, E. 2005. Derivation of expressions for the FCS correlation function. *Supplementary material for the F-Praktikum.*

Pink et al. (1980): Pink, D. A.; Green, T. J.; Chapman, D. 1980. Raman scattering in bilayers of saturated phosphatidylcholines. Experiment and theory. *Biochemistry, Volume 19, Issue 2, pp. 349-356.*

Robertson (1957): Robertson, J. D. 1957. New Observations on the Ultrastructure of the Membranes of Frog Peripheral Nerve Fibers. *The Journal of Biophysical and Biochemical Cytology, Volume 3, Issue 6., pp. 1043-1048.*

Schmidt et al. (2006): Schmidt, D.; Jiang, Q.; MacKinnon, R. 2006. Phospholipids and the origin of cationic gating charges in voltage sensors. *Nature, Volume 444, pp.775-779.*

Schwille and Haustein (2002): Schwille, P.; Haustein, E. 2002. Fluorescence Correlation Spectroscopy: An Introduction to its Concepts and Applications. *Biophysics Textbook Online (BTOL).*

Seeger et al. (2005): Seeger, H.; Fidorra, H.; Heimburg, T. 2005. Domain size and fluctuations at domain interfaces in lipid mixtures. *Macromolecular Symposia, Volume 219, pp. 85-96.*

Seeger (2006): Seeger, H. 2006. Kinetics of Domain Formation Processes in Lipid Membranes. *Ph.D. Thesis.*

Seeger et al. (2007): Seeger, H. M.; Gudmundsson, M. L.; Heimburg, T. 2007. On the influence of anesthetics, neurotransmitters and antibiotics on the relaxation processes in lipid membranes. *arXiv:physics/0703022v1 [physics.bio-ph] 2 Mar 2007. Submitted.*

Simons and Ikonen (1997): Simons, K.; Ikonen, E. 1997. Functional rafts in cell membranes. *Nature, Volume 387, pp. 569-572.*

Sinensky (1974): Sinensky, M. 1974. Homeoviscous Adaptation – A Homeostatic Process that Regulates the Viscosity of Membrane Lipids in Escherichia coli. *Proc. Nat. Acad. Sci. USA, Volume 71, Issue 2, pp. 522-525.*

Singer and Nicolson (1972): Singer, S. J.; Nicolson, G. L. 1972. The Fluid Mosaic Model of the Structure of Cell Membranes. *Science, Volume 175, pp. 720-731.*

Strom-Jensen et al. (1984): Strom-Jensen, P. R.; Magin, R. L.; Dunn, F. 1984. Ultrasonic evidence for structural relaxation in large unilamellar liposomes. *Biochimica et Biophysica Acta, Volume 769, pp. 179-186.*

Sugar et al. (1994): Sugár, I. P.; Biltonen, R. L.; Mitchard, N. 1994. Monte Carlo simulations of membranes: phase transition of small unilamellar dipalmitoylphosphatidylcholine vesicles. *Methods in Enzymology, Volume 240, pp. 569-593.*

Sugar et al. (1999): Sugár, I. P.; Thompson, T. E.; Biltonen, R. L. 1999. Monte Carlo Simulation of Two-Component Bilayers: DMPC/DSPC Mixtures. *Biophysical Journal, Volume 76, pp. 2099-2110.*

Tien and Ottova-Leitmannova (2003): Tien, H. T.; Ottova-Leitmannova, A. 2003. Planar Lipid Bilayers (BLM's) and Their Applications. *Elsevier Science, 1st Edition.*

Träuble and Haynes (1971): Träuble, H.; Haynes, D. H. 1971. The volume change in lipid bilayer lamellae at the crystalline-liquid crystalline phase transition. *Chemistry and Physics of Lipids, Volume 7, Issue 4, pp. 324-335.*

Turnheim et al. (1999): Turnheim, K.; Gruber, J.; Wachter, C.; Ruiz-Gutiérrez, V. 1999. Membrane phopholipid composition affects function of potassium channels from rabbit colon epithelium. *American Journal of Physiology - Cell Physiology, Volume 277, pp. 83-90.*

Venturoli and Sperotto (2005): Venturoli, M.; Sperotto, M. M. 2005. Simulation Studies of Protein-Induced Bilayer Deformations, and Lipid-Induced Protein Tilting, on a Mesoscopic Model for Lipid Bilayers with Embedded Proteins. *Biophysical Journal, Volume 88, pp. 1778-1798.*

Wannier (1945): Wannier, G. H. 1945. The Statistical Problem in Cooperative Phenomena. *Reviews of Modern Physics, Volume 17, Issue 1, pp. 50-60.*

Widengren (1996): Widengren, J. 1996. Fluorescence Correlation Spectroscopy, Photophysical Aspects and Applications. *Ph.D. Thesis*

Wilson (1979): Wilson, K. G. 1979. Problems in Physics with Many Scales of Length. *Scientific American, Volume 241, pp. 140-158.*

Woodbury (1989): Woodbury, D. J. 1989. Pure Lipid Vesicles Can Induce Channel-Like Conductances in Planar Bilayers. *Journal of Membrane Biology, Volume 109, pp. 145-150.*

Wu and McConnell (1973): Wu, S. H.; McConnell, H. M. 1973. Lateral Phase Separations and Perpendicular Transport in Membranes. *Biochemical and Biophysical Research Communications, Volume 55, Issue 2, pp. 484-491.*

Yafuso et al. (1974): Yafuso, M.; Kennedy, S. J.; Freeman, A. R. 1974. Spontaneous Conductance Changes, Multilevel Conductance States and Negative Differential Resistance in Oxidized Cholesterol Black Lipid Membranes. *Journal of Membrane Biology, Volume 17, pp. 201-212.*

Yeomans (1992): Yeomans, J. M. 1992. Statistical Mechanics of Phase Transitions. *Oxford University Press.*

Yoshikawa et al. (1988): Yoshikawa, K.; Fujimoto, T.; Shimooka, T.; Terada, H.; Kumazawa, N. 1988. Electrical oscillation and fluctuation in phospholipid membranes: Phospholipids can form a channel without protein. *Biophysical Chemistry, Volume 29, pp. 293-299.*

Zondervan et al. (2003): Zondervan, R.; Kulzer, F.; Orlinskii, S. B.; Orrit, M. 2003. Photoblinking of Rhodamine 6G in Poly(vinyl alcohol): Radical Dark State Formed through the Triplet. *Journal of Physical Chemistry A, Volume 107, Issue 35, pp. 6770-6776.*

Part V
Appendix

This part is included so other people may reproduce the work of this thesis. It should not be necessary to read it to understand the thesis itself, but is simply here as documentation.

A Extrusion procedure

The procedure for extruding the vesicles was as follows:

- Measure out an appropriate amount of lipids, making a 10mM solution. If the vesicles only consist of one type of lipid (e.g. DMPC or DPPC), then simply dissolve it in a 200mM NaCl solution. If a mix of lipids is necessary (e.g. DPPC and DPPG) dissolve the lipids in a 2:1 mix of dichloromethane:methanol, and then let the solvent evaporate in a desiccator (vacuum chamber) before dissolving the mix in a 200mM NaCl solution.
- Add sufficient rhodamine 6G chloride to the solution to make the concentration 50μM, which should result in approximately 20 ± 5 rhodamine molecules per vesicle.
- Wrap the vial in aluminium foil in order to prevent unnecessary photobleaching of the dye, and then heat it to about 10 degrees above the phase transition temperature while stirring it for an hour or so.
- Meanwhile, turn on the heat bath for the extruder, setting it to 49.6°C.
- Once the sample has been thoroughly heated and stirred, transfer it to the extruder syringe and put the filled syringe in the extruder for 15 minutes or so, thus allowing the syringe and the sample to get heated to the same temperature as the extruder itself.
- Extrude slowly (about one cycle per two minutes), and make sure that it's done an odd number of times, thus ending up with the sample in the opposite syringe. This should reduce the amount of dust and aggregates in the sample (as this will be left in the first syringe) and it will ensure that all of the vesicles have been through the filter at least once.
- Once done, transfer the extruded sample to a small vial and store it in the fridge. As there are no concentration gradients at this point, dye leakage will not be an issue.

B Chromatography guide

B.1 The G50 chromatography column

Before the actual separation (via. size exclusion chromatography) could be performed, the column needed to be preparation and equilibrated. This step is crucial to get decent results.

- Weigh out 5g of Sephadex G50 Superfine chromatography gel (Fluka, BioChemica).
- To pre-swell the gel, add approximately 200ml of Millipore water. Excess water is added to allow the gel to swell without the risk of drying out.
- Allow the solution to stand for 3 hours at 80°C or overnight at room temperature.
- Once pre-swelling has occurred, allow the gel to settle and then pour off the gel slurry supernatant to remove the gel fines. Failure to remove the gel fines may cause the chromatography column to become blocked during use, ruining the entire preparation.
- To ensure that the gel fines are removed, resuspend the gel in 200ml of Millipore water, allow it to settle, and pour off the gel slurry supernatant as before. Repeat until no more fines can be discerned.
- Resuspend in 100ml of Millipore water. The gel should now be ready for usage.

B.2 Chromatography procedure

Once the gel has settled, chromatography can be performed, using the following procedure. Also see Fig. (22) for guidance.

- Set up a clean disposable glass Pasteur pipettes (the longer the better) with a small piece of sterile glass wool plugged in the neck (use a long and narrow pipette to push the wool down the Pasteur pipette), and ensure that the column is vertical and well clamped into position. Add enough Millipore water or buffer to occupy about 20% of the column volume and drain to about 10% of the column volume to remove air from the column fittings.
- Mix the pre-swollen Sephadex G50 gel so that the gel slurry is homogeneous. Use another Pasteur pipette to fill the column with the gel slurry, taking care to avoid producing bubbles. Note that the gel slurry should not be too thick for pouring as air bubbles will become trapped in the column. Keep adding gel until it packs to a level $\approx$ 2cm below the top of the column. Also, make sure that the ambient temperature is at least 10 degrees below the phase transition temperature of the sample to prevent dye leakage during the separation procedure.
- Equilibrate the column with buffer. Ensure that the buffer is at room temperature before use, so as to reduce the risk of air bubbles forming in the column. It is suggested that a minimum of three column volumes are run through the column to block all non-specific binding sites on the column. This usually takes an hour or two.
- Pour the sample into the column and add more buffer as needed, in order to keep the column from drying out.

- Collect fractions (of about 200μl each) in five or six Eppendorf tubes, thus getting different grades of separation and concentration of the vesicles and the free rhodamine particles.
- Store the samples in a fridge to prevent leakage. When used for the actual FCS measurements, dilute the sample with buffer by a factor of 50-100.

C FCS procedure

The FCS measurements used the following procedure:

- Heat the entire instrument to approximately the desired temperature. This can be done by placing a hot air heater under the optical table. In addition, mount a water bath heated mantle/jacket on the objective, to get better temperature control. This part can easily take a couple of hours before everything has equilibrated.
- Clean a chambered coverglass[19] (i.e. a cuvette), taking care to avoid dust contamination.
- Transfer 500μl of solution to one of the wells and then degas it approximately 10 minutes. Remove any air bubbles that form in the well.
- Measure the temperature of the objective water drop using a thermocouple. Additionally, make a measurement in a cuvette well filled with an oil with a low evaporation rate (to reduce the cooling effect of evaporation).
- Seal the well with some Parafilm, mount the heating jacket and place the cuvette over the water immersion objective.
- When making measurements of rhodamine 6G, wait for at least 10 minutes, allowing rhodamine adsorption to the cuvette walls to reach equilibrium. This will also give the sample time to get heated to the desired temperature and for turbulence to die out.
- Make sure the focus is well inside the sample and not too near the cover glass, and calibrate the instrument until a maximum signal is achieved. Normally, simply adjusting the pinhole will suffice.
- Record a dozen correlation curves (30-60 seconds sampling) to check whether the system has fully equilibrated, and then determine the focus radius, characteristic diffusion time scale, and counts per second per rhodamine molecule.

Once the setup has been calibrated and good rhodamine data has been obtained, a systematic series of measurements were carried out. This was done by making short script that could control the laser shutter as well as the Flex5000 correlator card.

A typical series consisted of 50-100 correlation curves, where each curve had a sampling time of 50-60 seconds, and was separated by a 5-6 seconds pause with

[19] NUNC Lab-Tek Chambered #1.0 Borosilicate Coverglass System.

the shutter blocking the light path. Measurements at temperatures very close to the transition temperature used shorter sampling time (≈30 seconds) and longer sampling times (≈120 seconds) at low temperatures. The pause between measurements was always 10% of the sampling time, in order to eliminate differences in the photobleaching of the system.

D Structures of the dyes

The schematic structures of the dyes used in this thesis. For ease of reference the more colourful representations are also shown in Fig. (56).

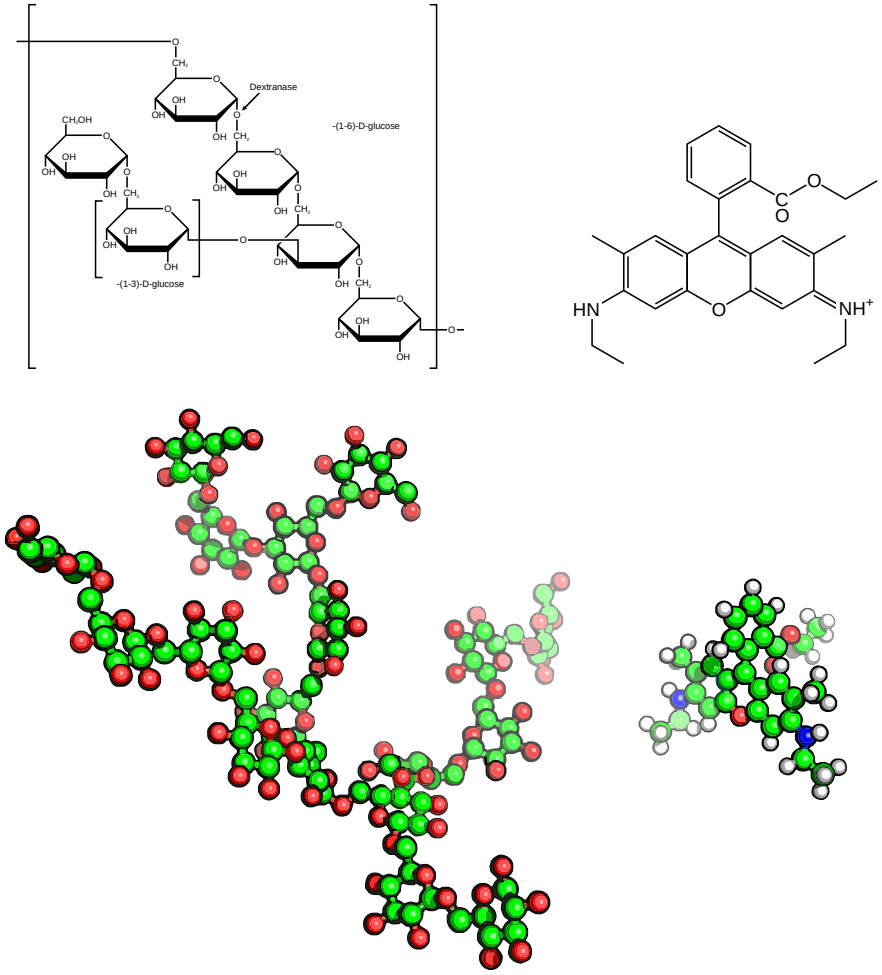

FIG. 56: *Left:* Dextran. *Right:* Rhodamine 6G chloride.

E Lattice complications

One complication associated with having a variable lattice size and periodic boundary conditions is that there are two of the sites which will have an ill-defined neighbourhood.

In my program this was solved by allowing these two sites to have only five nearest neighbours as shown in Fig. (57). The error that this produces should be negligible, as lipids are much more likely to have neighbours in the same state for $\omega_{fg} > 0$ (see Fig. (42)).

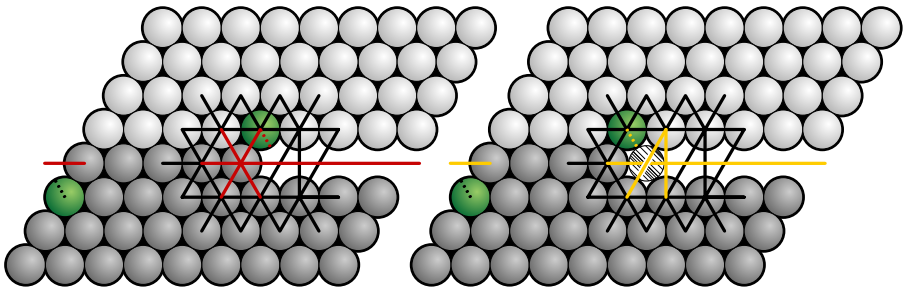

FIG. 57: The solution to the lattice oddity. The light grey lattice represents the periodic boundary conditions, and is therefore the bottom of the lattice. When adding or removing a particle from the lattice "end", only the yellow and the red interactions change. The green lattice sites are the sites with ill-defined neighbourhoods, where the dotted lines represent interaction with itself (in effect having no free energy cost and only five nearest neighbours).

F Estimating errors

As previously mentioned, there will always be a trade-off between having good sampling and acceptable computation time. The problem becomes immediately apparent when calculations one tries to calculate thermodynamic quantities near critical points – a phenomenon known as critical slowing down. While there are methods that can suppress this problem, doing so would in it self be a major undertaking, and has not been done in my program.

Even when far away from a phase transition, there is still the issue of finite sampling, which introduces statistical noise in any of the calculated thermodynamic observable.

As mentioned in Sec. (5.4), the time series that one obtains from the simulations show correlated fluctuations, which requires some additional considerations, as standard data analysis methods assume that the data points are uncorrelated, which is rarely the case in these kinds of simulations. The problem becomes more severe the nearer one is to a critical point, as the correlation times and lengths diverge at the critical point itself. However, a number of methods can be used to give estimates for the confidence intervals for a given quantity.

F.1 The moving blocks bootstrap

The most straightforward and primitive method is simply to make dozens of simulations, and then use the usual statistical methods for obtaining confidence intervals. This, however, is a very time consuming affair, as one would have to equilibrate the system for every simulation, and it might not be a realistic option, if one simulation takes, say, a week or more to perform.

A slight improvement over the method above would be to take the time series, and divide it into intervals of around 10 times the characteristic correlation time of the fluctuations (which can easily be obtained beforehand by autocorrelating the time series). This would ensure that the estimates of a thermodynamic quantity obtained from the different intervals would be (essentially) independent of each other, and one could proceed as before and obtain error estimates for the derived observable. In essence, this method simply does away with the need to re-equilibrate the system for each estimate.

Better yet would be to use the Moving Blocks Bootstrap method (see Efron and Tibshirani (1994) for a more thorough introduction). To generate the so-called *bootstrap realisation* of the time series, one first needs to choose an appropriate block length, ℓ, and then consider all possible contiguous blocks of this length. Then one samples (with replacement) from these blocks and connect enough of them to form a bootstrap time series, which is of roughly the same length as the original time series. So if the block length is ℓ, then we sample $k \approx n/\ell$ blocks.

Using this bootstrap, we can then estimate our thermodynamic quantity. This entire process is then repeated a couple of hundred times, after which we can perform the standard data analysis, as the estimates from each bootstrap time series are, to a good approximation, independent.

So the basic idea is to choose a block size, ℓ, that is large enough so that observations more than ℓ Monte Carlo apart will be practically independent of each other, while retaining any correlation present in the observations that is less than ℓ Monte Carlo cycles apart.

It should be noted that the choice of block size, ℓ, is quite important, though an effective methods for making this choice has still not been developed to the best of my knowledge.

F.2 The blocking method

Another very useful, though less general, method for obtaining error estimates on averages of correlated time series, is the so-called *blocking method* or *bunching method*. (see Flyvbjerg and Petersen (1989) for a more thorough discussion).

This method is quite powerful and should "combine maximum rigour with minimum computation and reflection."

In short, this method can be used to estimate the lower bounds for the variance, $\sigma^2(\overline{x})$, of averaged variable, $\overline{x}$, by iteratively "blocking" the data. The procedure is as follows.

Transform the data set $x_1, \ldots, x_n$ into half as large a data set $x'_1, \ldots, x'_n$, where

$$x'_i = \frac{1}{2}(x_{2i-1} + x_{2i}), \tag{131}$$

$$n' = \frac{n}{2}. \tag{132}$$

If we then define $\overline{x}'$ as the average of the n' "blocked" data points, we still have that

$$\overline{x}' = \overline{x}, \tag{133}$$

as the average of averages is, of course, the same as the average over the entire data set[20].

So if we start with a data set $x_1, \ldots, x_n$, we can compute c_0, where c_0 is defined as

$$c_0 \equiv \frac{1}{n(n-1)} \sum_{k=1}^{n} (x_k - \overline{x})^2. \tag{134}$$

This gives us a first estimate and a lower bound for $\sigma^2(\overline{x})$, as it can be shown that

$$\langle c_0 \rangle \leq \sigma^2(\overline{x}). \tag{135}$$

By iteratively applying the blocking transformations Eqs. (131)–(132) to the data set, one can compute c_0' as estimates for $\langle c_0' \rangle$. This sequence of estimates will increase until a fixed point is reached, where it will remain constant (within fluctuations).

This constant value is the best estimate for $\sigma^2(\overline{x})$, and one can even estimate the standard deviation on our estimate c_0' for $\sigma^2(\overline{x})$, namely

$$\sigma^2 \approx c_0' \pm c_0' \sqrt{\frac{2}{n'-1}}, \tag{136}$$

which can be useful to know when determining whether the fixed point has been reached yet.

In the case that the fixed point is not reached before $n' \leq 3$, one can the use the largest value obtained for c_0 as a lower bound on $\sigma^2(\overline{x})$.

One of the great advantages of this method is that due to the geometric nature of the blocking procedure, the number of operations needed for obtaining the estimate for $\sigma^2(\overline{x})$ is only $\mathcal{O}(2n)$.

In this thesis the blocking method was used to determine the uncertainties in the average number of pores ($x \equiv N_h$) and in the heat capacity ($x \equiv (H - \overline{H})^2$).

G Assorted curiosities from the simulations

During the development of the Monte Carlo program a great number of different bug checks and data outputs were made. Some of them might be of interest, and are therefore presented here.

G.1 Bifurcation

Out of simple curiosity, a bifurcation diagram of the system was also made. As can be seen from Fig. (58) a supercritical pitchfork bifurcation occurs at $T = T_m$ and $\omega_{fg} = 1434.77\text{J/mol}$ (if there were no finite-size effects). Though

[20] Except if there's an uneven number of data points, in which case some information will be lost, and the two values will differ slightly.

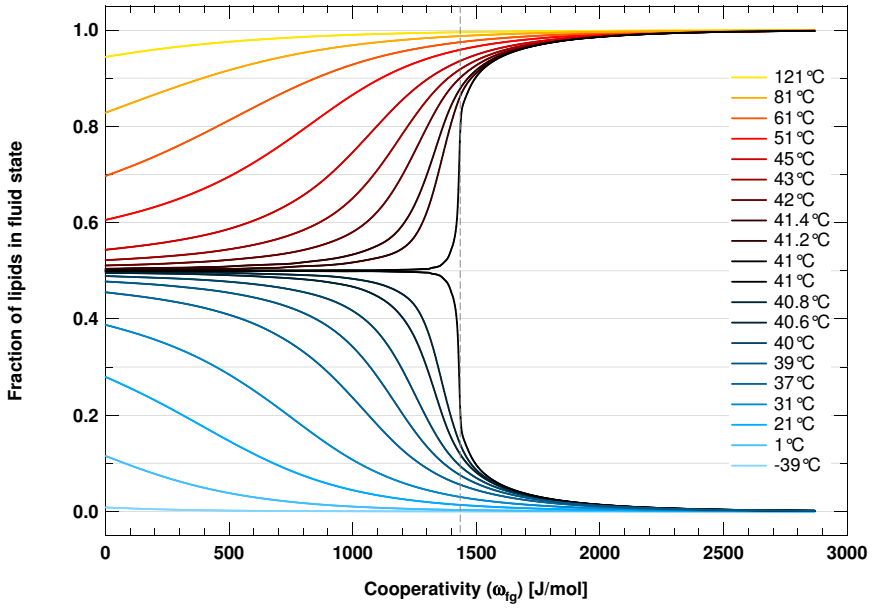

FIG. 58: Bifurcation diagram for a 50×50 system (DPPC), with no pore formation. The dashed lined is the theoretical critical value from Eq. (93). The finite-size effects are evident near the critical point at $T = 41°\text{C}$ and $\omega_{fg} = 1434.77$ J/mol.

the figure only shows the stable solutions, there is, for instance, also a solution for $T = T_m$ with a constant fluid fraction of 0.5. However, this solution is unstable for $\omega_{fg} > 1434.77$J/mol and will practically never occur due to the constant thermal disturbances of the system.

G.2 Cooperativity and domains

The average size of the domains is shown in Fig. (59). A domain is defined as a cluster of lipids (two or more) in the fluid state when below the melting temperature, and gel state lipids when above. The size is simply the number of lipids in the cluster.

A peculiar observation that was made, was that the distribution of domain sizes seem to be almost independent of ω_{fg} at $T = T_m$, as shown in Fig. (60).

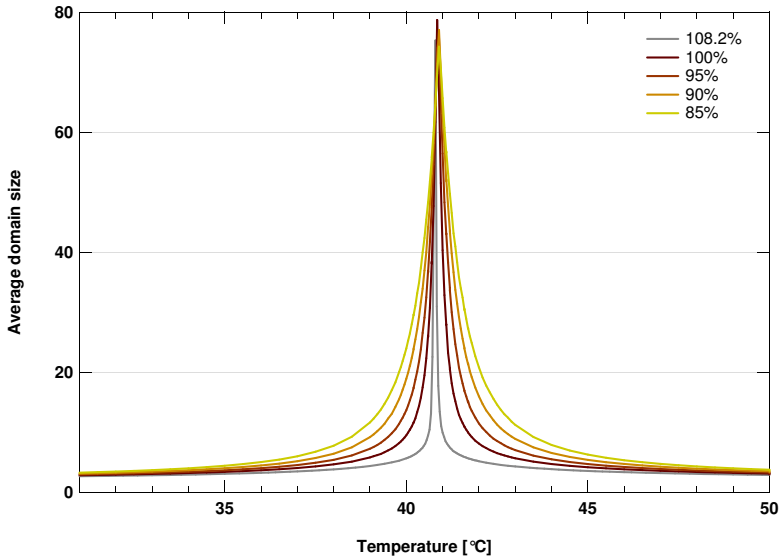

FIG. 59: Average domain sizes in a simulated one-component system (DPPC) with varying cooperativity, ω_{fg}. The reference value (100%) is $\omega_{fg} = 1326$kJ/mol. The 108.2% corresponds to $\omega_{fg} = 1434.77$J/mol, i.e. the critical value from Eq. (93) The slight shifts in the location of the maxima are due to different number of pores in the system.

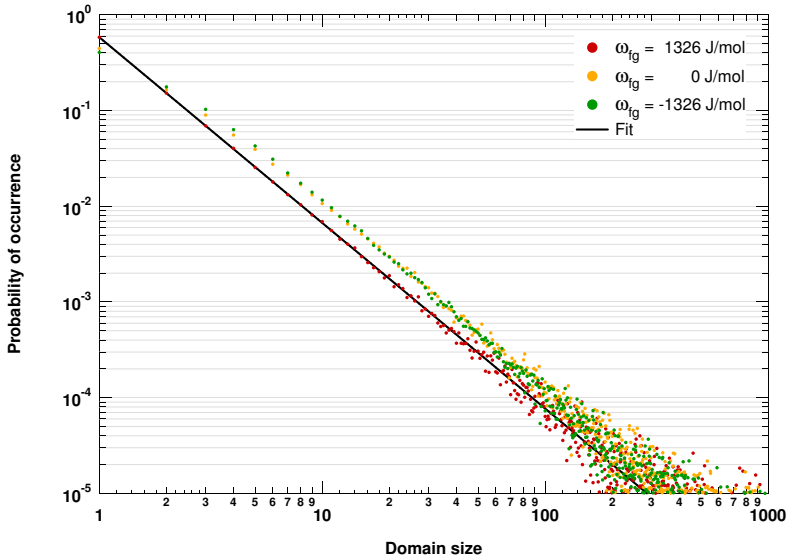

FIG. 60: The domain size distribution for different values of ω_{fg} at $T = T_m$ in a simulation without pores or anaesthetics involved. Note that the slope is independent of ω_{fg}, which is not immediately obvious from the snapshots shown in Fig. (61). The offset is due to the slight differences for very small domains ($l^\alpha < 3$). The fitted function shown is $f(l) = 0.58 \cdot l^{-1.94}$.

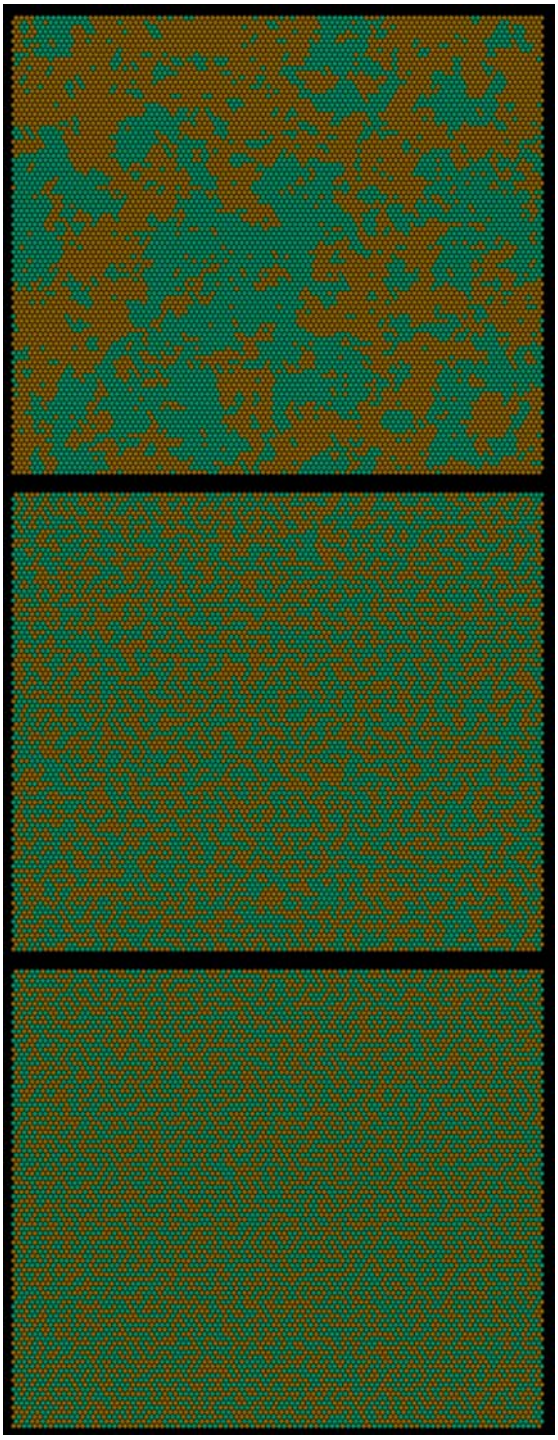

FIG. 61: Representative micro configurations for different values of ω_{fg} at $T = T_m$ in a simulation without pores or anaesthetics involved.